Technical Report Documentation Page

1. Report No.	2. Government Accession No.	3. Recipient's Catalog No.
FHWA/TX-97/1244-11		

4. Title and Subtitle	5. Report Date
INFLUENCE OF COARSE AGGREGATE IN PORTLAND CEMENT CONCRETE ON SPALLING OF CONCRETE PAVEMENTS	November 1995 Revised: October 1996
	6. Performing Organization Code
7. Author(s) Sanjaya P. Senadheera and Dan G. Zollinger	8. Performing Organization Report No. Research Report 1244-11
9. Performing Organization Name and Address Texas Transportation Institute The Texas A&M University System College Station, Texas 77843-3135	10. Work Unit No. (TRAIS)
	11. Contract or Grant No. Study No. 0-1244
12. Sponsoring Agency Name and Address Texas Department of Transportation Research and Technology Transfer Office P.O. Box 5080 Austin, Texas 78763-5080	13. Type of Report and Period Covered Interim: September 1992-August 1995
	14. Sponsoring Agency Code

15. Supplementary Notes

Research performed in cooperation with the Texas Department of Transportation and the U.S. Department of Transportation, Federal Highway Administration.
Research Study Title: Evaluation of the Performance of Texas Pavement Made with Different Coarse Aggregates

16. Abstract

Spalling is a form of distress in concrete pavements. However, the current state of knowledge and the available prediction models on spalling indicate a lack of understanding of the spalling mechanism. This research attempts to fill the need to develop a framework to incorporate spalling in the design of concrete pavements based on a mechanistic approach. The report presents results from a comprehensive field survey on spalling in concrete pavements in Texas. Based on the results from this field survey, a mechanism for spalling is proposed. According to this mechanism, spalling is the culmination of damage initiated as delaminations early in the life of pavements. The development of delaminations is related to the concrete mix design and conditions at the time of paving including ambient conditions and the method of curing. The delaminations are extended into spalls as a result of fatigue damage induced by traffic and temperature fluctuations in the pavement. Early-age analysis of concrete pavements was performed using a finite element program developed to predict stresses in the pavement caused by shrinkage. Results from the analysis indicated that a high level of stress sufficient to create delaminations may be generated at a very early age. The coarse aggregate type in concrete was noted to have a significant effect on the level of spalling. Based on results from laboratory studies, a mechanism on how the aggregate type influences spalling is proposed. This proposed spalling mechanism is included in a framework to incorporate spalling in the design of concrete pavements.

17. Key Words	18. Distribution Statement
Spalling, Cracking, Coarse Aggregate, Curing, Properties of Aggregates, Evaluation of Aggregates	No restrictions. This document is available to the public through NTIS: National Technical Information Service 5285 Port Royal Road Springfield, Virginia 22161

19. Security Classif.(of this report)	20. Security Classif.(of this page)	21. No. of Pages	22. Price
Unclassified	Unclassified	222	

Form DOT F 1700.7 (8-72) Reproduction of completed page authorized

INFLUENCE OF COARSE AGGREGATE IN PORTLAND CEMENT CONCRETE ON SPALLING OF CONCRETE PAVEMENTS

by

Sanjaya P. Senadheera
Research Assistant
Texas Transportation Institute

and

Dan G. Zollinger
Associate Research Engineer and Associate Professor
Texas Transportation Institute

Research Report 1244-11
Research Study Number 0-1244
Research Study Title: Evaluation of the Performance of Texas Pavement Made with Different Coarse Aggregates

Sponsored by the
Texas Department of Transportation
in Cooperation with
U. S. Department of Transportation
Federal Highway Administration

November 1995
Revised: October 1996

TEXAS TRANSPORTATION INSTITUTE
The Texas A&M University System
College Station, Texas 77843-3135

IMPLEMENTATION STATEMENT

The spalling research discussed in this report will assist in developing an understanding of the factors that cause spalling in concrete pavements.

Spalling was found to result from pre-existing delaminations just below the surface of the pavement. These delaminations were found to occur as early as one week after construction, which suggests that the development of these delaminations is strongly related to the early aged bond strength of the mortar and the coarse aggregate. Factors relative to the construction process were found to be important in terms of the rate of water loss from the surface of the pavement during the hardening process. Polyethylene curing was found to significantly reduce the formation of the delaminated fracture surface. The study also discusses other factors. Use of improved curing techniques can result in reduced maintenance costs for spall repair damage and other related cost benefits to the Texas Department of Transportation.

DISCLAIMER

The contents of this report reflect the views of the authors who are responsible for the facts and accuracy of the information presented herein. The contents do not necessarily reflect the official views or policies of the Federal Highway Administration or the Texas Department of Transportation. This report does not constitute a standard, specification, or regulation.

ACKNOWLEDGMENT

Research findings presented in this report are a result of joint efforts between the Texas Transportation Institute, Texas A&M University, and the Center for Transportation Research, University of Texas at Austin. The authors would like to thank the staff of the Texas Department of Transportation for their support throughout this study as well as the U.S. Department of Transportation, Federal Highway Administration.

TABLE OF CONTENTS

LIST OF FIGURES

LIST OF TABLES

SUMMARY

This research study verified the already established fact that the coarse aggregate type has a significant influence on spalling in concrete pavements. However, due to the lack of an established mechanism for spalling, researchers have not been able to explain other factors that may influence spalling. This research study enabled the researchers to establish a mechanism for spalling which was hitherto not available.

According to this mechanism, spalling is not just a time dependent phenomenon as it has long been understood. Spalling distress develops in two stages. In stage I, delaminations are formed very close to the surface of the pavement slab. These delaminations are primarily caused by the loss of moisture due to evaporation. Therefore, ambient conditions at the time of paving have a significant influence on the development of delaminations. Also, it was observed that the interfacial strength between the aggregate and the cement paste has a significant influence on the development of delaminations. Therefore, for delaminations to occur at an early age of the pavement life, two conditions must be satisfied. The ambient conditions cause the concrete to lose moisture from the top part of the pavement slab. At the same time, stresses develop as a result of differential shrinkage across the depth of the slab exceeding the tensile strength of concrete. This is where the interfacial strength at the aggregate-cement interface comes into the picture. In summary, the precondition for the development of spalls, which is the initiation of delamination, occurs at a very early age. This explains why in some situations, concrete pavements with siliceous river gravel aggregates which generally display significant spalling also display instances of zero spalling. Situations of no spalling probably arise because ambient conditions were not sufficiently harsh to result in a significant loss of moisture from the pavement slab during curing.

If these delaminations do not form, the pavement is unlikely to develop any significant spalling during its lifetime. However, when they do form, the development of delaminations into spalls appears to be by fatigue due to the application of wheel loads on the pavement and the presence of water in the delamination.

It is therefore, clear that in order to eliminate spalling, a preventive approach needs to be adopted to prevent delaminations from occurring. This can be achieved by following either one or a combination of the steps listed below.

1. Use of more effective curing methods, particularly if paving is done at times when harsh climatic conditions exist (i.e., high temperature and low relative humidity).
2. No concrete paving in harsh climates as indicated above in (1).
3. Improve the aggregate-cement paste interface either by treating aggregates or by using better mix design methods.
4. Blend certain aggregate types which manifest a high level of resistance to spalling distress.

The decision to follow one of these methods will have to be made based on local considerations governed primarily by economic aspects.

CHAPTER 1: INTRODUCTION

A satisfactory method of pavement design should incorporate distresses crucial to the performance of the pavement during its lifetime. Each significant pavement distress contributes to the failure of the pavement. Since the failure of a pavement is functional in nature, the additive nature of damage from each pavement distress needs to be considered in the design process. The incorporation of distresses in the design process involves the use of models to predict the distress magnitudes at any point during the life of the pavement. The trend in pavement design has been to develop pavement distress prediction models based primarily on empirical means. In many instances, models have been developed using data from pavement distress databases. The governing factors in these models were identified primarily by empirical means. These models often disregard the significant effect imposed on the pavement performance by local conditions. Some dependence of empiricism is inevitable in pavement design due to the variable nature of the pavement and related factors. However, satisfactory pavement distress prediction models can be developed by having this inevitable empiricism revolve around a sound understanding of the pavement distress mechanisms. Therefore, as a precursor to successful pavement distress model development, sufficient time and effort should be used to fully understand the mechanisms of pavement distress development.

Spalling is a distress in Portland cement concrete pavements where a visible surface distress is caused by pieces of concrete getting dislodged from the surface of the pavement. Fig. 1 illustrates a typical spall in a concrete pavement. Spalling primarily occurs at transverse cracks or joints in a concrete pavement. It is a form of distress which is common to both continuously reinforced concrete pavements (CRCP) and jointed concrete pavements (JCP). Spalling results in a rough ride, and it also gives the traveling public a negative perception of the integrity of the pavement. From a technical standpoint, loss of concrete due to spalling may lower the load transfer efficiency across the transverse random cracks (in CRCP) or joints (in JCP). A reduction in load transfer efficiency will increase the stress level due to traffic loading in the pavement and will

eventually lead to more severe forms of distress such as punchouts in CRCP and joint faulting in JCP.

FIG. 1. Typical Spall in Concrete Pavements

Several researchers have developed spalling models based on empirical means. They have tried to explain the mechanism of spalling as purely age-dependent. These spalling models have not performed particularly well in predicting spalling of known pavements. This is not surprising considering the fact that a comprehensive mechanism of spalling is not incorporated in these models. Some of these models are discussed in the chapter titled *Existing Knowledge Base on Spalling*. This research was directed at achieving a sound understanding of the mechanism of spalling. It has been postulated that freeze-thaw would result in D-cracking in the pavement near the joints and/or cracks, and these durability cracks would eventually result in spalls. Field investigations on spalling, undertaken as a part of this study, have shown that extensive spalling occurs in regions where no appreciable freeze-thaw exists.

A comprehensive investigation of the mechanism of spalling should include several important aspects including field studies, laboratory studies, and analysis methods. A detailed field study was first undertaken in this research to identify factors which

significantly affect the spalling distress. This field study incorporated the investigation of spall development among different pavements, spall development at different locations of a single pavement, and the rate of spall development. Some of the findings of this field study were then applied to several newly constructed pavement test sections for verification and further study.

Results from the field study revealed that several environmental and materials related factors significantly influence the development of spalling. A laboratory test program was conducted to further investigate the effect of the material properties involved. Field test sections were constructed to assess the effect of environmental factors on spalling. The laboratory test program concentrated on both strength and durability related factors. Prior research on spalling indicated a strong influence of the aggregate type on spalling. Also, evidence of damage very early in the life of the pavement was observed. Therefore, particular attention was given to the investigation of early-age properties of Portland cement concrete. These laboratory results provided data on the strength of Portland cement concrete with different types of coarse aggregates, aggregate treatments, and curing conditions.

The analysis model was based on the premise that spalling distress is a culmination of damage in the pavement which originates very early in the life of the pavement. Therefore, an attempt was made to analyze pavements at very early ages. Such analyses included the prediction of stresses caused by shrinkage in early-age concrete pavements. These stresses were then compared with the strength of Portland cement concrete at respective ages measured in the laboratory. These analyses revealed that significant stress levels can be developed in pavements at very early ages which may result in damage to the concrete pavements. Such early damage could then act as a precursor to subsequent damage in Portland cement concrete pavements.

It has been suggested in previous research that the formation of spalls occurs due to temperature induced stresses as well as stresses caused by freeze-thaw of the concrete pavement. When temperature in the pavement increases, the concrete expands. Unless there is room for this expansion, stresses will develop in the pavement depending on the level of restraint present for the expansion. In the absence of any restraint, no stresses

will develop, whereas, if there is full restraint which prevents the pavement from expanding, the maximum level of stress will develop. It has been argued that when debris gets deposited in joints and transverse cracks in concrete pavements, the debris acts as a restraint to the expansion of the pavement. For a concrete slab to develop spalls in this manner, either extremely high stresses (at least of the order of 20 mpa) have to develop for sudden failure, or there must be repeated action of stresses lower than the compressive strength, resulting in fatigue failure.

The most important observation from field studies undertaken in this research is that spalling is not just an age-dependent phenomenon. It is believed that de-bonding cracks at the aggregate-cement paste interface occur very early in the life of the pavement which then develop into a continuous flaw (a delamination). Subsequently, with time, these delaminations are developed into spalls due to fatigue damage. Delaminations may be the result of differential shrinkage stresses in the concrete pavement slabs at very early ages. Using the most recently developed techniques in the measurement of pore humidity in early-age concrete, analysis of concrete pavements is performed to investigate if sufficiently high stresses can develop as a result of shrinkage at early-ages.

It has long been established that micro-cracks exist in concrete even prior to the application of load. Most of these micro-cracks have been shown to locate at the interface between the coarse aggregate and the cement paste. It is possible that due to the action of external stresses, stress concentrations occur at the edges of these micro-cracks which eventually lead to a continuous flaw, such as a delamination. These factors indicate that in order to study the delamination and spall development in concrete pavements, it is important to study the properties of the interfacial region between the aggregate particles and the bulk cement paste, and how these interfacial properties change with properties of the concrete and the aggregate. These factors could then be combined with a number of other factors likely to affect the way spalls are developed in concrete pavements. A microscopical investigation of the interfacial region between the aggregate particles and the cement paste in concrete was undertaken to assess some of these concerns.

Once delaminations occur in concrete, its development into a spall can happen due to a number of mechanisms. It is believed that traffic stresses, shrinkage stresses, and thermal stresses contribute to this spalling. Once we understand the mechanisms of delamination and spalling, it is important to find out ways to minimize spalling through the use of improved materials, design methods, construction techniques, and quality control methods. The manner in which the findings of these analyses can be used to incorporate spalling in the design of Portland cement concrete pavements is also addressed.

A framework to incorporate spalling in the design of concrete pavements is proposed at the end of this report. A regression-based spalling prediction model is also presented. It is not feasible to develop a spalling prediction model based on the comprehensive spalling mechanism developed in this research because of limitations with spalling data available in the existing databases. Data needed to develop a comprehensive spalling prediction models are identified for possible incorporation in the development of pavement condition databases in the future.

CHAPTER 2: EXISTING KNOWLEDGE BASE ON SPALLING

Research on spalling in concrete pavements dates as far back as the early 1960s. The earliest research on the subject of spalling centered around the identification of factors affecting spalling and the discussion of possible mechanisms of spalling. These investigations addressed the investigation of both crack spalling and joint spalling. Zollinger and Barenberg (1990) defined crack spalling as "the breakdown of the pavement along the cracks leading to the loss of concrete and the disintegration of the load transfer mechanism." A Roadway Maintenance Evaluation User's Manual developed for the state of Texas (Epps et al. 1974) describes spalling as the breakdown or disintegration of slab edges at joints or cracks or directly over reinforcing steel, usually resulting in the removal of sound concrete. The same manual classifies spalling into three groups according to the number of spalled cracks or joints in the concrete pavement. The three groups are 1-15%, 16-50%, and over 50%.

Spalls are generally categorized by their depth and width. The Texas Pavement Evaluation System (PES) records spalling of CRC pavements in terms of the number of spalled cracks (Texas SDHPT 1985). For a crack to be considered as spalled, it must have spalling a width of 2.5 cm or more and a length of at least 30 cm. Only transverse cracks are considered in this distress manifestation. The pavement distress identification manual of the Strategic Highway Research Program (SHRP 1994) suggests recording of spalling data both numerically (number of spalled cracks/joints and length of cracks/joints spalled) and qualitatively (low, medium, or high severity). The severity of spalling is a measure of the depth, width, and frequency of spalling.

FIELD OBSERVATIONS

A study commissioned by the National Cooperative Highway Research Program (NCHRP 1979) categorized spalling into two groups, namely, minor and severe. Minor (or slight) spalling was observed in this study along most cracks in CRC pavements. It

was often attributed to the surface widening of cracks resulting from a fracturing of the mortar in the concrete pavement surface along the crack face. It was believed that such spalling consists of flaking of the mortar in the concrete mix on either side of the crack. Minor spalling was observed to remain stable, and it was not considered as a progressive form of deterioration or of any structural consequence.

Guitierrez de Velasco and McCullough (1981) indicated that severe spalling is usually produced as a result of construction operations. They also suggested that spalling is influenced by traffic, pavement age, and location along the transverse crack (distance from the pavement edge). McCullough et al. (1979) identified the primary causes of spalling as follows:

1. Entrapment of road debris in cracks, which may cause a stress concentration under a buildup of compressive force.
2. A combination of shear and tensile stress under wheel load.
3. Poor concrete at the surface due to overworking during the finishing process.

McCullough et al. (1979) also noted that even if minor spalling is a stable form of distress, its incidence increases with traffic and age of concrete. They also noted that severe spalling had no correlation to minor spalling or crack spacing; however, it was observed that spalling increased with increasing crack width.

In 1960, Shelby and McCullough noted that the coarse aggregate type may have some influence on spalling. Later in 1979, McCullough et al. noted that concrete made with limestone coarse aggregate showed less spalling than concrete with siliceous gravel coarse aggregate. They attributed this difference in performance to lower modulus of elasticity, higher concrete strength, and better bonding characteristics of the limestone concrete. McCullough et al. (1975) noted spalling as discontinuities that develop during the process of crack propagation as the forming crack takes the path of least resistance. In a related study (NCHRP 1979), it was noted that deeper spalls are generally related to structural weakness, while shallow and wide spalls are related to weakened horizontal planes in the surface of the concrete. It was also suggested that spalling can develop as a result of stress concentrations induced mechanically by load and deflection of pavement under traffic. Based on results from finite element analysis, Tayabji and Colley (1986)

showed that spalling may result from incompressible material lodged in the cracks under expansive strains during temperature increases. They indicated that restraint to volume change from temperature variation through the slab depth can cause spalling due to stresses caused by adjacent slabs butting together. Wright (1981) suggested that the use of a joint filler would retard the development of crack spalling by inhibiting edge raveling, admission of incompressible material, and corrosion of reinforcement.

With regard to the location of spalls along transverse cracks and/or joints, a study in Minnesota (Tracy 1978) noted from two projects that spalls generally occurred in the wheel path region. In the same study, it was noted that a majority of spalls which extended to the reinforcement were caused by chloride induced corrosion of the reinforcement. However, Zollinger and Barenberg (1990) indicated that spalling over reinforcement is not considered a widespread problem in CRC pavements.

Zollinger and Barenberg (1990) also reported results from an extensive analysis of CRC pavements for bending stresses. They reported that the loss of bending stiffness at the transverse crack is related to spalling in CRC pavements. Their analysis indicated that considerable stresses, both shear and normal, are created at the face of the transverse crack with the potential for spalls to be developed. Since the crack width and the depth to reinforcement influence the stiffness of the concrete, they indicated that, consequently, these variables will also influence the spall stresses. In addition, they also reported that the pavement support condition also significantly affects the spall stresses.

A number of studies on spalling have also been conducted for jointed concrete pavements. Smith et al. (1990) analyzed spalling data from the Michigan Road Test and made the following observations:

1. Incompressible material in the joints is the major cause of spalling, and it appears that preformed sealants are capable of keeping incompressible material from infiltrating the joints for a significant period of time.
2. There is a dramatic effect of D-cracking on joint spalling.

More observations were made from the results of the analysis of the Long Term Pavement Performance (LTPP) database for spalling in jointed pavements. Results from

such analyses were revealed in a report published by the SHRP (SHRP 1994) and included the following:

1. Joint seal type has been found to significantly influence spalling in some studies, but in others, its influence has been found to be insignificant.
2. A high number of freeze-thaw cycles will tend to increase spalling in jointed plain concrete pavements.

MODELING OF SPALLING

Available literature on spalling indicates attempts to model it as a function of age. One such model developed for JCP is the PEARDARP model (van Wijk 1985, Kopperman 1986) shown in Eq. 1.

$$F_S = 1 - e^{-\alpha(J - 8)} \tag{1}$$

where F_s = fraction of joints spalled; $\alpha = 0.0000162\, A^{3.0806}$; J = transverse joint spacing in feet; and A = age of pavement in years.

Smith et al. (1990) found that the PEARDARP model is unable to predict spalling satisfactorily and that it tended to over predict transverse joint spalling for spalling data from every environmental region in the database. Their studies further showed that, in general, spalling was observed on pavements of all ages and with different joint spacing. They noted spalling in pavements where material problems such as non-durable aggregates under harsh climates existed, or the dowel bars had corroded or locked up the joints. Based on the analysis of spalling data from the Michigan Road Test, Smith et al. (1990) proposed the spall models given by Eqs. 2 and 3 for jointed plain concrete pavements (JPCP) and jointed reinforced concrete pavements (JRCP), respectively.

$$JTSPALL = AGE^{2.178}(0.0221 + 0.5494\ DCRACK - 0.0135\ LIQSEAL - 0.0419\ PREFSEAL + 0.0000362\ FI) \quad (2)$$

$$JTSPALL = AGE^{4.1232}\ (0.00024 + 2.69E\text{-}05\ DCRACK + 3.07E\text{-}04\ REACTAGG - 3.3E\text{-}05\ LIQSEAL - 0.0003\ PREFSEAL + 1.4E\text{-}07\ FI) \quad (3)$$

where *JTSPALL* = number of medium-high severity joint spalls per mile; *AGE* = age of pavement since original construction in years; *DCRACK* = 0, if no D-cracking exists, and 1, if D-cracking exists; *LIQSEAL* = 0, if no liquid sealant exists in the joint, and 1, if liquid sealant exists in joint; *PREFSEAL* = 0, if no preformed compression seal exists, and 1, if a preformed compression seal exists; *FI* = freezing index in degree days below freezing; and *REACTAGG* = 0, if no reactive aggregate exists, and 1, if reactive aggregate exists. The model for JPCP (Eq. 2) had a coefficient of determination (R^2) of 0.59 and a standard error of estimate (SEE) of 9 joints per km. The model for JRCP (Eq. 3) had an R^2 of 0.47 and a SEE of 8 joints per km.

Results from sensitivity analysis of selected pavement distresses (SHRP 1994) indicate two more spalling prediction models for jointed concrete pavements. Based on statistical analysis using a number of candidate variables likely to affect spalling, the models shown by Eqs. 4 and 5 were developed for JPCP and JRCP, respectively.

$$SPALLJP = 9.79 + 10.09\ [-1.227 + 0.0022\ (\ 0.9853\ AGE + 0.1709\ FT\ )^2] \quad (4)$$

$$SPALLJR = -79.0 + 0.604\ (\ AGE\ )^{1.5} + 0.129\ (TRANGE)^{1.5} \quad (5)$$

where *SPALLJP* = predicted mean percentage of transverse joint spalling (all severities) as a percentage of total joints for JPCP; *SPALLJR* = predicted mean percentage of transverse joint spalling (all severities) as a percentage of total joints for JRCP; *TRANGE* = mean monthly temperature range (mean maximum daily temperature minus mean minimum daily temperature for each month over a year); *FT* = number of mean annual air freeze-thaw cycles; and *AGE* = age since construction (in years).

For JPCP, 56 survey sections were used in the analysis, with a model R^2 of 0.335 and a root mean square error (RMSE) of 11.05% joints. For JRCP, 25 survey sections were used in the analysis, with a model R^2 of 0.644 and a RMSE of 16.06% joints. Significant differences between the actual data and predictions were observed in both these models.

RESULTS FROM OTHER STUDIES ON SPALLING DATA ANALYSIS

Dossey and Hudson (1993) analyzed spalling data from the Texas concrete pavement database. This spalling database contained minor and severe spalling for each pavement section surveyed. Minor spalling was defined in the database as "edge cracking where the loss of material has formed a spall of one half inch wide or less" (Dossey and Weissmann 1989). All other spalling was considered as severe spalling. Since minor spalling as defined is not likely to be considered, only severe spalling from the database was considered in the analysis. The survey sections included in the database have information such as pavement thickness, coarse aggregate type in concrete, subbase treatment, type of subgrade soil (likelihood of swelling/shrinkage), yearly temperature range, average annual rainfall, and the estimated average daily traffic and its projected rate of growth. Preliminary analysis of spalling data by Dossey and Hudson (1993) using the Texas Rigid Pavement Database indicated the following:

1. 85 percent of survey sections were more than five years old at the time of first survey.
2. 72 percent of survey sections displayed no spalling whatsoever.
3. An analysis of variance was performed to determine the factors which had the most significant influence on the level of spalling. Only the two-way interactions between each factor and age of pavement were considered. The

following factors and interactions were found to be excellent predictors of spalling in descending order of significance:

a. interaction between age and coarse aggregate type.
b. interaction between age and rainfall.
c. age itself.
d. interaction between age and subbase type/treatment.

Previous studies on spalling, as identified above, have identified some factors which may influence spalling. However, these factors have not been verified using either laboratory or field studies in any of these studies. This research included verification of such factors as well as identification of other factors that influence spalling.

CHAPTER 3: FIELD STUDY OF CONCRETE PAVEMENTS

INTRODUCTION

In the previous section of this report, the existing knowledge based on spalling was presented. A number of studies on spalling identified several factors which appeared to affect spalling. None of the studies mentioned in the previous chapter made any attempt to address the spalling distress from a mechanistic standpoint. The spalling prediction models presented in the previous chapter were regression-based models obtained using parameters which displayed the best correlation with spalling data. Also, those spalling prediction models did not have satisfactory statistical predictors that one might expect to have for these models to be used with confidence in pavements from different geographical regions with a wide variety of environmental conditions. Therefore, before embarking on the development of a prediction model for spalling, it was decided to undertake a detailed field study of concrete pavements within the state of Texas with the idea of coming up with a sound mechanism for spalling.

In this field study, two types of pavement sections were studied. These were the pavement survey sections and pavement test sections. First of all, several pavement survey sections were identified from existing concrete pavements within the state of Texas. Pavement sections both with and without the spalling distress were identified as survey sections. These survey sections were scrutinized with regard to their construction history, spalling history, and the traffic history. These studies highlighted some factors which were believed to significantly influence spalling. Some of the findings from these survey sections were then applied to two pavement test sections which were constructed under the auspices of this research study. Therefore, it was possible to monitor the spalling distress development in these test sections from an early age. Since all the construction conditions were known for these test sections, they could be related to the development pattern of spalling. All pavement sections in this field study were CRC pavements.

In addition to the study of pavement survey and test sections, a preliminary analysis of existing spalling data obtained from the Texas rigid pavement database was performed as a means of verifying the findings from the field survey. The Texas rigid pavement database consists of a large number of CRC pavement sections from throughout the state. Another objective of such an analysis was to narrow down the factors to be investigated later in the laboratory testing phase of this research.

FIELD SURVEY SECTIONS

Selection of Survey Sections and Performance of Field Surveys

As a part of this field investigation, several CRC pavement survey sections within the state of Texas were selected for investigation. In order to select these survey sections, a statewide telephone survey was conducted among the district maintenance engineers of the Texas DOT to find out their experiences with regard to spalling of concrete pavements. Some districts were not contacted based on the assumption that they did not have significant lengths of concrete pavements under their jurisdiction. Information obtained from this telephone survey is summarized in Table 1. Based on the results of this telephone survey, pavement sections identified in Table 2 were selected from different parts of the state. Factors such as the locality of the pavement section (urban or rural), type of coarse aggregate used in concrete, pavement thickness, and pavement age were incorporated in this selection. The field survey of the selected pavement sections included visual surveys, video recording of concrete pavement sections, and coring. Later, the cores were subjected to a microscopical examination in the laboratory. Equipment and personnel for these activities were provided by the Texas Department of Transportation (TxDOT). Video recordings were obtained from some of these survey sections. The ARAN (Automatic Road Analyzer) truck of the TxDOT was used for this purpose.

TABLE 1. Summary of Telephone Survey Among District Maintenance Engineers of the Texas Department of Transportation (TxDOT)

District	City	Remarks
1	Paris	District has approx.105-113 km of JCP and CRCP. Spalling does exist, but it is not a major problem. Spalling occurred very early in life of JCP pavements, whereas CRCP took much longer to spall.
2	Fort Worth	Spalling exists. In one instance, spalling occurred very early in the life of pavement.
3	Wichita Falls	Not contacted
4	Amarillo	Not contacted
5	Lubbock	Not contacted
6	Odessa	Not contacted
7	San Angelo	Not contacted
8	Abilene	Not contacted
9	Waco	District has spalling on IH-35E in Hillsboro.
10	Tyler	IH-20 was constructed with Portland cement concrete (PCC), but it is now overlaid with HMAC. They have had a lot of problems with punchouts, but very little spalling was observed.
11	Lufkin	Not contacted
12	Houston	There are a number of sections which have spalled. They are Beltway 8 near Bellaire street, IH-610 west loop, and IH-10 westbound just before entering the downtown area between mileposts 760-770.
13	Yoakum	There are PCC pavement sections of IH-10 and US-59 with servicing concrete pavements. Spalling has been a problem particularly in US-59. Punchouts have been a major problem in the IH-10 section in Gonzales county.

TABLE 1. (Continued)

District	City	Remarks
14	Austin	Not contacted
15	San Antonio	District has only about 16 km of servicing concrete pavements, and spalling is not a problem.
16	Corpus Christi	District has only about 16 km of servicing concrete pavements, and spalling is not a problem.
17	Bryan	District has two major CRCP sections, one in SH-6 bypass in Bryan/College Station (21 km) and another in IH-45 in Buffalo (27 km). SH-6 section is heavily spalled but the IH-45 section is not.
18	Dallas	District has lots of spalling in its concrete pavements. However, no study has been done at district level.
19	Atlanta	Not contacted
20	Beaumont	District has spalling in IH-10 (JCP & CRCP).
21	Pharr	Not contacted
23	Brownwood	Not contacted
24	El Paso	District has approx. 32 km of CRCP in service. Spalling is not a major problem.
25	Childress	Not contacted

Cores were obtained from the two survey sections (SH-6 in Bryan/College Station and BW-8 in Houston) and from both test sections (SH-225 in La Porte and US-290 in Cypress). Cores were taken either adjacent to or on the transverse cracks at spalled locations. When the observations from these cores were recorded, a distinction was made among cores taken from the two sides of a crack with reference to the direction of traffic. Fig. 2 indicates the positions at which most cores were taken by the numbers 1, 2, and 3. According to the notation used, cores 1, 2, and 3 were taken downstream of the crack, upstream of the crack, and on top of the crack, respectively.

TABLE 2. Survey Sections Selected for Field Studies on Spalling

Highway	County/ Closest City	No. of Lanes	Length (km)	Year of Constr-uction	Sub-grade	Coarse Aggregate
SH-6	Brazos County, Bryan/College Station	4	4.8	1972	Clay	Siliceous gravel (calcareous traces)
BW-8	Harris County, Houston	6	12.9	1987	Clay	River gravel
US-59	Wharton County, Wharton	4	9.6	1971-72	Clay	River gravel
IH-10	Harris County, Houston	8	3.2	1971	Clay	River gravel
IH-45	Leon County, Buffalo	4	32.1	1972	Sand	Crushed stone, Siliceous gravel
IH-10	Gonzales County, Gonzales	4	48.3	1970-71	Sand/ Clay	Crushed stone

In addition to the field survey methods mentioned earlier in this chapter, interviews were conducted with the personnel of TxDOT to gain an insight to their experiences with regard to spalling, particularly those who had associated themselves with the selected survey sections. In some cases, we were fortunate enough to interview personnel who were associated with the construction of the pavement sections 10-20 years ago.

Spalling prediction models in existing literature suggest that spalling depends on factors listed below:

1. age of pavement
2. potential for D-cracking in the pavement
3. reactivity of the coarse aggregate

4. freezing index
5. properties of the joint filler material (for jointed pavements)
6. joint spacing (for jointed pavements)

At the beginning of the survey, particular attention was given to the factors indicated above. Initial observations were directed to verify if all or a part of the factors influence spalling in concrete pavements in the state of Texas.

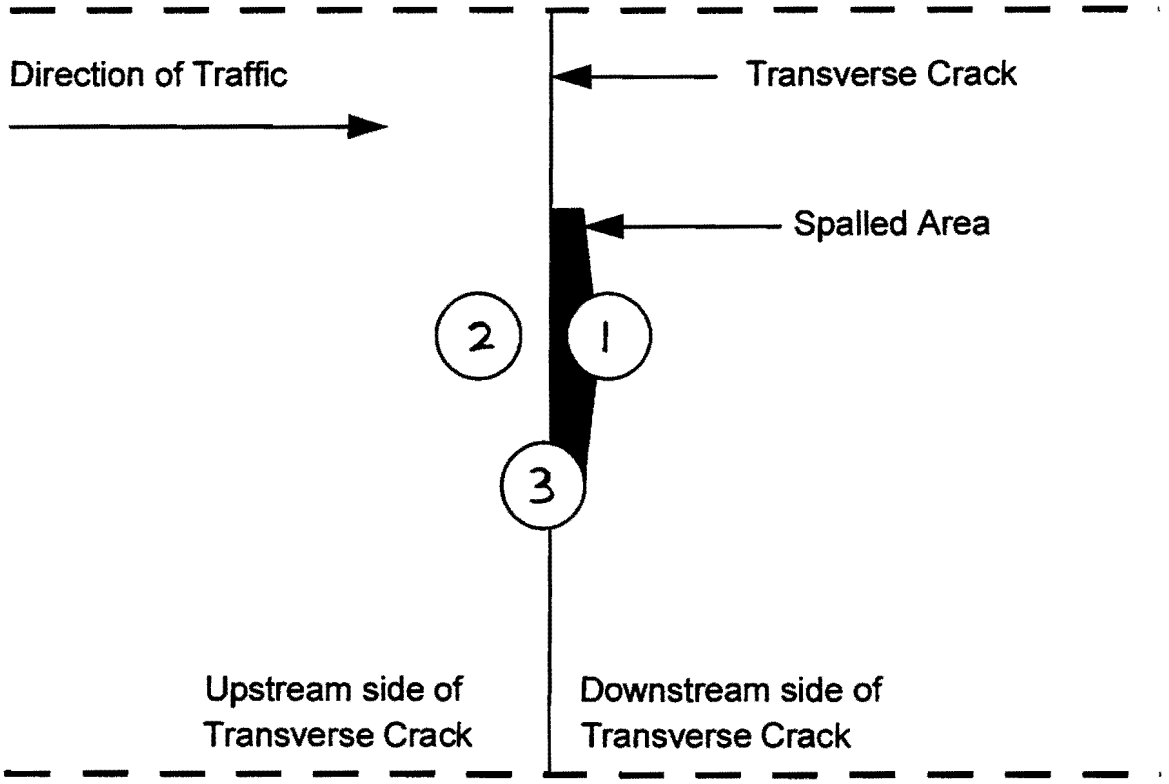

FIG. 2. Schematic Diagram for Coring, Indicating Coring Positions and Notations

Observations from Field Surveys

General Observations

Table 3 summarizes the important observations made from each survey section indicated in Table 2. A detailed compilation of information from the field survey,

including data on field survey sections, results from the petrographic analysis of concrete cores, and general observations from concrete cores, are given in Appendix A.

Engineers from TxDOT associated with the survey sections in BW-8, SH-6, and US-59 indicated that these sections started to spall approximately 12-24 months, 18-24 months, and 5-7 years after construction, respectively. General observations suggest that spalling could be first seen in a pavement as early as 12 months and as late as 7 years. These observations suggest that there are other factors involved in spalling than just age.

TABLE 3. Summary of Observations From Survey Sections

Highway	Survey Method	Modes of Distress	Remarks
SH-6	Visual Survey, Coring	Spalling	Extensive spalling present. There is more spalling in the inside lane. 75% of spalls are downstream of crack. Spalling is predominantly in wheel path. Planes of weakness at a depth of 2.5 cm at most transverse cracks.
BW-8	Video Record, Coring	Spalling	There are isolated areas of extensive spalling, and spalling distributed among all 3 lanes. Concrete cores from pavement showed planes of weakness at 2.5 cm depth.
US-59	Visual Survey	Spalling	Extensive spalling present. More spalling in the inside lane. Most spalls were downstream of crack. Spalling in wheel path.
IH-10 Houston	Video Record	Spalling	Extensive spalling present. Most of the spalling is located in the two inside lanes.
IH-45	Visual Survey	Punchouts	Virtually no spalling.
IH-10 Gonzales	Visual Survey	Punchouts	Virtually no spalling.

It was also interesting to note that most of these survey sections which showed extensive spalling were located in regions where only a very small number of freeze-thaw cycles take place per year. There were also very few, if any, durability problems (D-cracking) seen near transverse joints or cracks of these pavements. This may indicate that neither a high number of freeze-thaw cycles nor the presence of D-cracking would significantly affect spalling. There was ample evidence of spalling along the wheel paths. In SH-6 and US-59 sample sections, most spalls were only seen to occur on the downstream side of the transverse crack. This was quite noticeable in other sample sections as well. In SH-6, US-59, and IH-10 (Houston) sample sections, there was more spalling in the inside lane(s) than in the outside lane(s).

Types of Spalling

Based on this field survey, two types of spalls were identified. They are illustrated in Fig. 3. Type-I spalls are deep spalls which are likely to occur due to a branching of a crack originating from transverse re-bar. This branching most likely occurs due to the positioning of a large aggregate particle in the way of the advancing crack. According to the field survey undertaken as a part of this study, Type-I spalls are not very common. Type-II spalls are relatively shallow spalls where a whole block of concrete adjacent to the transverse crack is removed from the pavement. The maximum depth observed on these spalls was approximately 9 cm. Most of the spalls observed in this field survey were Type-II spalls.

Type-II spalls were observed in two different forms (Fig. 4). The first form is where the spall extends from the transverse crack. The second form of the Type-II spall is where a small flaky piece of concrete close, but not adjacent, to the transverse crack gets dislodged first. A further investigation of this form of the Type-II spall indicated that even though there is a block of concrete still intact between the spalled area and the transverse crack, a failure plane is present underneath that concrete block. Coring done at locations where this form of Type-II spall was observed indicated that there is a fracture surface at a depth of 2 to 4 cm from the surface, and the spalled piece of

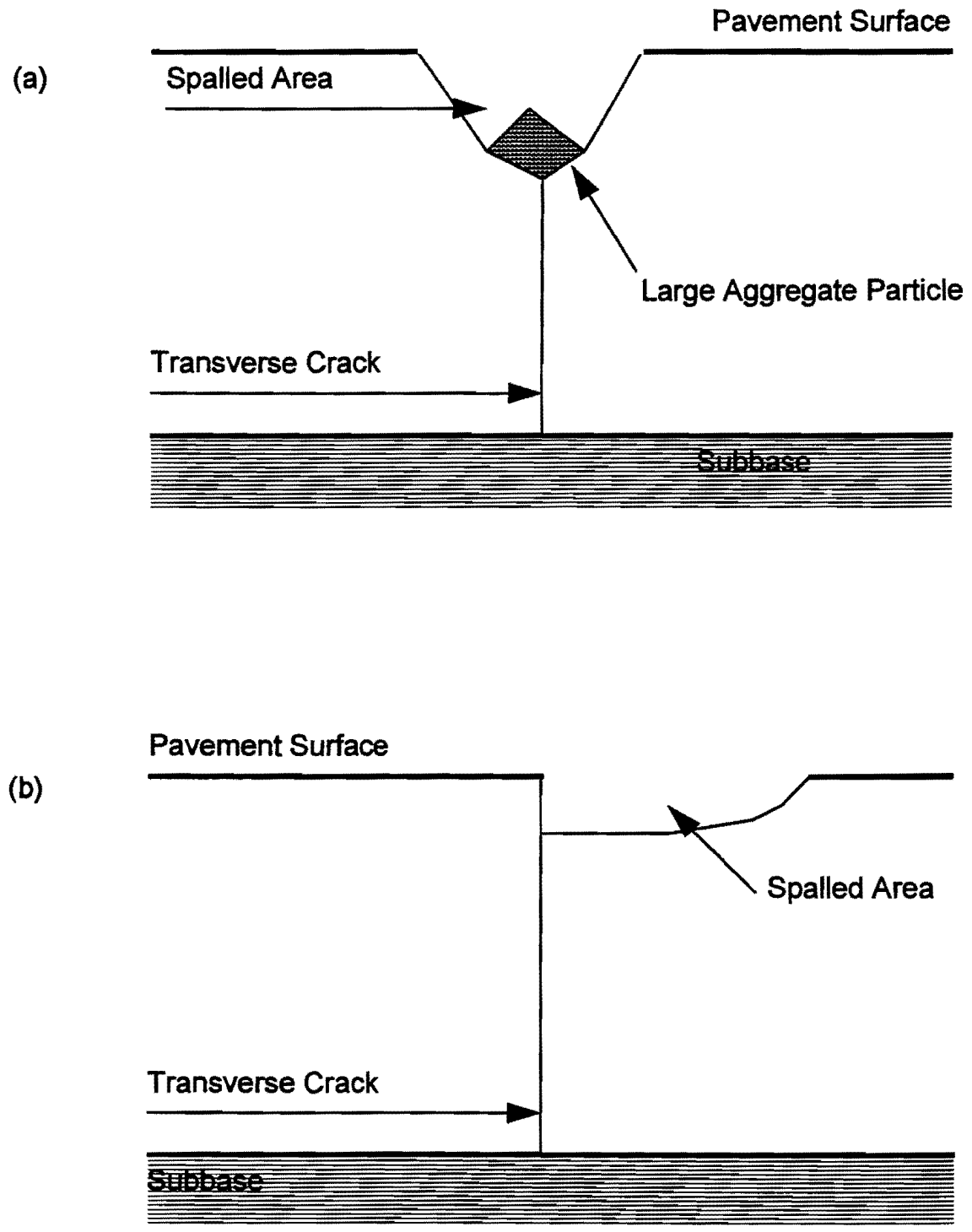

FIG. 3. Types of Spalls (a) Type-I, and (b) Type-II

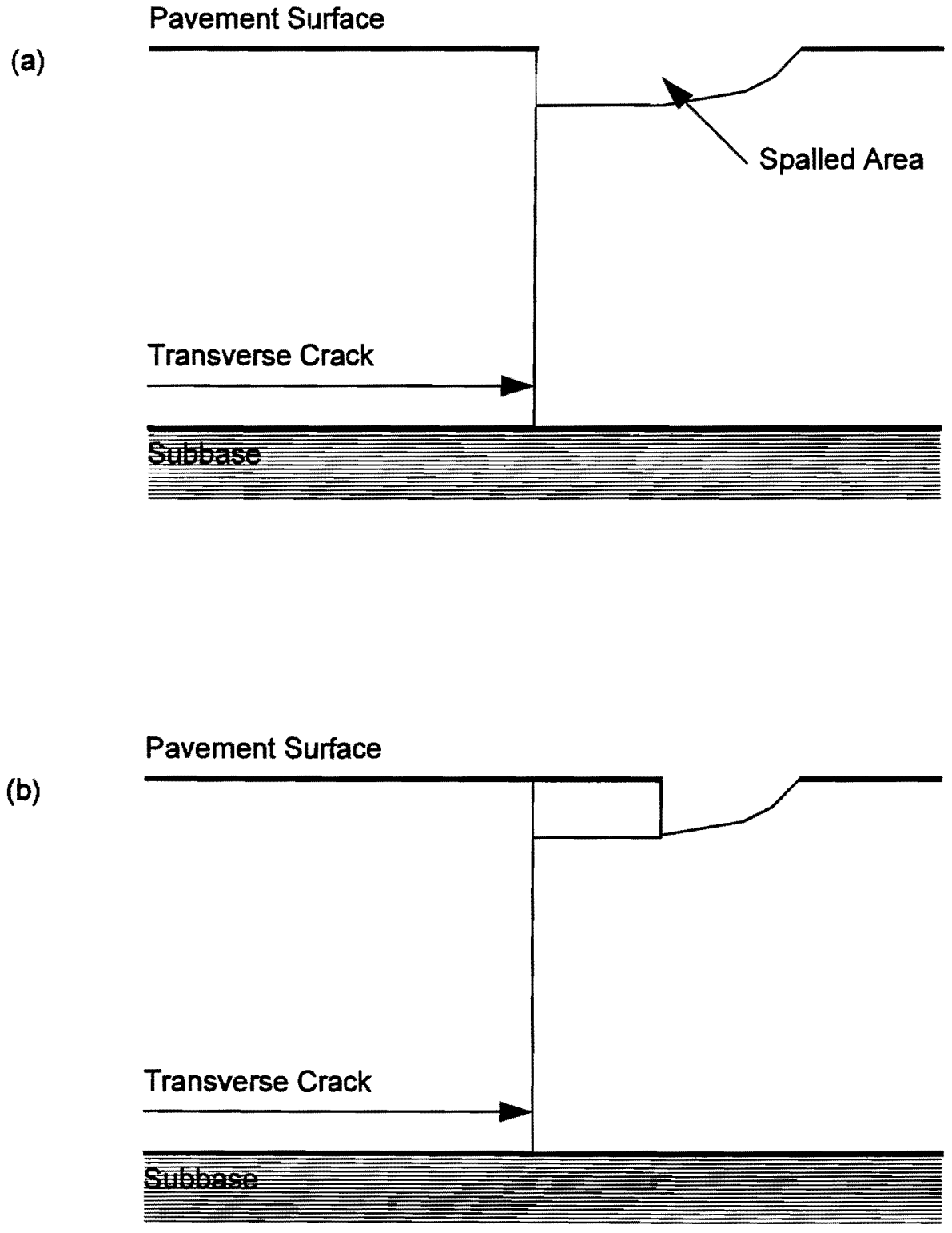

FIG. 4. Two Modes of the Type-II Spall (a) Mode-I, and (b) Mode-II

concrete is actually an extension of this same horizontal crack. Apparently, this crack is originating from the transverse crack.

Spalling Mechanism

During the coring operation, cores were also taken at some transverse cracks which did not show any spalling. In some of these cores, it was observed that at locations where there were no spalls, there were horizontal cracks present very close to the surface. These cracks were almost parallel to the pavement surface, and they appeared to originate at the transverse crack. Fig. 5 shows a photograph of a core taken at the BW-8 survey section. In that photograph, these horizontal cracks are clearly visible at depths of approximately one inch and three inches from the surface.

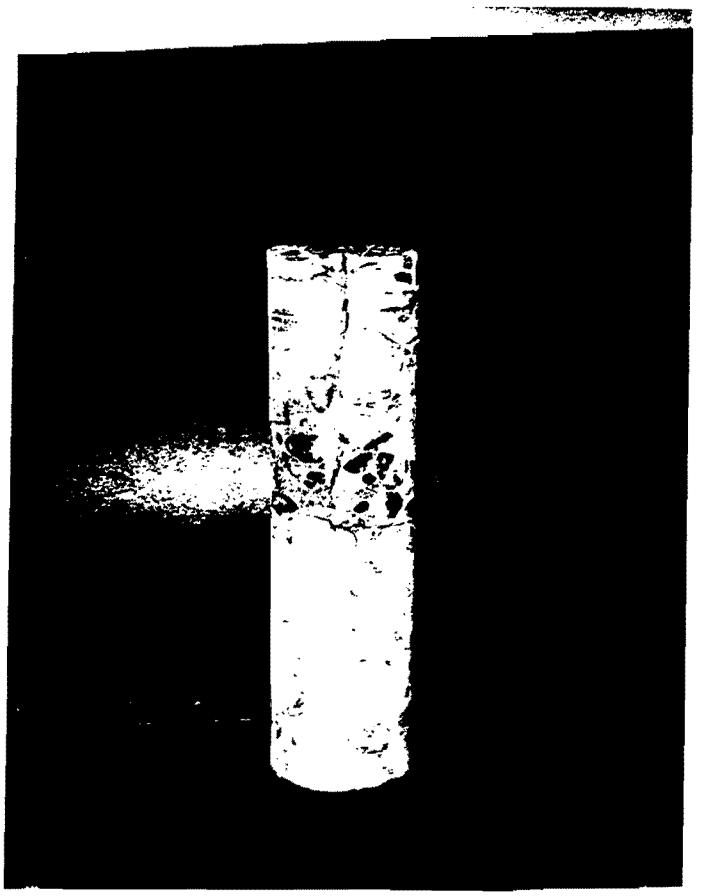

FIG. 5. Concrete Core Taken at a Transverse Crack Indicating Delaminations

Fig. 6 is a schematic diagram showing the location at which this core was obtained. It was quite evident from these observations that these sub-surface flaws (horizontal cracks) act as nuclei for subsequent spalling. Since these sub-surface flaws start horizontally, the term *delamination* seemed appropriate to describe it. Cores taken at the locations of spalls also indicated that these horizontal cracks (delaminations) sometimes extend beyond the spall itself (Fig. 7).

The mechanism of spalling, as it was derived from field surveys, is illustrated in Fig. 8. The first stage in the spalling distress, shown by Fig. 8(a), is the formation of hair line cracks at the interfacial zone between the aggregate particles and the cement paste. In the second stage, shown by Fig. 8(b), the crack faces de-bond due to traffic load and the action of water intrusion forcing the crack to abrade and to widen. The third stage is when these delamination cracks extend to develop into spalls. A delamination crack is propagated until it reaches the pavement surface, and then the piece of concrete between the transverse crack and the delamination is removed, thus showing a visible spalling distress, as shown in Fig. 8(c). The progression from the stage of de-bonding cracks to the stage of spalling may be taking place as a result of stresses due to wheel load, thermal expansion of concrete, and shrinkage.

During the coring of survey sections, it became important to identify the location of delaminations which cannot be seen from the pavement surface by using non-destructive methods. It was noted that delaminations could be detected by dropping a heavy steel bar on the pavement and listening to the sound emanating from the pavement. When the steel bar is dropped on homogeneous solid concrete, it provides a ringing sound, whereas, when it is dropped on a delaminated concrete segment, the sound emanated has a dull tone. Using this simple non-destructive method, also referred to as the *sounding method*, it was possible to identify locations where delaminations were present. In order to verify the accuracy of the steel bar method of detecting delaminations, cores were taken at several locations. The results indicated that the steel bar method is an effective method of detecting delaminations when the delaminations are well developed. Use of this technique

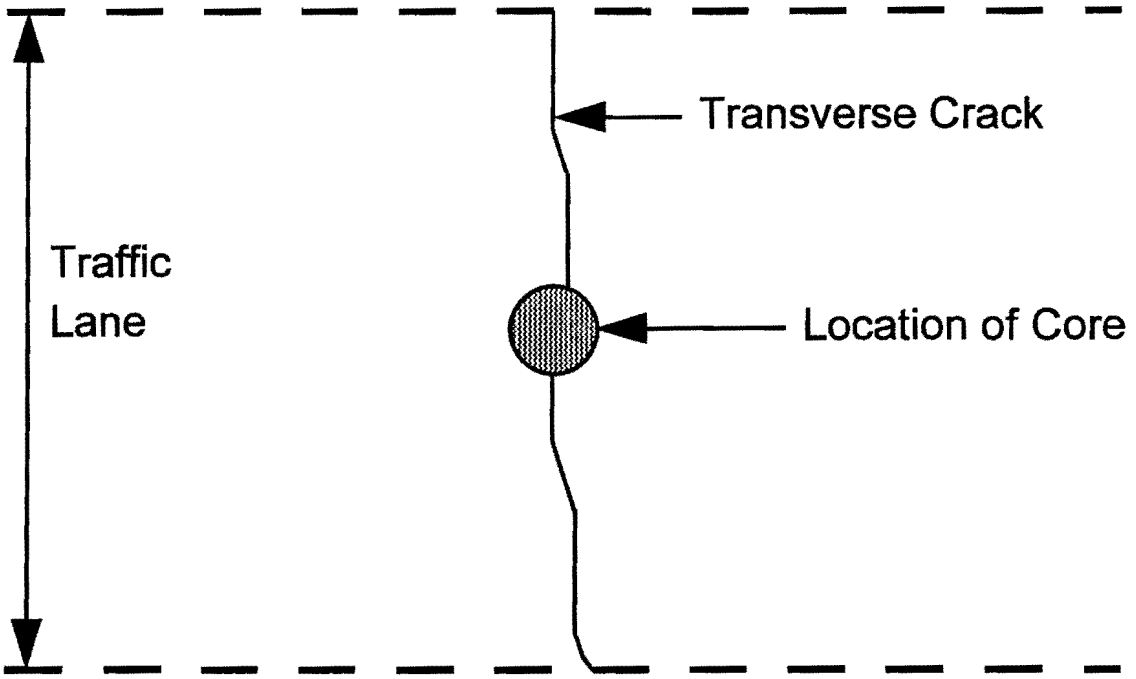

FIG. 6. Schematic Diagram Indicating the Location of the Core Shown in Fig. 5

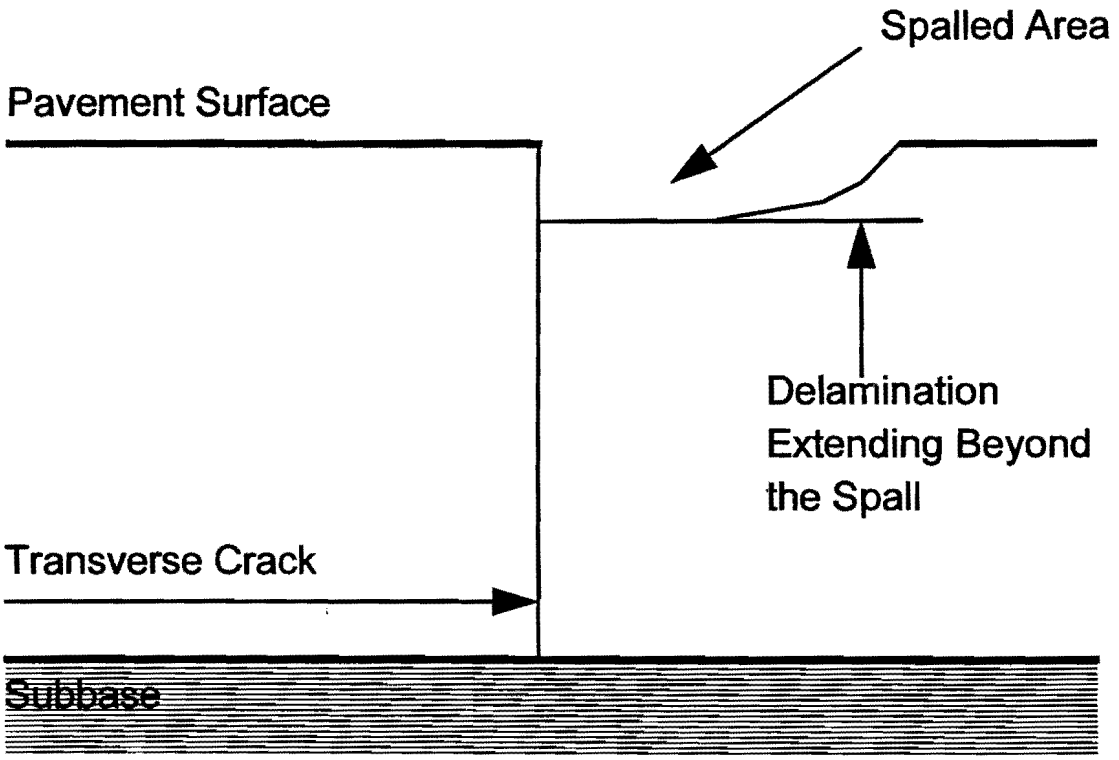

FIG. 7. Type-II Spall With Delamination Extending Beyond the Spall

indicated the following observations:

1. Delaminations are generally present on both lanes.
2. Delaminations occur adjacent to a transverse crack or joint.
3. Delaminations are present on either or both sides of the transverse crack.

Petrographic Analysis of Concrete Cores

Petrographic analysis was performed on concrete cores taken from the SH-6 survey section in Bryan/College Station and from the BW-8 survey section in Houston. Two cores from each test section were subjected to a petrographic analysis, and the results of this analysis are listed in detail in Appendix A. The important observations from the petrographic analysis can be summarized as follows:

1. There is evidence of secondary deposits, such as calcium hydroxide and ettringite along transverse cracks and delaminations.
2. An analysis of the delaminated area indicates that the delamination runs through many interfacial zones between the coarse aggregate particles and the cement paste.
3. In the cores from BW-8 survey section, the bulk of the interfacial fractures occurred at the interface between the weathered brown chert particles and the cement paste. No evidence of alkali-silica reactivity was observed.
4. There were delaminations at several depths in the 33 cm high cores from BW-8. The width of these delamination cracks appeared to reduce with increasing depth. The cores from SH-6 (20 cm high) showed only one delamination at a depth of approximately 2 to 4 cm from the pavement surface.
5. The degree of cement hydration along the transverse cracks and delaminations seemed to be much lower than for the rest of the cement matrix.

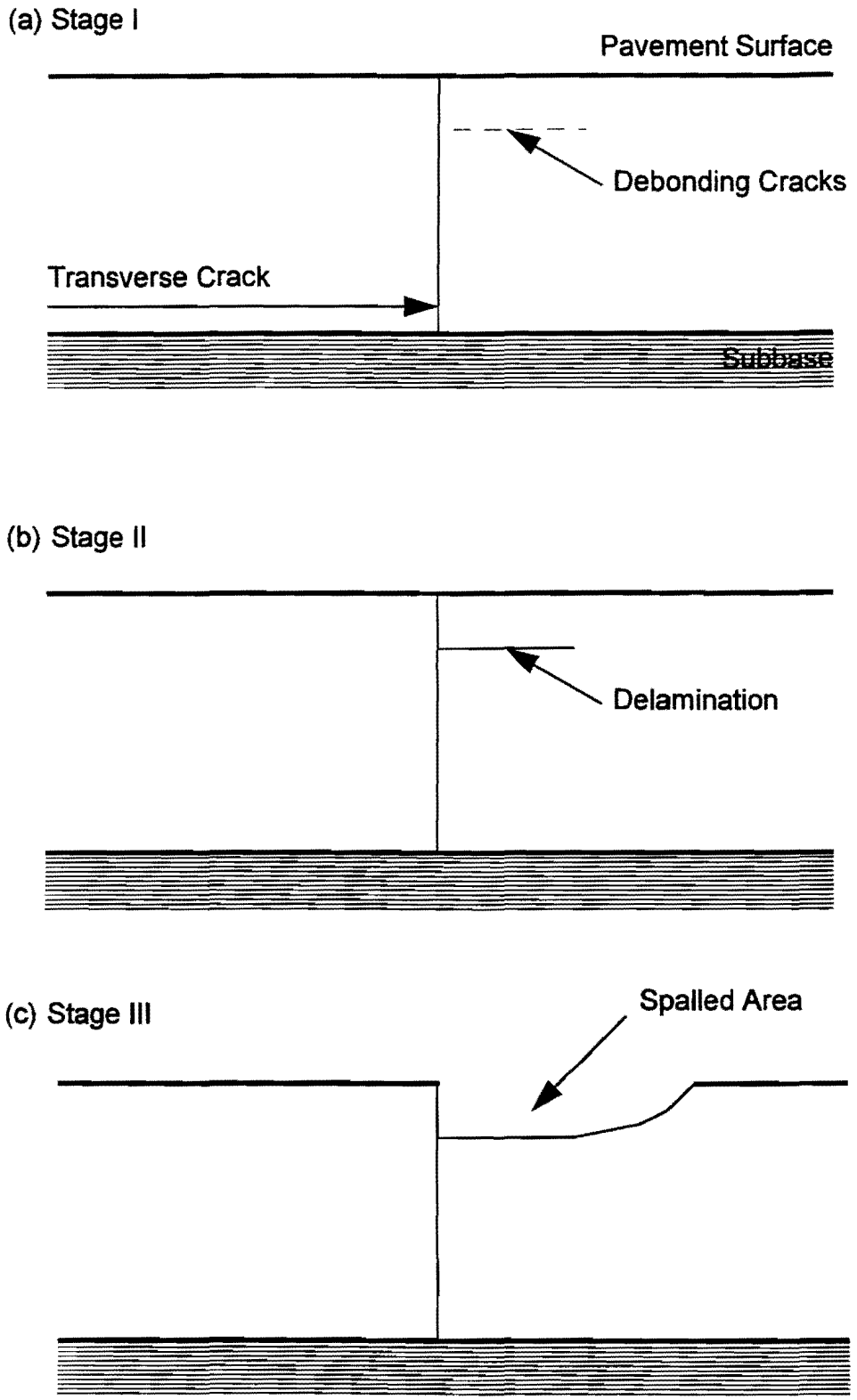

FIG. 8. Stages of Spall Development (a) De-Bonding Cracks at the Aggregate-Paste Interface, (b) Delamination, and (c) Spalling

Since the degree of hydration at the delamination and transverse crack faces was observed to be much lower when compared with the rest of the cement matrix, it may be an indication that both the delaminations and the transverse cracks occur early in the life of the pavement. In summary, results from the petrographic analysis of concrete cores appear to support the theory that delaminations occur at an early age, along preferential paths at the interfacial region between the aggregate particles and the cement paste, and where highly oriented secondary deposits such as calcium hydroxide are present.

Other Important Observations from Field Surveys

From the field surveys, several key factors affecting spalling in concrete pavements were identified. The field survey included only continuously reinforced concrete pavements (CRCP). However, these same factors are likely to be applicable for jointed concrete pavements as well, since the mechanism of spalling is similar for both types of pavements. The manner in which these factors may affect spalling are discussed below.

Orientation of the Spall

Spalling in concrete pavements may take place on either one or both sides of a transverse crack (Fig. 9). However, some pavement sections showed that spalling may occur predominantly on one side of the transverse crack only. Such observations were noted from SH-6 and US-59 survey sections. Cores taken from these survey sections showed that even if only one side of the crack showed spalling, delaminations were nevertheless present on both sides of the crack. An interesting feature in the SH-6 sample section was that more than 75% of the pavement section was spalled on the downstream side of the transverse crack (in the direction of traffic flow), and the rest of the section was spalled on the upstream side (Fig. 10). Discussions with TxDOT personnel involved with the construction of this project indicated that this reversal in spall orientation occurred near a place where the concrete mixing plant was located during construction. It was also believed that the location of the concrete plant resulted

in a reversal in the paving direction. If this is accurate, in the SH-6 pavement section, spalls are always positioned downstream of the crack in the direction of paving. Based on this, it can be speculated that the formation of delaminations may be influenced by the direction of paving.

Restraint to shrinkage may be one of the factors governing this phenomenon. Shrinkage of concrete in the longitudinal direction causes the pavement to crack in the transverse direction. When shrinkage strains occur, the level of restraint would dictate the magnitude of stresses created in the concrete. When concrete is paved from one end to the other, and when shrinkage strains occur, the older concrete would gain more strength and hence would offer a higher level of restraint compared to the more recently placed concrete. Since there would be a difference in the level of restraint at the two ends of the pavement section, one end is likely to create a longer delamination due to the higher level of restraint. It is quite possible that this sequence of events may create delaminations with different lengths on either side of the crack (Fig. 11). Fracture mechanics principles show that the likelihood of longer cracks propagating is much higher than for shorter cracks. This may be a reason why, in some pavements, only one side of the crack would spall. Verification of this phenomenon was not possible during this research because the data on paving direction was not available for all survey sections.

Uneven Distribution of Spalls Between Lanes

Sample sections on SH-6, US-59, and IH-10 (Houston) showed evidence of more spalling on the inside lane(s) of the highway (Fig. 12). During the construction of SH-6 and US-59 survey sections, the inside and outside lanes were placed together under the same paving conditions. The only difference between the two lanes is the amount of traffic carried by each lane.

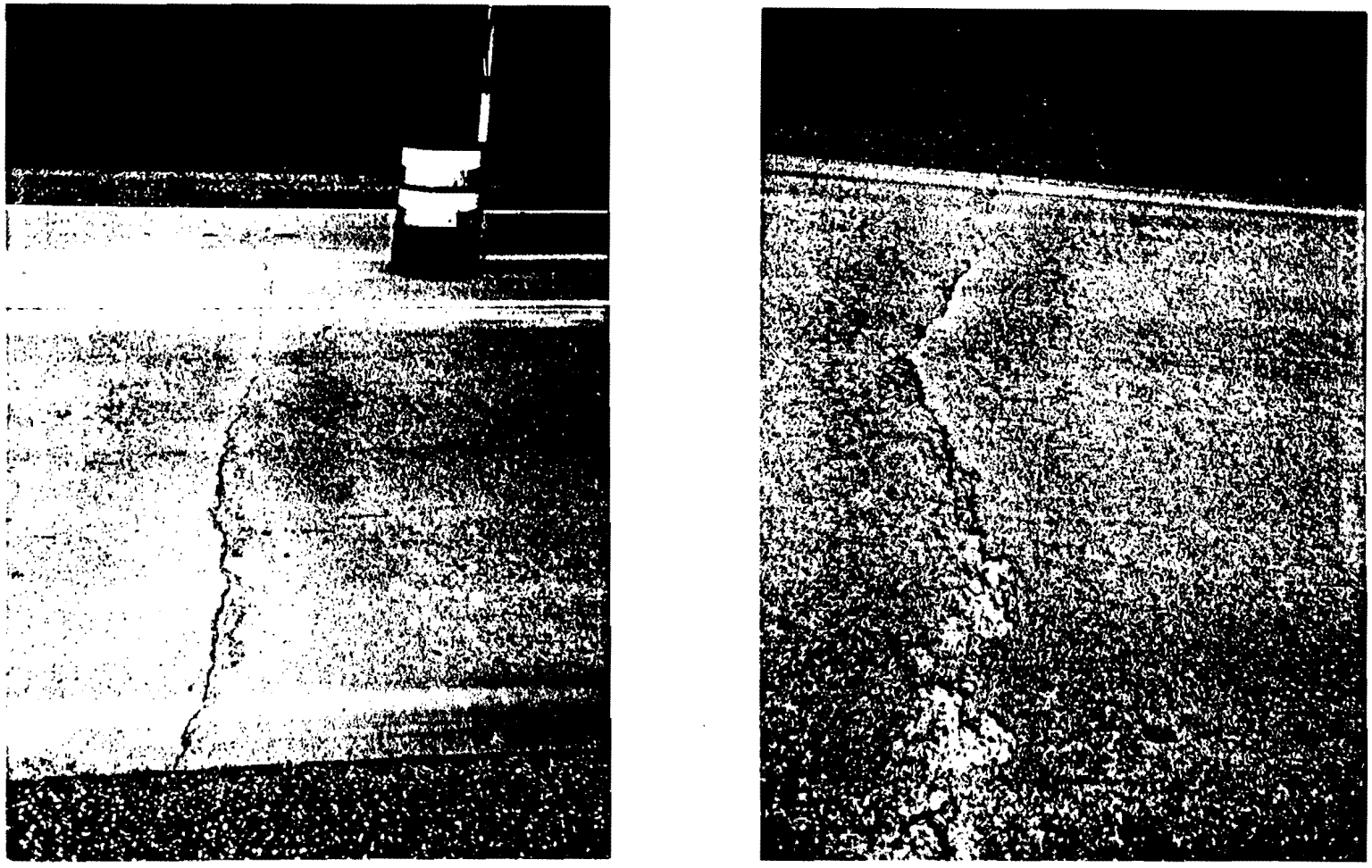

FIG. 9. Orientation of Spalling in SH-6 East Bypass in Bryan/College Station: (a) Spalling Only on Upstream Side of the Crack, and (b) Spalling on Both Sides of the Crack

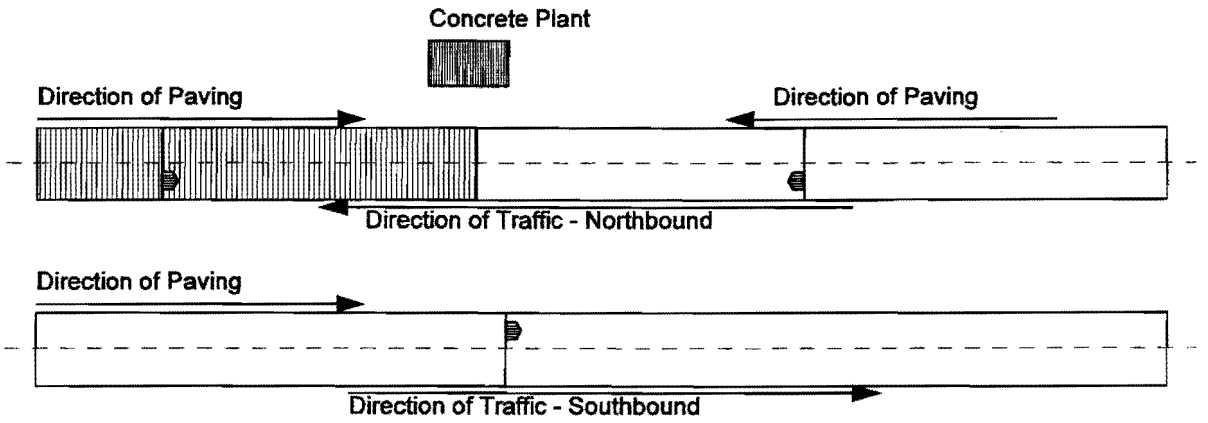

FIG. 10. Schematic Diagram of SH-6 Survey Section Showing Possible Relationship Between Paving Direction and Spall Orientation

Tayabji and Colley (1986) pointed out the important role played by the restraint to pavement expansion at the transverse cracks in generating large enough stresses which may lead to spalling. Zollinger and Barenberg (1990) performed stress analysis and demonstrated that crack width can significantly affect the development of spalling. Observations from the field investigations of this study using the *sounding method* indicated that when a pavement shows signs of spalling, both the inside and outside lanes may be delaminated. Therefore, the differences in the level of spalling between the lanes may suggest a difference in the level of restraint provided at the inside and outside lanes.

This restraint is likely to be affected in two ways. One scenario is when incompressible materials are deposited inside the transverse crack, which result in the generation of compressive stresses when the concrete slab expands. The other scenario is when water is present inside the delaminations, and the friction between the delaminated faces is reduced, thus, reducing the restraint to the movement of concrete above the delamination. This results in increased stress levels at the tip of the delamination. Results from a finite element analysis of a delaminated pavement will be presented in a later chapter illustrating the change in stress level with friction at the delaminated faces.

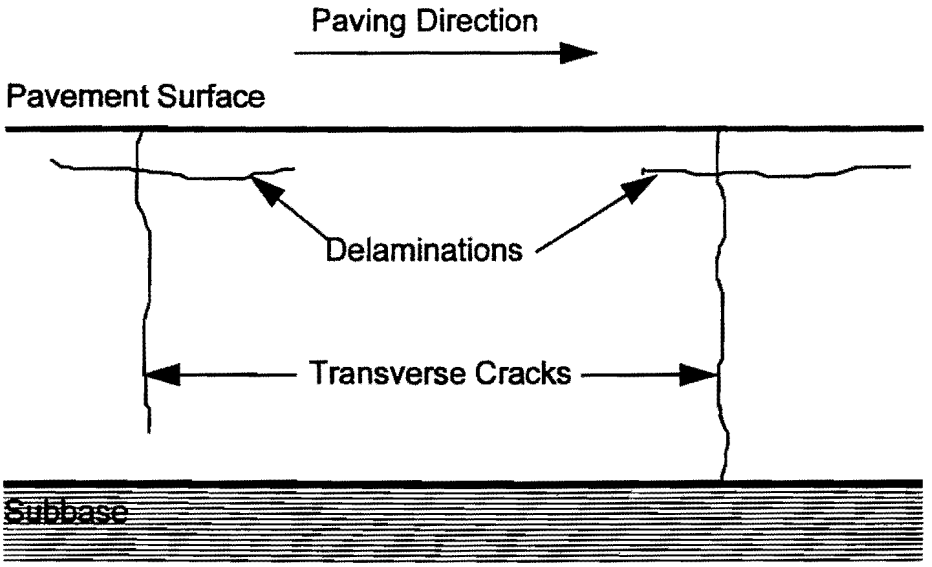

FIG. 11. Illustration of the Effect of Paving Direction on Delamination Length

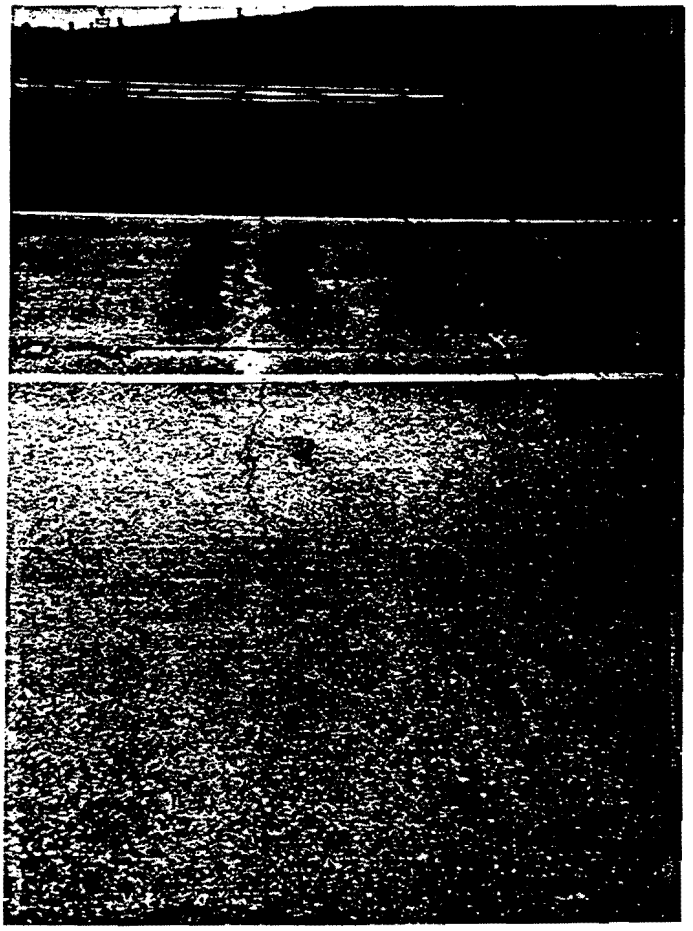

FIG. 12. Uneven Distribution of Spalling Between Inside and Outside Lanes of a 4-Lane Highway

Less spalling in the most traveled lane (outside lane) may be due to the action of the rolling tire during rainstorms, which may remove water and incompressible material entrapped inside the cracks, thus reducing the restraint to expansion. In the same way, there would be more water and incompressible materials left in the cracks or joints of the inside lane(s) causing them to provide more restraint to pavement deformation.

Coarse Aggregate Type in Concrete

Of the six pavement survey sections investigated, four sections had siliceous gravel as coarse aggregate, one had crushed limestone, and the other had a blend of crushed calcareous sandstone and gravel. The two sections which used crushed stone aggregates did not show any significant spalling. They only displayed cracking and punchout distresses. The four survey sections with siliceous gravel as course aggregate showed significant spalling. This evidence may suggest that coarse aggregate type may have a significant influence on spalling. This observation is consistent with previous observations made by Shelby and McCullough (1960) who noted a relationship between the coarse aggregate type and the level of spalling. Later, Guitierrez de Velasco and McCullough (1981) observed that concrete pavements with limestone as coarse aggregate showed less spalling than concrete pavements with siliceous river gravel. Even though coarse aggregates in concrete can be broadly categorized as limestone, siliceous river gravel, granite, sandstone, etc., there is considerable variability in the properties of aggregates within each of these categories. Therefore, it is expected that the tendency for spalling of a concrete pavement with a particular coarse aggregate would depend on the characteristics of the aggregate. A detailed discussion on the characteristics of coarse aggregate which influence spalling will be presented in the chapter titled *Effect of Aggregates on Spalling*.

Factors Related to Pavement Construction

Method of curing and the mix design are two aspects of pavement construction that may have an effect on spalling in concrete pavements. It can be expected that an effective method of curing may result in a decrease in shrinkage stresses, thus reducing the likelihood of delaminations. Mix design parameters such as the cement content, water-cement ratio, and the coarse aggregate content have an influence on the shrinkage of concrete. These mix design parameters will also influence the characteristics of the interfacial zone between the aggregate particles and the cement paste. The concrete mix design and the curing method may be selected in such a way to reduce the shrinkage stresses, but at the same time, to increase the development of strength, particularly at the interface between aggregate and the cement paste. A detailed analysis of the effect of the curing method and the mix design on spalling of concrete pavements is presented in the chapter titled *Delamination of Concrete Pavements.*

Field Test Sections

SH-225 Test Section in La Porte, Texas Fig. 13 indicates the layout of experimental sections within the SH-225 test section in La Porte, Texas. These test sections were located in the two outside lanes in the eastbound direction of the eight-lane highway. This test section was designed to investigate the effect of several parameters on the performance of continuously reinforced concrete pavements. The effect of curing method, rebar placement, and very early-age saw-cutting on cracking and spalling of CRC pavements were observed (Table 4).

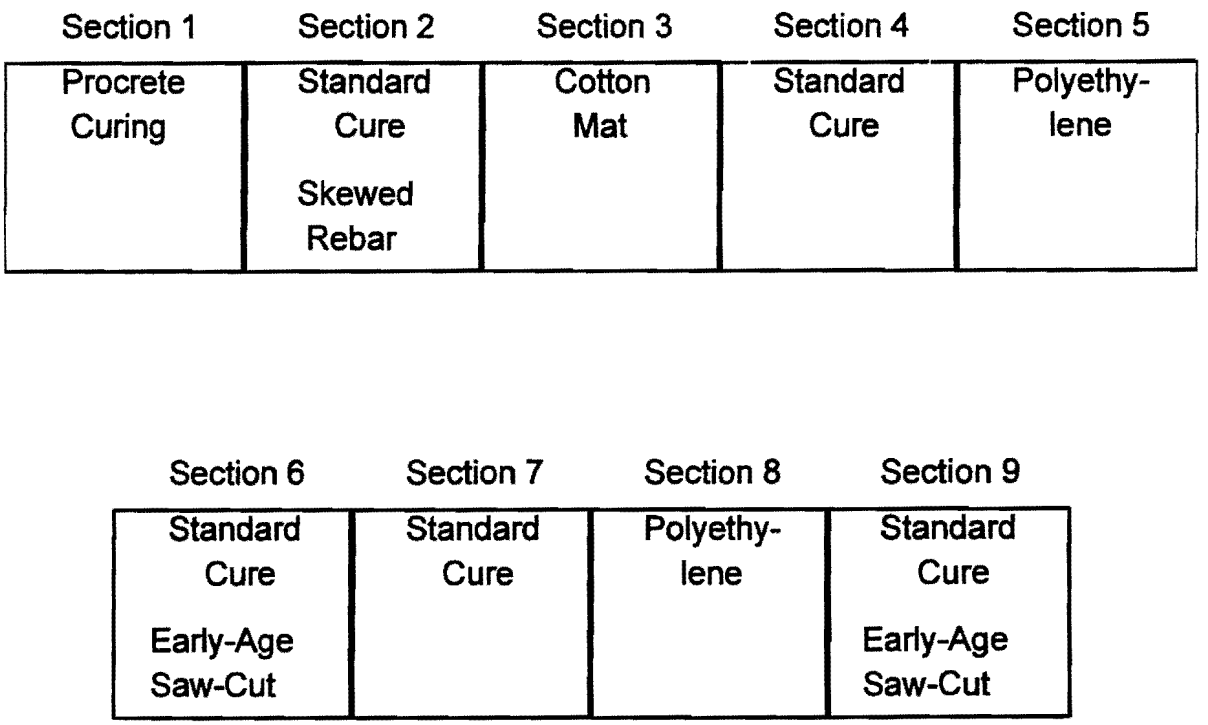

FIG. 13. Layout of Experimental Sections Within SH-225 Test Section in La Porte, Texas

As indicated in Table 4, other than the standard TxDOT curing compound, the effect of three other curing methods were studied. These were procrete compound, cotton mats, and polyethylene sheets. Another important variable considered in this test section was the effect of very early-age saw-cutting of the pavement. This saw-cutting was done as soon as the concrete initially hardened, which was anywhere from 12 to 24 hours after paving, depending on the ambient environmental conditions. The intention of the saw-cutting operation was to force the transverse cracks to initiate at the tips of these notches (Fig. 14). This way, a uniform transverse crack spacing can be achieved. Two saw-cut spacings of 1 to 1½ m were used in this study. The other variable considered was the orientation of the transverse rebar. Both a standard transverse rebar orientation and a skewed rebar orientation (transverse rebar not being perpendicular to the longitudinal rebar) were used.

TABLE 4. Test Factorial in SH-225 Test Section in La Porte, Texas

Parameter	Parameter Value
Method of curing	Procrete
	Standard TxDOT curing compound
	Cotton mat
	Polyethylene sheet
Very early-age transverse saw-cutting	.9 m spacing between saw-cuts
	1.5 m spacing between saw-cuts
	No saw-cuts
Orientation of transverse rebar	regular transverse orientation
	skewed orientation

The main objective of the coring operation in this test section was to see if there were any delaminations being developed in the pavement. This concrete pavement test section was paved on November 11, 1991 and was opened for traffic on December 12, 1991. Coring was performed on September 24, 1992. This made the pavement a little over ten months old and in use for more than nine months at the time of coring.

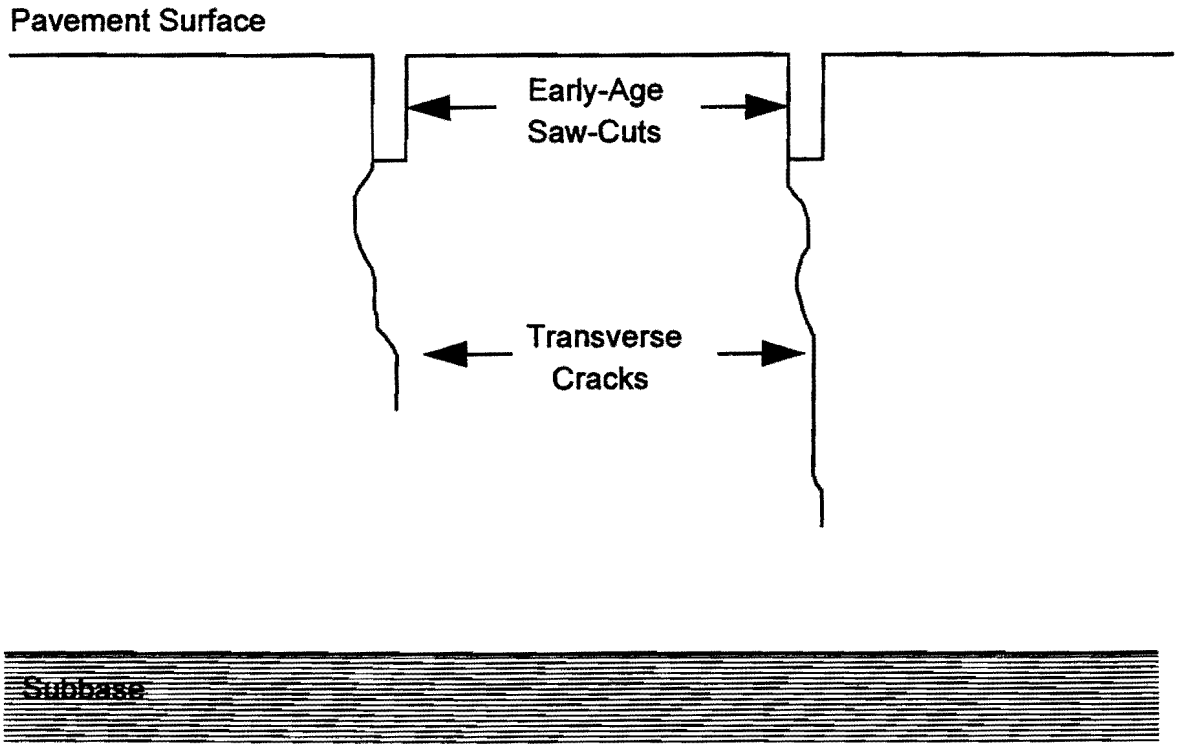

FIG. 14. Illustration of Transverse Cracking Induced by Early-Age Saw-Cutting

Observations from the coring investigation are summarized in Appendix A. Cores taken at the SH-225 test section indicated that there were delaminations present in the slab. Even though these delaminations were not as pronounced as those seen in much older pavements, they were clearly visible. This adds credence to earlier assertions that the process of delamination indeed starts at a very early age in the pavement, even as early as during the first few days after paving.

Cores were taken both along the transverse cracks and transverse saw-cuts. In all cores taken at random transverse cracks, transverse cracks were clearly visible down to level of the bottom rebar layer (10 cm from the bottom of the slab). Fig. 15 illustrates the crack pattern of some typical cores taken at both random transverse cracks as well as at

transverse saw cuts. Some notable observations from the SH-225 La Porte test section are listed below:

1. There were delaminations present near random transverse cracks in sections under all curing methods except polyethylene.
2. There was no indication of delamination in cores taken at the transverse saw-cuts.
3. The delaminations at random transverse cracks occurred during the first ten months of the life of pavement.
4. Minor spalling was already visible, mostly in the wheel paths.

It is important to note that the very early-age saw-cutting seemed to have eliminated delaminations at shallow depths. This is probably related to the discussion on the effect of restraint to concrete shrinkage. Since these saw-cuts are done at a very early age, they may help in releasing some of the strain energy generated due to shrinkage and temperature change in the pavement. This may indicate that adequate restraint is essential to the development of delaminations.

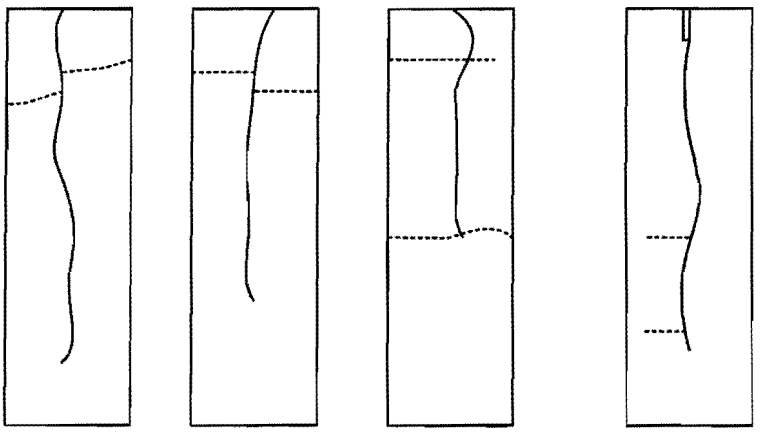

(Random Crack) (Random Crack) (Random Crack) (Saw Cut)

Note: Horizontal and vertical lines indicate delaminations and transverse cracks, respectively.

FIG. 15. Illustration of Cracking and Delaminations in Representative Core Samples From SH-225

US-290 Test Section in Cypress, Texas This test section was constructed in August 1992, and coring was performed in June 1993. At the time of coring, the pavement section was not opened for traffic. The main objectives of this test section were to investigate the effect of aggregate type/blend and the curing method on the behavior of CRC pavements. Table 5 illustrates the test factorial adopted for this test section. Detailed observations from this coring investigation are summarized in Appendix A.

Important observations from cores taken from this test section are listed below:

1. De-bonding cracks at the aggregate-cement paste interface were visible. Since the pavement was not open for traffic, these de-bonding cracks developed prior to the application of vehicle loads.
2. De-bonding cracks were visible in cores from the section with 100% siliceous gravel and a 67% siliceous gravel-33% limestone blend.
3. De-bonding cracks were also visible in sections which had a single coat of the regular curing compound. Sections which had the polyethylene and double application of regular curing compound did not show any de-bonding cracks.

TABLE 5. Test Factorial in US-290 Test Section in Cypress, Texas

Description of Variable	Variable
Method of curing	1 coat of standard TxDOT curing compound
	2 coats of standard TxDOT curing compound
	Polyethylene film
	Water-based curing compound
Coarse aggregate blend	100 % Limestone
	67 % Limestone and 33 % Siliceous gravel
	33 % Limestone and 67 % Siliceous gravel
	100 % Siliceous gravel

Preliminary Analysis of Spalling Data

The Texas Rigid Pavement Database (TRPD) was used to perform the preliminary analysis of data to investigate factors affecting spalling. This preliminary data analysis was performed to verify the effect of factors identified earlier in this chapter. Statistical correlation was performed on a large number of possible factors that may have an effect on spalling.

Texas Rigid Pavement Database (TRPD)

TRPD has hundreds of test sections from all over the state of Texas. The data were collected for a period of more than 20 years on a number of distress types. Also, the inventory of the database includes information on test sections such as location information, construction year and month, concrete slab thickness, type of subgrade, coarse aggregate type in concrete, rainfall, average minimum temperature at test section, estimated traffic data, etc. These data were collected based on a hierarchy indicated by Fig. 16. The Texas Rigid Pavement Database (TRPD) consists of a large number of master sections located around the state. Each of these master sections are selected such that throughout the section there is the same design, construction method, performance, and environmental effects. Each master section is further sub-divided into a number of survey sections each of which is 304 m long. Pavement condition data (in this case, the spalling data) is collected for each survey section so that for each master section, there is a population of data sets. The same concept is illustrated in Fig. 16. In this database, spalling is recorded as the number of spalled transverse cracks within a 304 m long survey section.

Results

A summary of the master sections including their geographical distribution and the maximum level of spalling within the geographical region is outlined in Table 6. The

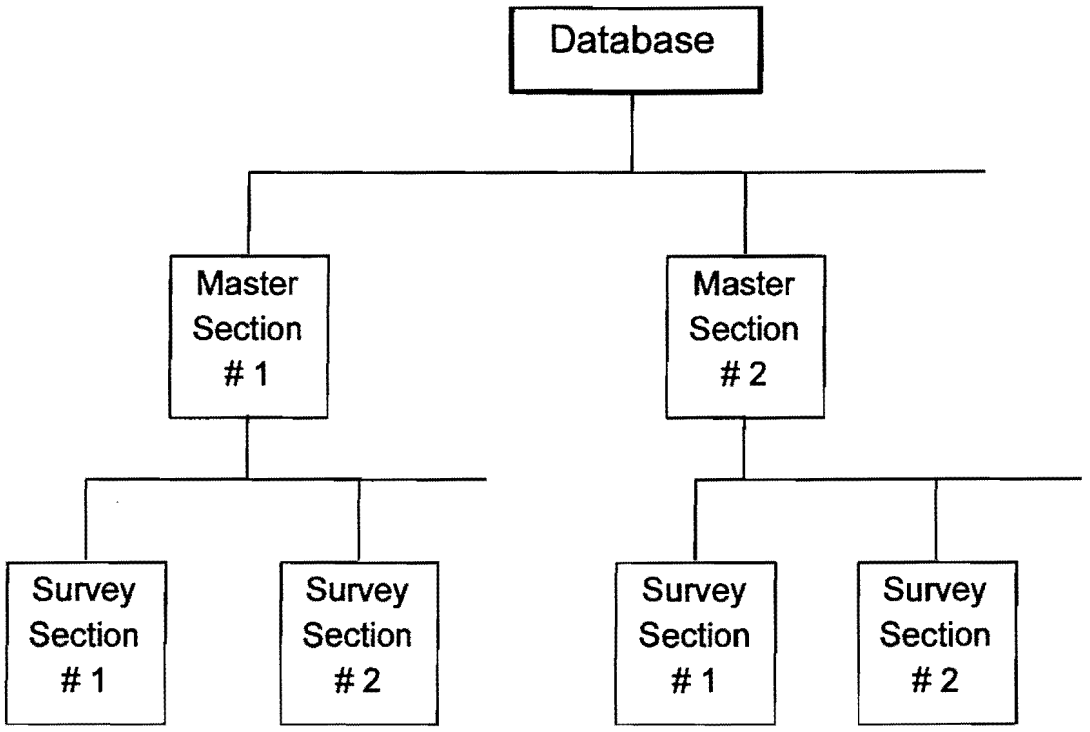

FIG. 16. Data Collection Framework for Texas Rigid Pavement Database

master sections were in service at the time of the condition survey for periods between 1 and 20 years. The distribution of master sections by paving month and coarse aggregate type and the distribution of the number of survey sections by the paving month are presented in Appendix B.

Since it was established that the conditions at the time when the pavement was constructed may be a criterion in the development of delaminations, it was decided to present some of the results of the preliminary analysis by the month of construction. Also, since it was observed earlier that the coarse aggregate type in concrete has some influence in spalling, the same results were also presented with respect to the type of coarse aggregate used in the concrete slab.

The influence the coarse aggregate type has on spalling is evident from Fig. 17 where the number of spalled cracks is averaged for the two most commonly used coarse aggregate types in Texas, siliceous river gravel and crushed limestone. The high degree of spalling in

TABLE 6. Geographical Distribution of Master Sections in Spalling Database

Region	Closest City	Number of Master Sections	Mean Number of Spalled Cracks per 304 m	Max. Number of Spalled Cracks per 304 m
Southeast	Beaumont	13	25.1	126
Southeast	Houston	3	7.7	63
Central	Buffalo	3	2.2	68
Central	Madisonville	1	24.7	128
Central/ North Central	Waco	2	6.9	18
Central/ North Central	Fort Worth	3	2.0	5
Northeast	Marshall	5	13.3	81
Northeast	Paris	2	11.2	57
Northeast	Texarkana	5	50.1	251
Northwest	Lubbock	2	0.1	18
West	Fort Davis	3	0.5	10

pavements with siliceous gravel is evident. The same spalling data is also presented against the month of paving (Fig. 18). There appears to be a definite relationship between the level of spalling and the month of paving, particularly during the summer months. The reason for the very high level of spalling for pavements constructed during the month of November was most likely due to bias in the data since there was only one master section constructed during this month. This one master section has an unusually high level of spalling, most likely related to factors such as mix design, aggregate properties, and curing conditions, which are not recorded in the database.

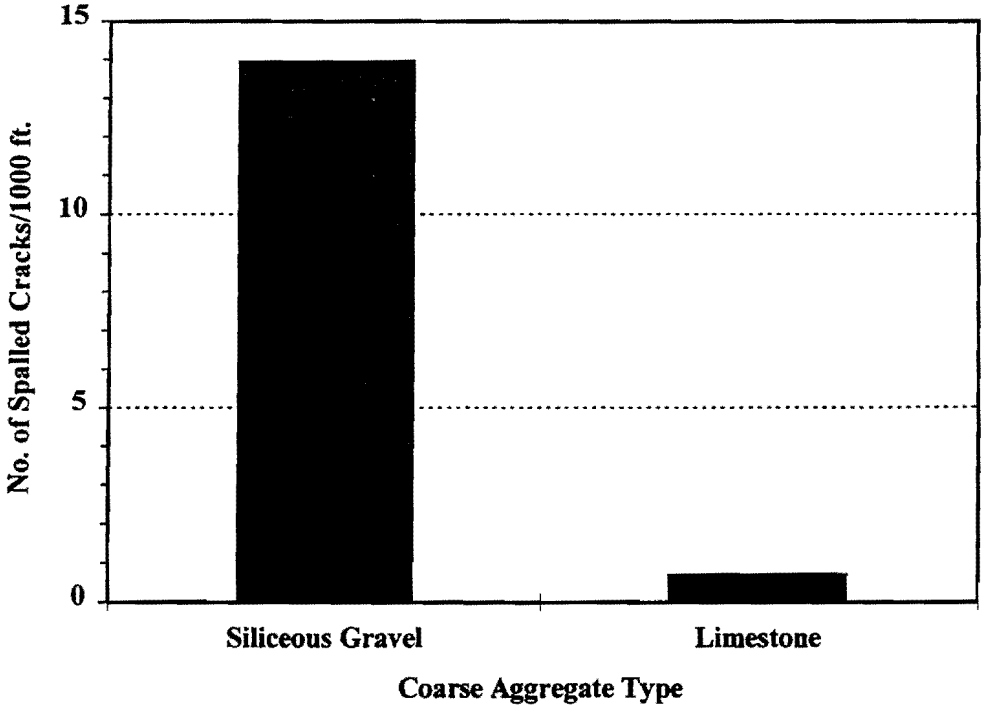

FIG. 17. Number of Spalled Cracks Per Survey Section Averaged by Coarse Aggregate Type and by Master Section (1 ft = .305 m)

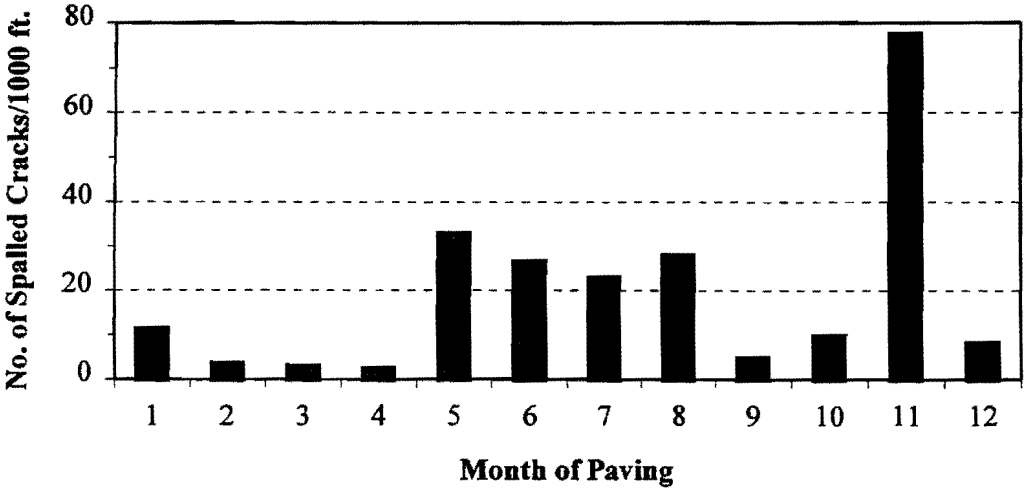

FIG. 18. Number of Spalled Cracks Per Survey Section Averaged by Master Section and by Paving Month (1 ft = .305 m)

CHAPTER 4: EFFECT OF AGGREGATES ON SPALLING

Field studies undertaken as a part of this research and preliminary analysis of spalling data discussed in the previous section on field studies highlighted the influence the coarse aggregates have on spalling in concrete pavements. Field observations on spalled fracture surfaces as well as petrographic analysis of concrete cores indicate a high incidence of interfacial fracture. This may point to a weak link in concrete that may very well be causing the initiation of the spalling fracture. Such evidence calls for an investigation into the role of the coarse aggregate in concrete aimed at explaining its effect on spalling. First, a review of available literature on aggregates in concrete is discussed. Later, results from laboratory testing of concrete is presented.

Aggregate is the major constituent in Portland cement concrete in terms of volume. Early classifications viewed aggregate in concrete as an inert and inexpensive material which can produce large volumes of concrete required to form various structural shapes. However, recent research has shown that aggregate in concrete is not the inert material it was once thought to be, and that its physical and chemical properties influence the performance of the concrete in terms of strength and durability.

Concrete aggregates can be either natural or artificial. Natural aggregates are either directly used or processed by artificially crushing a large parent mass. Properties of crushed natural aggregates can be categorized into two groups, namely, properties inherited from its parent material and properties independent of the parent rock. Some properties inherited from the parent rock are petrography, chemical and mineral composition, specific gravity, hardness, strength, physical and chemical stability, pore structure, and color. Properties not directly inherited from the parent rock may include particle shape and size. Properties of aggregates likely to affect the behavior of concrete can be divided into two classes, namely, physical properties and chemical properties. Some of these properties believed to be pertinent to the performance of the bond between aggregate and cement paste are given below.

PROPERTIES OF AGGREGATES IN PORTLAND CEMENT CONCRETE

Physical Properties

Gradation

Gradation affects the workability of concrete which may, in turn, affect the segregation of constituents, bleeding, water-cement requirements, handling, placing, and finishing characteristics. These factors may then affect strength, volume change, durability, and the economy of concrete.

Mineralogic and Chemical Composition

This affects the surface texture and the chemical reactions at the cement paste-aggregate interface. Therefore, these are very important properties in the investigation of aggregate-cement paste interfacial zone.

Electro-Static Condition of the Aggregate Surface

The geophysical aspects of aggregates are very important in determining the formation of different interfacial compounds in the interface. It is believed that in some siliceous aggregates, the presence of electro-static charges on the aggregate surface enables the attraction of bipolar water molecules (internal bleeding), thus, creating a weak bond at the interface (Sherwood 1964).

Thermal Properties

This is important in the context of differential thermal expansion between the aggregate and the cement paste, which can create stresses at the interface. It has been found that the coefficient of expansion is important only in the case of low expansive

rocks such as granite, limestone, and marble. The specific heat and conductivity are important in case of mass concrete.

Strength and Elasticity

This depends not only on the strength of the mineral aggregate, but also on the internal bond of the crystals (i.e., granites which comprise hard quartz crystals, show low strength, elasticity, and abrasion resistance due to poor bonding between crystals).

Coatings

These are usually deposited from ground water which runs through aggregate deposits. Some notable coatings are clay, silt, calcium carbonate, iron oxide, opal, gypsum, manganiferous substances, and soluble phosphates. Coatings can be either beneficial or detrimental to the concrete, and their effects depend on the physical nature and the mineral or chemical composition of such coatings. The effects of these coatings on the particles may relate to the adhesion between the particles and the cement paste, the chemical stability of the aggregates, and the contribution of excess material to the plastic mixture.

Chemical Properties

It is generally accepted that differences exist in the bonding of cement paste with different aggregate types. Carbonate aggregates appear to react chemically with the cement hydration products, forming a good interfacial bond. In contrast, silicate aggregates do not seem to bond well with the cement paste, as evidenced by more abundant cracking at the cement paste-aggregate boundary (Farran 1956).

Often mentioned aggregate reactions in concrete are alkali-aggregate reactions. These reactions could be in the form of either alkali-silica or alkali-carbonate reactions. With alkali-silica reactions, the alkalis in the cement react with aggregates having various forms of silica such as opal, chalcedony, chert, flint, tridymite, cristobalite, microcrystalline, strained quartz, etc. (Gillott 1975). Consequences of alkali-silica reactions are in the form of cracking in concrete as a result of stresses caused by expansion of compounds resulting from the reactions. The time taken for such action may be as rapid as several months or as slow as 30 years or more.

Alkali-carbonate aggregate reactions may be beneficial, innocuous, or deleterious. As for beneficial effects, it is commonly believed that the bond between the aggregate and the cement paste is enhanced by the epitaxial overgrowth of the calcium hydroxide of the cement paste on the calcium carbonate crystals of limestone or dolomite aggregates (Mather and Meilenz 1960). Rims of discoloration are often seen within the aggregate particle, both in concrete showing distress, as well as in good durable concrete. Usually, these rims are believed to show differences in solubility between the periphery and the center of the aggregate. The most deleterious of the chemical reactions between carbonate aggregates and the cement paste is the expansive de-dolomitization reaction. Some of the other aggregate properties associated with chemical reaction of aggregates are listed below:

1. Solubility - few rocks are soluble enough to cause problems.
2. Oxidation, Hydration, and Carbonation - oxidation, hydration, and carbonation of iron, magnesium, and calcium compounds give problems such as pop-outs and staining of the concrete. Iron sulfides such as pyrite and marcasite undergo oxidation and hydration to give hydrated iron oxides and sulfates, which can result in expansion of the concrete.
3. Reactivity with Portland Cement - sulfates added with aggregates can form calcium sulfo-aluminate, gypsum, and other minerals which can create problems. Minerals such as opal, chalcedony, tridymite, cristobalite, and heulandite, and also rocks such as glassy or crypto-crystalline rhyolites,

dacites, andesites, opaline cherts, chalcedonic cherts, and phyllites react with alkalis in the cement and create deleteriously expansive reactions.

Geometric Properties

Scrivener (1989) indicated that the physical characteristics of aggregate particles such as particle size distribution, particle shape, and surface texture affect the properties of concrete. The grading of the aggregate will affect both the packing of the particles and the surface area of the particles which must be covered by the cement paste. Some quantitative parameters have been used to describe particle shape. However, their use has been limited in practice due to the lack of a technique to measure them for a sample of aggregate comprising a reasonable number of particles. Ozol (1978) mentioned that "in the hardened concrete, the compressive and flexural strength, elastic properties, and the stress distribution are influenced by the aggregate particle orientation, degree of adhesion of particles to the cement paste, and the mechanical behavior of the cement paste-aggregate interface." He also said that these properties are influenced by equi-dimensionality, angularity, surface texture, and surface area of the particles. Ozol also observed that "concrete suitable to a purpose can be made with coarse and fine aggregates of very different sphericity, roundness, surface texture, surface morphology and surface area." However, based on research findings on the cement paste-aggregate interface, the importance of the above mentioned factors can be considered as crucial for both strength and durability of the concrete structure.

The fundamental attributes of particle geometry are shape and surface texture. The shape, surface area, surface texture, and the kind of intrinsic coating present on the particle surface can each be related back to the geology of the deposit, especially in the case of sand and gravel (Ozol 1978). The concept of particle shape incorporates three geometrical ideas, namely, sphericity, roundness, and form. These are distinct and separately definable properties in a mathematical sense. Folk (1968) included a fourth property, the surface features (texture) under the broad heading of particle morphology. Texture of an aggregate rock particle involves the degree of crystallinity (mineral

composition in the context of surface texture), grain size, shape, and relative sizes and arrangement of the mineral grains. The particular size, shape, and distribution of voids in a porous surface may be more important for the bond and other mechanical properties of the interface between aggregate and the cement paste than the absolute numerical value of the porosity.

The surface texture of aggregates could either be random or uniform in nature. Granite reflects the irregular grain boundaries and size and shape of several minerals, each with its own characteristic cleavage or fracture. In contrast, a fair amount of regularity or periodicity may be present on broken surfaces of sedimentary or metamorphic rocks with strong cleavages, equi-granular textures, or other sorts of preferred orientations of minerals. The petrographic factors shaping surface texture are perhaps more relevant to the production of texture on crushed stone surfaces. The surface features of sand and gravel are rather different and bear the results of preferred solution, etching, leaching, precipitation, etc.

It is not a simple task to quantify the effect of aggregates, particularly its shape, size, and surface texture in terms of the behavior of concrete materials. This is so because the aggregate particles have random natural shapes which are not uniform in nature. If they were uniform, a single particle or a group of particles would have been characterized to represent the whole mass of aggregates. One of the most promising ways of assessing these properties would be to use computerized imaging techniques such as that used with the fractal analysis method (Li et al. 1993). The fractal analysis method of concrete aggregates is an extension of the concept applied by Peleg and Normand (1941) to characterize the shape and texture of "instant coffee" particles. The existing methods available to characterize aggregate shape and texture determine the deviation of a particle from a sphere. A fractal is a geometric shape which differs from a topological ideal, such as a sphere. A fractal dimension is calculated for the silhouette of each particle, preferably obtained from a photographic image. This fractal dimension is an indication of how deviant the shape of that particle is from a topological ideal such as a sphere, a cube, or a tetrahedron.

Previous studies have indicated that fractal dimension can be obtained from automated means and that the fractal dimension differs for different aggregate types (Li et al. 1993). For example, siliceous river gravel particles have a lower fractal dimension for surface texture than crushed limestone (Li et al. 1993). This is an indication of a higher contact surface area at the aggregate-cement paste interface for concrete with limestone as the coarse aggregate. This increases the interfacial friction and will result in enhanced bonding properties between the aggregate and the cement paste. This method of fractal analysis gives a very satisfactory tool to characterize the surface texture of aggregate which is a very important characteristic to be considered in the study of the interfacial bond between aggregate and cement paste. Table 7 shows the results from the fractal dimension measurements made by Li et al. (1993) of surface texture of aggregates from sources within the state of Texas.

TABLE 7. Fractal Dimension of Surface Texture of Aggregates (Li et al. 1993)

Aggregate Source/Company	Aggregate Type	Fractal Dimension of Surface Texture
Gifford Hill (Wardlaw Pit)	Siliceous River Gravel	0.25
Gifford Hill (OSR)	Siliceous River Gravel	0.26
Thorstenburg	Siliceous River Gravel	0.23
Pioneer	Siliceous River Gravel	0.40
Redland	Limestone	0.36
Vulcan	Limestone	0.35
East Texas Stone (Blue Mountain)	Sandstone	0.32
Texas Crushed Stone	Limestone	0.33

INTERFACIAL BOND BETWEEN CEMENT PASTE AND AGGREGATE

It has been shown that very fine bond cracks can exist at the interface between the cement paste and the aggregate in concrete, even prior to the application of load (Glucklich 1968). Such micro-level cracking is believed to occur as a result of differential thermal behavior between aggregate and cement paste, and the unique structure and properties of the interfacial bond between cement paste and aggregate. An investigation of the stress-strain properties of aggregate, cement paste, and concrete reveals that even though the aggregate and the cement paste individually display linear elastic behavior, the concrete composite shows signs of non-linearity, particularly at the higher stress levels. This indicates that the interface between these two constituent media contribute to the apparent ductility of the concrete (Neville and Brooks 1987).

Investigation of this interfacial bond between aggregate particles and the cement paste indicate that the nature of the hydrated cement paste at the interface is different from the bulk paste. The structure of the interfacial compounds have been shown to depend on the physical and chemical properties of the aggregate, the properties of cement, and the mix design parameters of the concrete. Strubl et al. (1980) presented a comprehensive summary of the research findings on the cement paste - aggregate bond published up to that time. They stated that the bond between cement paste and aggregate results from some combination of mechanical interlocking between cement hydration products and the aggregate surface, and a chemical bond resulting from a reaction between aggregate and cement paste. They categorized the nature of the cement-aggregate bond according to its morphological, chemical, and mechanical properties.

Morphological Nature of the Bond

Study of the morphological nature of the aggregate-cement paste bond typically involves examination of the cement hydration products at the interface by microscope. Farran (1956) first concluded that the bond strength was due to a combination of chemical reactions between aggregate and cement paste, and epitaxial growth of $Ca(OH)_2$

on the aggregate surface. Several other researchers (Buck and Dolch 1966; Schwiete et al. 1968; Bertacchi 1970) provided evidence of $Ca(OH)_2$ precipitation on calcite aggregate surfaces. Suzuki and Mizumaki (1975, 1976) observed that the quantity and crystallinity of these products varied with different aggregates. Farran et al. (1972) described "an aureole" of hydrated paste surrounding the calcite aggregate. Within this aureole, they observed that the hydration products were less dense than in the mass of the paste. They also observed evidence of less mechanical resistance of the aureole. Micro-hardness measurements across the cement-aggregate interface were made by Lyubimova and Pinus (1962). They concluded that quartz grains were covered with a layer of epitaxic calcium silicate hydrate and that micro-hardness values at the interface are lower than those for the aggregates and the hydrated cement paste.

Scrivener and Pratt (1986) reported that "the relative movement of the sand and cement grains during mixing, and possibly settling of the aggregates before the cement paste sets, may lead to regions of low paste density around grains and to areas of localized bleeding at the aggregate-cement interface in which large $Ca(OH)_2$ crystals precipitate." From previously published literature on the subject, it is clear that the interface regions are, in general, much different from the bulk cement paste in terms of morphology, composition, and density. At least in part due to bleeding referred to earlier, the interface region between aggregate and cement paste is more porous than the bulk paste, leading to lower densities. In addition, there are generally large crystals of calcium hydroxide in the interfacial zone with a preferential orientation. It is likely that these large calcium hydroxide crystals occur because of the extra space available within the interface.

Many models of the interfacial region have been presented in published literature. In spite of the differences in detail, they all show that the thickness of the interfacial region is approximately 40 to 50 μm, with the major difference in characteristics from the bulk paste occurring within the first 20 μm from the physical interface. The weakest part of the interface of this interfacial zone lies not right at the physical interface, but 5 to 10 μm away from it within the paste fraction. The fracture path often runs along the cleavage planes of the oriented calcium hydroxide crystals. Mehta (1986) stated that "in

mature pastes, the fracture surface generally contains unusually large areas of calcium hydroxide crystals." Due to the large crystal size and, therefore, a small surface area, the inter-particle bonding forces between calcium hydroxide crystals or between calcium hydroxide crystals and other particles in the cement paste are weak. Microscopic examination of polished concrete surfaces by Diamond et al. (1982) revealed that the mean spacing between the aggregate particles is only about 75 to 100 μm. Even though the variability of this spacing is large, it suggests that with an interfacial zone thickness of approximately 50 μm, most of the hydrated cement paste (HCP) lies within the interfacial zone and only a small volume of bulk HCP exists. This indicates that the representation of the actual concrete in the models is far from satisfactory.

Chemical Nature of Bond

Chemical bonds form as a result of chemical interaction between the hydrated cement compounds and the constituent minerals of the aggregate. Bond strength measurements made by Hsu and Slate (1963) and Farran (1956) for various types of aggregate show that, generally, carbonate aggregates produce higher bond strengths than silicate aggregates. These bond strength measurements were done on specimens made by casting cement paste onto prismatic aggregate pieces. The bond strength was modeled based on the shear strength as well as the flexural strength of these samples. Graves and Eades (1987) reported on results obtained by Alexander et al. (1968) that extrusive siliceous aggregates may develop high bond strengths. This is likely due to the amorphous nature of some extrusive aggregate components, producing a pozzolanic type reaction with the cement paste due to silica dissolution in the highly alkaline environment. However, they went on to say that it is doubtful whether that same mechanism would occur for the more commonly used non-extrusive siliceous aggregates of a highly crystalline nature, such as quartz gravel and crushed granite, due to their much lower silica solubility. Graves and Eades (1987) listed two commonly used

models of reaction between limestone aggregates and cement paste:

1. Bonding of $Ca(OH)_2$ formed at the interface to the calcite surface either by epitaxial overgrowth or non-homogeneous nucleation.
2. Formation of the carbo-aluminate. Some studies have concluded that the formation of carbo-aluminate is the most beneficial for providing a strong cement paste-aggregate bond (Yuan and Guo 1987; Yuan and Odler 1987).

The surface chemical properties of common silicate minerals, such as quartz and feldspar, are different than those of the carbonate minerals because quartz, which is composed of Silicon (Si) and Oxygen (O) atoms linked in tetrahedral coordination, yields a negatively charged surface through dissociation of hydrogen atoms. This results in a negative charge in the quartz surface and positive charges in the adjacent water medium. This structure is termed the double-layer structure at the quartz-water interface. This strong affinity to water results in a poor bond.

Mechanical Nature of Bond

Alexander et al. (1968) reported that bond strength varied widely according to the rock type and surface roughness of the aggregate, with the strengths varying by a factor of as much as two between different aggregates. Some researchers have used this as indirect evidence of chemical reaction between cement and rock types. Ozol (1978) pointed out that varation in bond strength could alternatively be explained by different roughness factors of different aggregate. However, regardless of whether the bond is primarily due to either mechanical interlocking or chemical reaction, the true surface area of the aggregate available for bonding is an important aspect of bonding. The true surface area entails the size, shape, and surface texture of aggregate particles.

Effect of Bond on Concrete Performance

Field observations made on concrete pavements within the state of Texas indicate that a large fraction of the fractured surfaces of spalls are interface failures between the cement paste and aggregate. This appears to suggest that the aggregate-cement paste bond may be the primary cause of spall development.

Concrete Strength

Conflicting evidence has been reported as to what extent the bond strength affects the strength of the concrete. Some researchers have concluded that the bond strength has very little or no effect on the concrete strength, whereas others have reported findings in which the bond strength has some effect on the strength by way of micro-crack propagation rate. Glucklich (1968) illustrated his findings on the micro-crack growth in concrete under load. Based on his findings he hypothesized that non-linearity of the stress-strain behavior of concrete is primarily caused by the growth of bond cracks.

Concrete Durability

Valenta (1961) measured flexural strength and durability of bond between cement paste and aggregate using rock types with different degrees of smoothness. He did not find any significant influence of the aggregate surface characteristics on the strength. But their effect on the durability was well established. He measured durability as the number of freeze-thaw cycles required to produce a 50% reduction in flexural strength of the bond. Based on this evidence, one might conclude that the morphological nature of the bond has a greater influence on the durability of concrete, whereas the chemical nature has a greater influence on concrete strength.

Methods of Improving Cement Paste-Aggregate Bond

There are still no standard methods either for analyzing the interfacial regions in concrete or for measuring interfacial bond strengths. In many of the earlier investigations, specimens were prepared either by casting cement paste against polished aggregate faces, or by carefully embedding fibers in cement or mortar matrix. It is a subject of argument whether these are appropriate simulations of what actually happens in concrete in practice.

Use of Improved Materials

The use of improved materials may be done in several ways. Ways of improving the interfacial strength between aggregate and cement paste can be done by improved mix design or the use of better performing aggregates. Several researchers, including Scholer (1967), suggested that the stress level for initiation of micro-cracks in concrete is primarily a function of mortar strength. Therefore, one way of achieving higher interfacial strength is to improve the strength of the mortar. However, this needs to be compatible with the other functional needs of the concrete. For example, if a higher cement content is used to increase the mortar strength in concrete, the shrinkage strains in concrete may also be increased, thus alleviating any benefit that may have been garnered from the increased mortar strength. Also, one may argue that the use of aggregates which improve the bond between aggregate and cement paste should be used. However, this is governed by the availability of these aggregates locally since a major part of the cost of aggregate is the cost of transportation.

Processing Methods

The evidence given by Valenta (1961) that the surface of aggregate particles has some influence on at least the durability of the aggregate indicates that the texture of the aggregate changes the bond strength. This is enough motivation to think about ways to

further study the effect of aggregate texture and shape on the strength and durability of the concrete. Two methods suggested were to crush uncrushed aggregates such as river gravel to increase the roughness of its surface texture, and also to use different crushing methods which would enhance the shape properties of the aggregate. These crushing methods would have to incorporate the grain size, fracture properties, and hardness of the parent rocks. The effectiveness of crushing aggregate particles is in question based on the results of some studies done recently.

Use of Admixtures

Monteiro and Mehta (1986) showed an increase in bond strength as a result of the addition of silica fume during the mixing of concrete. They attributed the improvement in bond strength to less free water (less bleeding) at the interface during specimen preparation and a reduction in size of the transition zone due to the pozzolanic reaction between calcium hydroxide and the silica fume, thus reducing the preferred orientation of the calcium hydroxide crystals. They also showed that bond strength can be improved by grain refinement. Grain refinement replaces large crystals with smaller ones in the interfacial zone. They indicate that grain refinement occurs either with the use of silica fume or with the use of carbonate aggregate.

Improved Mixing Methods

It is reported that cement-aggregate can also be improved by modifying the concrete mixing method where the cement and aggregate are premixed with only a part of the mixing water. Hayakawa and Itoh (1982) showed that this way, bleeding within the interfacial zone for concrete made with siliceous aggregate can be reduced, thus increasing its strength.

Coating of Aggregate Particles

Graves and Eades (1987) studied the calcium hydroxide treatment of aggregates to enhance their properties. They found that such treatment improves the compressive strength of Portland cement concrete containing siliceous aggregate. They recommended a procedure of mixing the siliceous aggregate with a calcium hydroxide solution, followed by drying the aggregate before concrete preparation. It was found that this procedure improves the cement paste-silicate aggregate interfacial bond. They thought the enhancement in bonding strength was due to increased adsorption of Ca^{2+} ions onto the negatively charged silica surface, thereby providing a bridging mechanism between the cement paste and aggregate.

LABORATORY STUDIES ON CONCRETE MADE WITH DIFFERENT COARSE AGGREGATES

It has been well established both in prior research (Shelby and McCullough 1960; Guitierrez de Velasco and McCullough 1981) as well as findings from this research that the coarse aggregate type used in Portland cement concrete has a significant influence on spalling in concrete pavements. Fig. 17 illustrated that concrete pavements with siliceous river gravel coarse aggregate are more likely to spall than those with crushed limestone coarse aggregate. It was also established that first, de-bonding cracks at the aggregate-cement paste interface or delamination cracks occur in concrete pavements. Subsequently, these delaminations develop into visible spalling distresses. Since it is believed that these de-bonding cracks and/or delaminations occur very early in the life of the concrete pavement, from that point on, the spalling distress becomes a fracture mechanics process due to the presence of these initial cracks. Therefore, it was decided to conduct fracture tests on concrete specimens to investigate if there are any significant differences in the fracture behavior of concrete with different coarse aggregates. Since it was also established that the strength of the cement paste-aggregate interface in concrete is important in spalling, it was thought that the type of fracture parameters that would be

obtained from the fracture tests would be a reflection of the performance of the aggregate-cement paste bond. The criteria that need to be met in selecting a fracture test for this purpose are listed below:

1. It is best if the test is simple, economical, and quick.
2. The test should provide information on "material" properties of the concrete.
3. The results from the tests should be a reflection on the characteristics and strength of the aggregate-cement paste interface in concrete.

As it was explained in the previous section on field studies, the formation of delaminations in concrete pavements and the development of these delaminations into spalls involves the creation and propagation of cracks within the concrete. Once cracks are formed in any elastic body, stress concentrations are created at crack tips where the stresses may be several times higher than the applied stress. Therefore, fracture mechanics principles can play an important role in the modeling of such phenomena. This phenomenon can be explained using the following analytical solution (Inglis 1913).

Fig. 19 shows a plate with an elliptical flaw in the middle. The major and minor axis dimensions of the elliptical hole are 2a and 2b, respectively. When a direct tensile stress σ is applied on the plate as shown in Fig. 19, the stress at point A is given by the solution:

$$\sigma_A = \sigma \left(1 + 2\sqrt{\frac{a}{\rho}} \right) \tag{6}$$

where ρ is given by:

$$\rho = \frac{b^2}{a} \tag{7}$$

If we consider a crack with a length of 3.75 cm and a width of .25 cm, the stress at the crack tip A is sixteen times the applied external stress of σ. This shows that in the presence of a crack, if one were to still consider a continuum mechanism approach (assuming that there is no crack within the body), the strength of the body would be severely underestimated. Therefore, fracture mechanics principles ought to be applied in such situations to take care of the stress concentration effects at the crack tips.

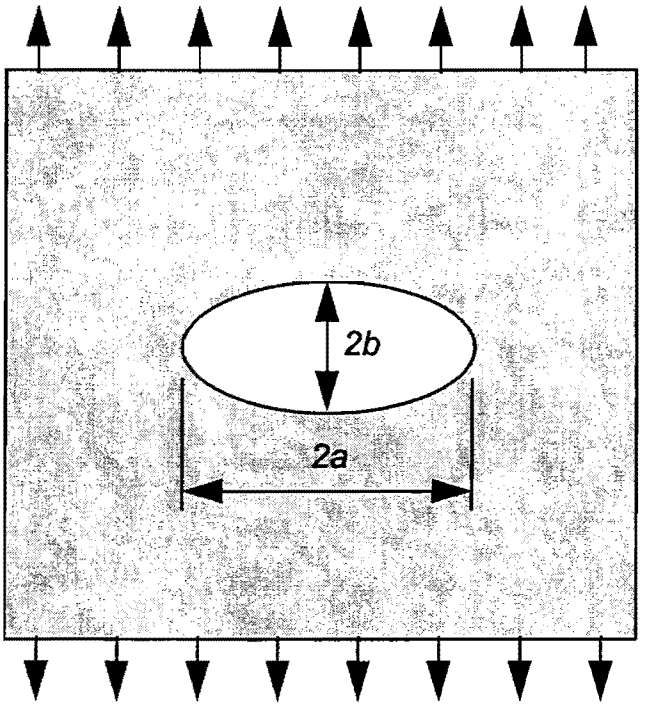

FIG. 19. Elliptical Hole in a Plate

Fracture Mechanics Concepts

Qualitative evidence of the root cause of fracture in materials was evident several centuries ago when Leonardo da Vinci observed that the strength of iron wires varied inversely with wire length, suggesting that fracture is related to flaws in the material.

However, a quantitative approach to fracture as a scientific study was first adopted by Griffith (1920). He extended an already available solution for a stress analysis around an elliptical hole (Inglis 1913) to come up with a relationship between fracture stress and crack size. A brief overview of some of the fracture mechanics concepts used in the study of concrete is given below.

Griffith's Energy Balance Principle

According to the First Law of Thermodynamics, when a system goes from a non-equilibrium state to equilibrium, there will be a net decrease in energy. Griffith (1920) applied this idea to the formation of a crack, and his solution was based on a simple energy balance. According to this principle, fracture occurs when the change in strain energy that results from an increment of crack growth is sufficient to overcome the surface energy of the material. Griffith used this model successfully to analyze fracture in glass. Griffith's solution for the fracture strength of an infinitely wide plate with a through thickness crack (which extends from one end of the plate to the other) subjected to a remote tensile stress σ (Fig. 19) , is given by:

$$\sigma_f = \sqrt{\frac{2\,E\,\gamma_s}{\pi\,a}} \tag{8}$$

where 2a is the flaw size and γ_s is the surface energy of the material (i.e., energy required to create a unit surface of the material). Subsequently, Irwin (1948) and Orowan (1948) independently modified the Griffith expression to account for different types of materials. They introduced a general term of fracture energy in place of the surface energy of the material. This fracture energy term includes the expended plastic energy in the propagation of the crack. Conceivably, Griffith's expression can be used for several types of materials, such as ideally brittle materials, quasi-brittle elastic-plastic materials, and brittle materials with crack meandering and branching.

Energy Release Rate Principle

Irwin (1956) proposed another approach for fracture which was much in line with the Griffith energy criterion. He defined an energy release rate, *G*, which is a measure of the energy available for an increment of crack extension. The energy release rate is expressed by:

$$G = -\frac{d\pi}{dA} \tag{9}$$

where π is the potential energy provided by the internal strain energy and external forces, and *dA* is the incremental increase in crack area. *G* is also referred to as the crack extension force or the crack driving force. Crack extension occurs when *G* reaches a critical value, G_c, which is a measure of the fracture toughness of material.

Stress Intensity Factor

Several researchers worked on attaining a closed form solution for stress distribution in a cracked body assuming isotropic, linear elastic conditions (Westergaard 1939; Sneddon 1946; Irwin 1957; Williams 1957). It was shown that the stress field in any linear elastic cracked body is given by:

$$\sigma_{ij} = \left(\frac{k}{\sqrt{r}}\right) f_{ij}(\theta) + \textit{higher order terms} \tag{10}$$

where σ_{ij} is the stress tensor, *r* and θ are defined in polar coordinates (Fig. 20), k is a constant, and f_{ij} is a dimensionless function of θ. The higher order terms depend on the geometry, and they come into play at a significant distance away from the crack tip (away from the stress singularity zone). As *r* approaches zero (near the crack tip), the leading term approaches infinity, but the second term (higher order term) remains finite or approaches zero. The stress near the crack tip varies proportionally to $1/\sqrt{r}$,

regardless of the configuration of the cracked body. A crack can undergo three modes of loading. These modes are illustrated in Fig. 21. Under Mode-I, the principal load is applied normally to the crack plane which tends to open the crack. Mode-II is when in-plane shear loading is applied which will try to slide one crack face with reference to the other. Mode-III loading causes out-of-plane shear. A crack can be loaded in any one or a combination of these modes.

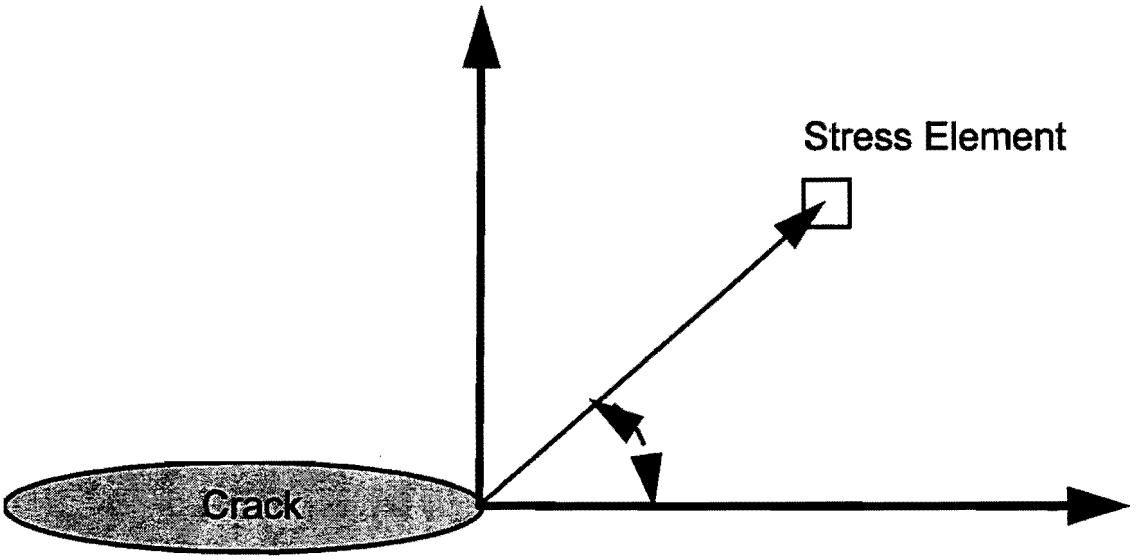

FIG. 20. Definition of the Coordinate System for Stress Analysis Ahead of Crack Tip

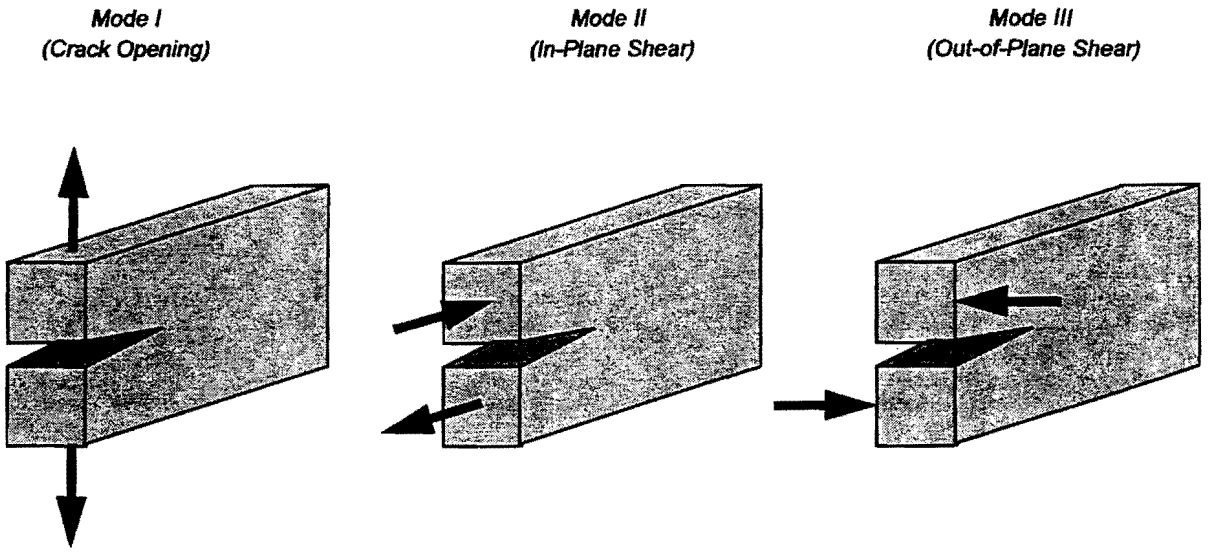

FIG. 21. Three Modes of Loading Applied to a Crack

Each mode of loading produces the singularity at the crack tip, but the proportionality constant k and f_{ij} depend on the mode. For convenience, k is replaced by a term called the Stress Intensity Factor (K) where

$$K = k\sqrt{2\pi} \tag{11}$$

The stress intensity factor K defines the amplitude of the crack tip singularity, and a subscript I, II, or III is used with the stress intensity factor to denote the mode of loading. Therefore, the stress field ahead of a crack tip in an isotropic linear elastic material under mode I loading can be written as:

$$\lim_{r\to 0} \sigma_{ij}^{(I)} = \frac{K_I}{\sqrt{2\pi r}} f_{ij}^{(I)}(\theta) \tag{12}$$

It was later shown that the stress intensity factor (K) and the energy release rate (G) are related by:

$$G = \frac{K_I^2}{E'} + \frac{K_{II}^2}{E'} + \frac{K_{III}^2}{2\mu} \tag{13}$$

for the general case of combined mode loading, where E' is equal to E for plane stress, and $E/(1-\nu^2)$ for plane strain.

Even though linear elastic stress analysis of sharp cracks predict infinite stresses at the crack tip, in real materials, stresses at the crack tip are finite because the crack tip radius is finite. This elastic stress analysis becomes increasingly inaccurate at the inelastic region as the crack tip grows. Several corrections are available to account for

moderate crack tip yielding. However, for more extensive yielding, alternative crack tip parameters need to be considered which take nonlinear material behavior into account.

If a material were to fail locally at some combination of stresses and strains, then crack extension must occur at a critical K value (K_c). This value of K_c is a measure of fracture toughness, and it is a material constant independent of the geometry of the cracked body. However, there is evidence that in some materials, even when the plastic zone is very small, fracture may not nucleate in the singularity dominated zone. This raises the important question of whether stress intensity is a useful failure criterion in materials that exhibit inelastic deformation at the crack tip. It is seen that under conditions where the plastic zone is small compared to geometry of the specimen, K_c can still be a useful failure criterion. It is observed that fracture toughness decreases with increasing thickness of the specimen, and it reaches a plateau where further increase in thickness has little or no effect on toughness. The critical K_I value at the plateau is defined as K_{IC}, which is the plane strain fracture toughness under mode I (tensile) loading. Therefore, as long as the specimen and the structure are large compared to the plastic zone, K_{IC} can be a useful failure criterion.

Application of Fracture Mechanics to Concrete

Neville and Brooks (1987) stated that "even when we eliminate one source of heterogeneity in concrete, viz. the aggregate, we find that the actual tensile strength of the hydrated cement paste is very much lower than the theoretical strength estimated on the basis of molecular cohesion of the atomic structure, and calculated from the energy required to create new surfaces by fracture of a perfectly homogeneous and flawless material." Griffith's postulated law of crack growth (Griffith 1920) is used to explain this discrepancy of strengths.

The structure of the cement paste is complex, and several sources of flaws and discontinuities exist, even before the application of any load. Neville and Brooks (1987) also mentioned that up to 50% of the volume of the cement paste may consist of pores. The presence of aggregate enhances this number of flaws, and it also provides larger-

sized pores. These cracks are randomly distributed and vary in size and orientation. The first experimental work on fracture mechanics of concrete was performed by Kaplan (1961). He found that the critical strain energy release rate, G_c, for cement mortar is much higher than the theoretical maximum of twice the surface energy of the material. Glucklich (1968) later explained that this was because fracture of concrete was not limited to a single crack, but a number of microcracks formed at the highly stressed zone located just ahead of the tip of the advancing primary crack. The size of this highly stressed zone and the number of microcracks present were believed to be based on the characteristics of the concrete such as the aggregate type, aggregate content, and the aggregate size. Glucklich noted that the presence of this highly stressed zone results in a true fracture area much higher than that of the apparent single primary crack. Later, researchers named this highly stressed zone as the *fracture process zone*. Glucklich also showed that high strength elements in normal strength concrete such as the aggregate act as crack arresters, resulting in increased energy demand.

With regard to the aggregate shape and texture, Alford and Poole (1979) found a general increase in the critical strain energy release rate (G_{IC}) required for crack growth with increasing angularity and surface texture of aggregate. Various other investigators have conducted investigations to evaluate fracture toughness for concrete. Several measures of the fracture toughness used in fracture mechanics studies were discussed previously. The most commonly used of these is the critical stress intensity factor (K_c) criterion. This means that one has to assume concrete to be an ideally brittle, linearly elastic material, with its fracture dominated by the singularity zone ahead of the crack tip. Hillemeier and Hilsdorf (1977) measured the fracture toughness of aggregate, hardened cement paste, and the aggregate-cement paste interface. Based on their results (Table 8), it can be concluded that for the materials they used, the strength of the interface is the lowest.

The values reported for K_c in literature seem to vary widely. Even though researchers have used test specimens of different size and also different methods of creating the notch, etc., it is believed that one of the primary reasons for this discrepancy is the effect of the slow-stable crack growth caused by the presence of microcracking or

fracture process zone ahead of the crack tip (Shah 1979). This would necessarily mean that the size of the specimen, which would relate to the size of this fracture zone and its effect on the specimen, would have a significant effect on the test results. The size of this fracture would likely depend on the properties of the concrete composite such as size and volume of aggregate, microstructure of the cement paste, properties of the cement paste-aggregate interface, etc. Since the notch depth relative to the characteristic specimen dimension becomes important, the concept of geometrically similar specimens was introduced.

TABLE 8. Typical Measured Values for Fracture Toughness of Concrete and Its Constituents (Hillemeier and Hilsdorf 1977)

Material	Fracture Toughness K_{IC} ($MN/m^{3/2}$)
Quartz	3.4
Marble	1.9
Hardened Cement Paste, w/c=0.4	0.31
Hardened Cement Paste-Quartz Interface	0.13

Some very important work on this subject was performed by Walsh (1972) who tested flexural beams with depths varying from 5-25 cm, but they all had the same ratio (of 0.5) between the notch depth and the specimen depth. His test results indicated that in a plot of nominal flexural stress vs. depth of the beam, the nominal stress remained somewhat constant at low specimen depths, and then showed a gradually decreasing trend as the specimen size increased beyond a "critical" size. Based on these results, he concluded that for a valid fracture mechanics test, the beam should be at least 25 cm deep. This is because the effect of the fracture process zone (Fig. 22) is dominant in specimens of smaller size. Bazant (1984) later introduced the size effect law for concrete fracture specimens.

The size-effect method for determining fracture energy and process zone size in concrete, is a standard test procedure of the RILEM (RILEM 1990). Since the size-effect law (Bazant 1984) is incorporated in this method, it presents the fracture toughness as a material property which is independent of the effect of the specimen size. This RILEM recommended method is used to determine the fracture energy of concrete by measuring the maximum loads of "geometrically similar" notched concrete beams of different sizes. Geometrically similar specimens have the same ratio between the characteristic dimensions. For example, in a notched concrete beam test, several sizes of beams are tested with the same span/depth and initial notch length/depth ratios. Since specimens of several sizes are used in this test, the fracture energy (energy per unit crack area) obtained from this test is analogous to the fracture of a large specimen such as a pavement slab. In theory, fracture toughness obtained in this manner is independent of both the specimen size and shape.

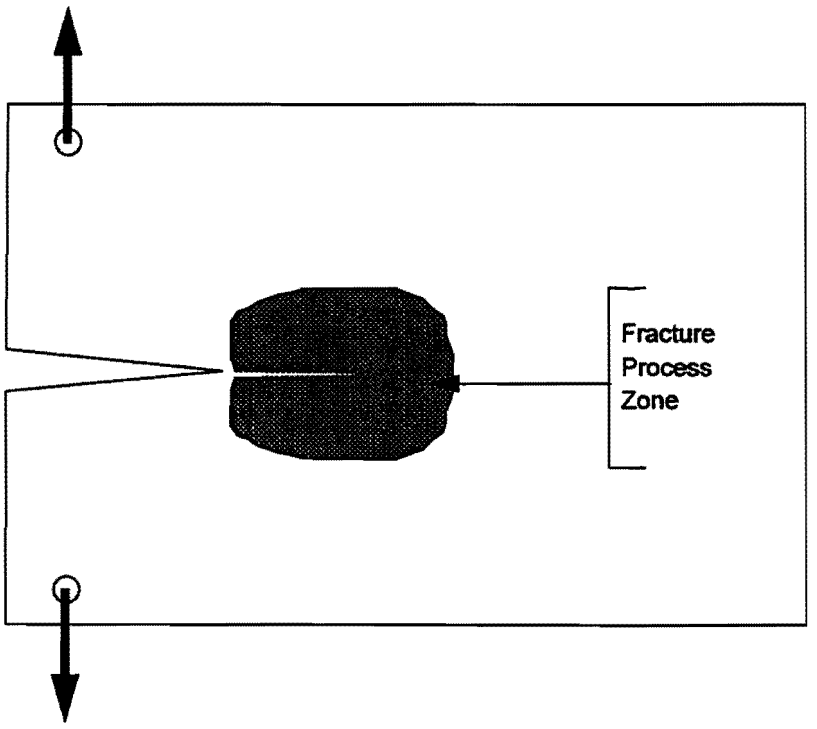

FIG. 22. Fracture Process Zone in Concrete

The fracture toughness (K_{If}) obtained from the size-effect method (RILEM 1990) is different from the critical stress intensity factor (K_{IC}) which is obtained from testing specimens of one size. For materials which do not display a fracture process zone (i.e., materials for which linear elastic fracture mechanics are applicable), K_{IC} may be used as a material property. But for a particulate composite such as Portland cement concrete, the fracture process zone needs to be taken into account, and K_{IC} cannot be used as a material property. In addition to the fracture toughness K_{If}, the size effect test also provides information such as the brittleness number for the concrete and the effective length of the fracture process zone.

Experimental Program

Based on results from prior research and from the field survey conducted in this research, it was determined that the coarse aggregate type in Portland cement concrete has a significant influence on spalling. The primary objective of this laboratory experimental program was to relate spalling to the properties of concrete made with different coarse aggregate types. The previous section on field studies discussed that spalling is caused by the extension of delaminations formed early in the life of the concrete pavement. It was theorized that, initially, small cracks formed very early at the aggregate-cement paste interface eventually developed into delaminations and finally into spalls. It was also argued that spalling involves the fracture of concrete. This laboratory experimental program, aimed at relating aggregate properties to spalling, was designed with emphasis on fracture testing of Portland cement concrete, and it consisted of the following:

1. A fracture test that was a modified form of the indirect tensile test,
2. Analysis of the fracture surface area of notched split tensile test specimens after they were tested for maximum load,
3. Size-effect fracture test on notched concrete beams, and
4. Microscopical examination of concrete specimens.

The size-effect fracture test on concrete beams was selected because it provides a fracture toughness for concrete that is independent of the specimen size, and therefore, can be considered as a material property. It also provides estimates of the effective length of the fracture process zone and the brittleness number of the material. These properties of concrete provide a basis on which the properties of concrete made with different coarse aggregate types can be compared. The following factors were incorporated in the experimental design:

1. coarse aggregate type
2. coarse aggregate treatment
3. paste additives
4. curing temperature
5. aggregate gradation

It was clear at the beginning of this test program that due to the large number of tests involved, it will be practically impossible to conduct size-effect fracture tests to investigate all the factors indicated above. To perform the size-effect test, concrete beams of several sizes need to be cast and tested with a number of replicates. Therefore, it was decided to conduct a simpler type of a fracture test to determine the critical stress intensity factor, K_{IC}, to compare the performance in concrete by incorporating factors 2-5 above. The size effect fracture test was performed only to evaluate the performance of concrete made with different coarse aggregate types. It was decided that the best way to determine the critical stress intensity factor (K_{IC}) was to perform a modified form of the indirect (split) tensile test. In this test, a concrete cylinder with a notch inserted axially was tested in a manner similar to the split tensile test in concrete. From the ultimate load, critical fracture toughness (K_{IC}) can be calculated.

Indirect (Split) Tensile Test of Notched Cylinders

Analytical Solution

This type of test is also known as the notched Brazilian disk test (Ojdrovic and Petroski 1985). Fig. 23 show the schematic diagram of the test configuration.

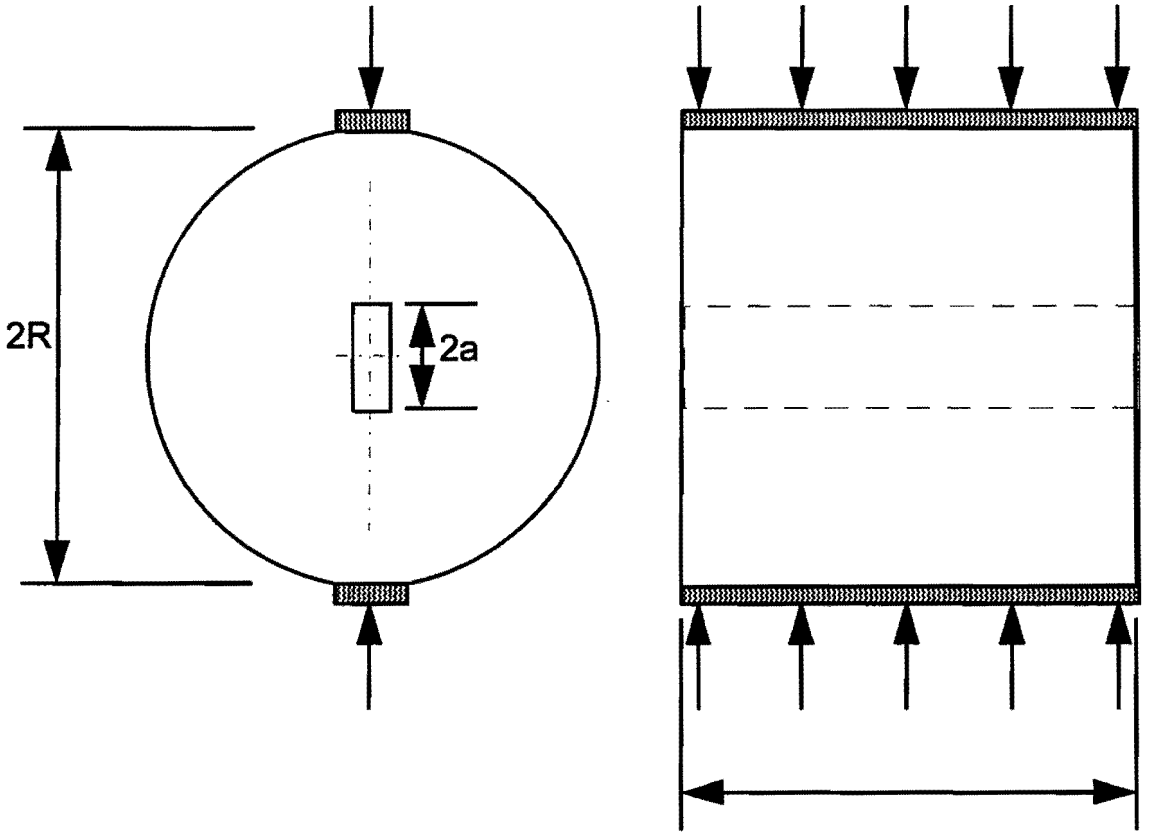

FIG. 23. Schematic Diagram for Notched Brazilian Disk Test

The analytical solution for fracture toughness for a specimen similar to the one shown in Fig. 23 was derived by Atkinson et al. (1982) and was presented in the form of normalized stress intensities N_I and N_{II}.

$$N_I = \sum_{i=1}^{n} T_i \left(\frac{a}{R}\right)^{2i-2} A_i(\theta) \tag{14}$$

$$N_{II} = 2 \sin 2\theta \sum_{i=1}^{n} S_i \left(\frac{a}{R}\right)^{2i-2} B_i(\theta) \tag{15}$$

where $N_I = K_I/\sigma_0 \sqrt{\pi a}$; $N_{II} = K_{II}/\sigma_0 \sqrt{\pi a}$; $\sigma_0 = P/\pi R$; P = load per unit length; R = radius of the cylindrical specimen; L = length of the cylindrical specimen; T_i and S_i are constant coefficients; and A_i and B_i are angular constants based on the angle between the crack plane and the loading plane. N_I and N_{II} are normalized stress intensities in the normal and shear, respectively. The angle θ is the angle between the initial crack plane and the loading plane. When this angle is zero, as illustrated in Fig. 23, fracture is in pure tension (Mode I), and hence, $N_{II} = 0$, and N_I is approximated by the fourth degree polynomial:

$$N_I = 1.00415 - 0.0844\left(\frac{L}{a}\right) + 2.077\left(\frac{L}{a}\right)^2 - 1.66\left(\frac{L}{a}\right)^3 \tag{16}$$

Materials Used

Table 9 highlights information on the constituent materials used to make Portland cement concrete for the indirect tensile fracture test. For aggregates, the saturated-surface-dry (SSD) specific gravity, loose unit weight, and the percent solids were measured. Properties for the cement, flyash, and silica fume were obtained from the manufacturer. Table 10 indicates the concrete mix design used for all the indirect tensile fracture tests.

Specimen Preparation

For the Indirect tensile fracture tests, concrete was cast at a temperature of 21.1°C and a relative humidity of approximately 50%. All specimens were cast in cardboard cylindrical molds which were 15 cm high and 15 cm in diameter. A notch was created along the axis of the cylindrical specimen by first casting a high-density polyethylene strip with the concrete. Then the polyethylene strip was carefully pulled out of concrete after a few hours when the concrete was set.

TABLE 9. Data on Materials Used for Indirect Tensile Fracture Tests

Constituent Description	Material Type	Source	Specific Gravity
Coarse Aggregate	Siliceous River Gravel	Pioneer Arena Plant	2.60
Coarse Aggregate	Crushed Limestone	Vulcan Materials Cancun, Mexico	2.55
Fine Aggregate	Siliceous Sand	Pioneer Arena Plant	2.65
Cement	Type I	Holnam Galena Park, Texas	3.1
Fly-Ash	Class C	JTM Industries Stafford, Texas	2.6
Silica Fume	Uncompacted	Fritz Chemical Co. Dallas, Texas	2.3

The molds were originally long, but they were cut in half because of the difficulty in keeping the polyethylene strip in place during casting. Nevertheless, a special attachment was designed to keep the top end of the plastic strip in place during casting. Under these conditions, the best time to pull out the polyethylene strip was 5 to 6 hours after casting. Once the strips were removed, the concrete cylinders were

transported to a moist curing room and cured at a temperature of 21.1 °C until the time of the test. The load was applied by way of a 3.1 mm, 2.5 cm wide plywood strip.

TABLE 10. Concrete Mix Design Used for Indirect Tensile Fracture Tests

Constituent	Siliceous River Gravel as Coarse Aggregate	Siliceous River Gravel as Coarse Aggregate
Yield (m^3)	19.7	19.9
Coarse Aggregate	2033	2033
Fine Aggregate	921	921
Portland Cement	451	451
Fly-Ash	97	97
Free Water (gallons)	30	30
Water/Cement Ratio	0.46	0.46

(All proportions are by mass, in lbm)

The polyethylene strips were 3.1 mm thick, and the initial crack length was taken at 3.2 cm. This provided a ratio between the initial crack length and characteristic dimension (2a/2R) of 0.2083.

Phase I of the Indirect Tensile Test of Notched Cylinders

Test Factorial

Split tensile fracture tests were performed in two phases. The test factorial for Phase I is given in Table 11. In Phase I, the effect of gradation on the critical stress intensity factor of concrete (K_{IC}) was investigated, and two types of gradations, well graded and gap graded, were used along with two maximum coarse aggregate sizes (3.8 cm and 1.9 cm). Data from the tests on concrete with these gradations are shown in Table 12. A well-graded aggregate is one that has a bell shaped curve as shown in Fig. 24(a). As shown in Fig. 24(b), aggregate is labeled as gap-graded when the intermediate

aggregate sizes are deficient and the gradation curve is not bell-shaped. In the test factorial, a letter 'x' in a cell is an indication that the test was performed.

TABLE 11. Test Factorial for Phase I of the Indirect Tensile Fracture Tests

Gradation	Maximum Coarse Aggregate Size (cm)	
	1.9	3.8
Well-Graded	x	x
Gap-Graded	x	x

Results

Concrete cylinders from Phase I of the indirect tensile fracture tests were tested 3 and 7 days after casting. Two replicates were used for each test. A summary of the results on fracture toughness is shown in Table 13. A detailed listing of data, including those for replicate samples, is presented in Appendix C. The results from Table 13 were subsequently analyzed as a ratio of K_{IC} for the gap-graded and well-graded concrete. Those results shown in Table 14 indicate that for both aggregate types, the gap-graded mix has a higher critical stress intensity factor (K_{IC}) when compared with the well-graded mixture. Also, the K_{IC} ratio decreased with decreasing maximum aggregate size, indicating that as the maximum aggregate size decreases, the effect aggregate gradation has on K_{IC} decreases. This may be an important observation in enforcing the aggregate gradation specifications for concrete with different maximum coarse aggregate sizes.

Phase II of the Indirect Tensile Test of Notched Cylinders

Test Factorial

For the second phase of the indirect tensile fracture test, several factors including coarse aggregate type, curing temperature, coarse aggregate treatment, and the paste additive were investigated. The test factorial and gradation data for Phase II of the indirect tensile fracture test are given in Tables 15 and 16, respectively.

TABLE 12. Aggregate Gradation Data for Phase I of the Indirect Tensile Fracture Test on Concrete with Different Aggregate Gradations

ASTM C-33 Gradation No.	467	467	67	67
Max. Aggregate Size (cm)	3.8	3.8	1.9	1.9
Coarse Aggregate				
Sieve Size/ID	Gradation (Percent Retained on Each Sieve)			
	Well-Graded	Gap-Graded	Well-Graded	Gap-Graded
37.5 mm	0	0	0	0
25 mm	10	0	0	25
19 mm	18	10	10	13
12.5 mm	22	25	28	20
9.5 mm	25	30	28	25
4.75 mm	20	29	25	15
2.36 mm	5	4	9	2
1.18 mm	0	2	0	0
Fine Aggregate				
Sieve Size/ID	Gradation (Percent Retained on Each Sieve)			
	Well-Graded	Gap-Graded	Well-Graded	Gap-Graded
2.36 mm	24	7	14	7
1.18 mm	26	21	30	21
600 μm	20	27	24	28
300 μm	17	32	20	31
150 μm	13	13	12	13
-150 μm	0	0	0	0

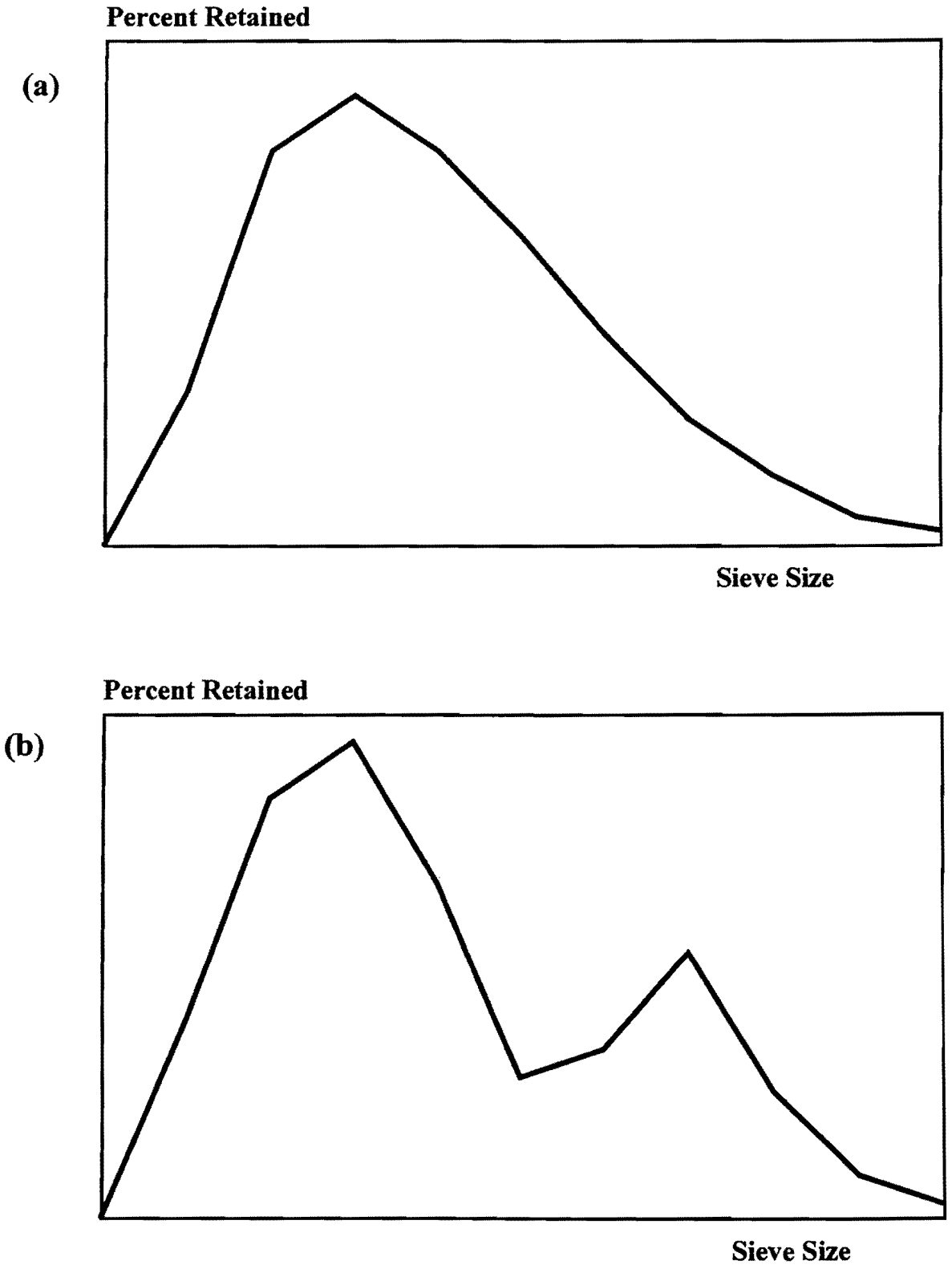

FIG. 24. Illustration of Well-Graded and Gap-Graded Aggregate Gradation Curves Used in Laboratory Experiments

TABLE 13. Results on Critical Stress Intensity Factor From Phase I of Indirect Tensile Fracture Tests for Concrete With Different Gradations

Coarse Aggregate Type	Max. Aggregate Size: Gradation	Critical Stress Intensity Factor (K_{IC})*	
		3-Day	7-Day
Siliceous Gravel	38 cm:Gap-Gr.	487.02	609.03
	38 cm:Well-Gr.	455.03	496.60
	19 cm:Gap-Gr.	468.49	622.10
	19 cm:Well-Gr.	483.00	606.39
Limestone	38 cm:Gap-Gr.	555.06	651.26
	38 cm:Well-Gr.	586.86	619.59
	19 cm:Gap-Gr.	496.99	593.73
	19 cm:Well-Gr.	589.50	613.92

* Fracture Toughness is calculated in mpa · $\sqrt{m}$.

TABLE 14. Results on Ratio of Critical Stress Intensity Factors for Different Gradations From Phase I of Indirect Tensile Fracture Tests

Coarse Aggregate Type	Max. Aggregate Size (m)	K_{IC} (Gap-Graded) / K_{IC} (Well-Graded)	
		3-Day	7-Day
Siliceous Gravel	38	1.07	1.23
	19	0.97	1.03
Limestone	38	0.95	1.05
	19	0.84	0.97

TABLE 15. Test Factorial for Phase II of the Indirect Tensile Fracture Tests

Test Factor		Coarse Aggregate Type	
		Siliceous Gravel	Limestone
Curing Temperature	21.1°C	x	x
	40.5°C	x	-
Aggregate Treatment	Untreated	x	-
	Lime Treated	x	-
Paste Additive	No Additive	x	-
	Silica Fume	x	-

TABLE 16. Gradation Used for Phase II of the Indirect Tensile Fracture Tests

ASTM C-33 Gradation No.	467
Gradation	Well-Graded
Max. Aggregate Size (mm)	38
Coarse Aggregate	
Sieve Size/ID	Percent Retained on Each Sieve
37.5 mm	0
25 mm	10
19 mm	22
12.5 mm	24
9.3 mm	24
4.75 mm	16
2.36 mm	4
1.18 mm	0
Fine Aggregate	
2.36 mm	18
1.18 mm	26
600 μm	22
300 μm	18
150 μm	14
-150 μm	2

Results

Concrete cylinders for Phase II of the split tensile fracture tests were tested 12, 24, and 72 hours after casting. All specimens were cured in a moist room at the

temperatures indicated. The tests at the ages of 12 and 24 hours were tested with three replicates, and the test after 72 hours had 2 replicates. Results from these tests are presented in Table 17. The same results are illustrated in Fig. 25. A more detailed form of these results, including those results for replicate samples, is presented in Appendix C. In Fig. 25, critical stress intensity factors (K_{IC}) calculated at 12, 24, and 72 hours of age are illustrated, and the following labels are used.

1. SRG_LTC: Concrete with untreated siliceous gravel, cured at 21.1°C
2. SRG_CH: Concrete with lime treated siliceous gravel, cured at 21.1°C
3. SRG_HTC: Concrete with untreated siliceous gravel, cured at 40.5 °C
4. CLS_LTC: Concrete with crushed limestone, cured at 21.1°C

TABLE 17. Summary of Results From Phase II of Indirect Tensile Fracture Tests on Concrete

Age of Concrete (Hours)	Critical Stress Intensity Factor (K_{IC})*			
	Siliceous River Gravel Coarse Aggregate			Limestone Coarse Aggregate
	Moist-Cured at 21.1°C (SRG_LTC)	Moist-Cured at 40.5°C (SRG_HTC)	Moist-Cured at 21.1°C, with Lime-Treated Aggregate (SRG_CH)	Moist-Cured at 21.1°C (CLS_LTC)
12	168.74		231.2	122.9
13		745.7		
24	646.42	1262.9	768.4	
26				597.5
72	1417.8	1672.5	1544.1	1192.7

* Critical stress intensity factor is calculated in mpa · $\sqrt{m}$.

The results presented in Fig. 25 can be summarized as follows:

1. For concrete with untreated siliceous gravel and untreated limestone (both cured at 21.1 °C), siliceous river gravel shows a higher critical stress intensity factor (K_{IC}) for the ages of concrete considered.

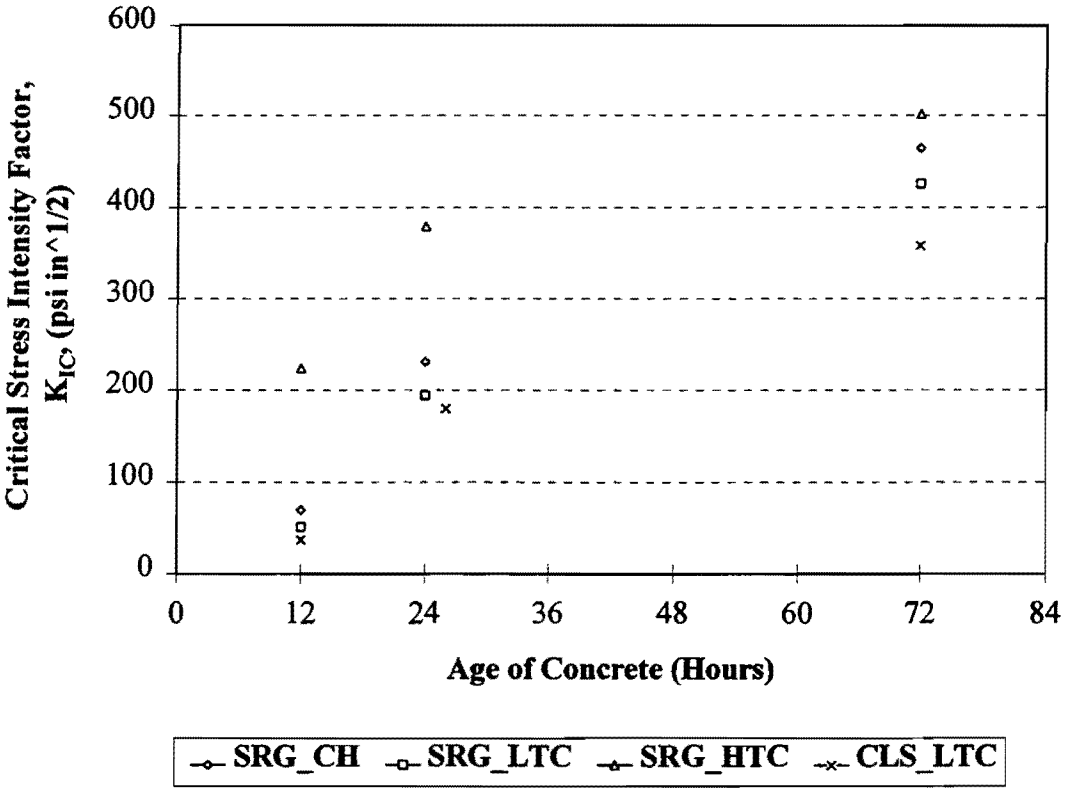

FIG. 25. Critical Stress Intensity Factors From Phase II of the Indirect Tensile Fracture Test (1 psi - √in - 1.099 mpa - √m)

2. The curing temperature appears to have a significant effect on K_{IC} of concrete made with siliceous gravel. The higher curing temperature provided a significantly higher K_{IC} during the first 7 days of concrete age. However, it is expected that this difference will diminish with time and the ultimate strength of concrete cured at different temperatures will be fairly close.
3. There is a somewhat significant increase in K_{IC} when siliceous gravel coarse aggregate is treated with lime at 21.1 °C curing.

Analysis of Fracture Surface Area of Failed Indirect Tensile Fracture Test Specimens

Several cylindrical test specimens from Phase II of the indirect tensile fracture test were used to evaluate their fracture surfaces. The failed surfaces of cylindrical specimens, which were square in shape, were digitized, and a special computer based technique developed at the Texas Transportation Institute was used to calculate the plane surface areas of different components within the fracture surface. These different components were failures at the coarse aggregate-cement paste interface, mortar and coarse aggregate particles. The area of air voids on the failure plane was also measured. Results from these measurements are presented in Table 18. The same results are illustrated in Fig. 26. Except for the high temperature cured specimens denoted by HT, all the other specimens were cured at 21.1 °C.

TABLE 18. Results From the Analysis of Fracture Surface Area of Indirect Tensile Fracture Test Specimens

	Age (Hrs)	Fracture Surface Area (cm^2)					
		SRG LT	SRG HT	SRG SF	CLS LT	CLS HT	CLS SF
Agg. Breaks	12	8.13	4.00	1.94	24.45	10.77	5.10
	24	9.10	9.03	5.35	10.52	39.16	14.06
Interface	12	62.65	73.48	78.97	47.71	56.39	75.81
	24	66.13	66.39	68.77	67.16	46.39	58.65
Air Voids	12	0	1.23	1.23	0	0	1.48
	24	0.45	0	0.97	1.74	0.58	1.61
Mortar	12	113.03	105.10	101.74	84.71	116.64	101.42
	24	108.19	108.52	108.77	104.45	97.74	109.55

Fig. 26 shows that for early-age concrete, the interfacial failures in the fracture surface could be as much as 30-35%. Even at the early age of 12-24 hours after casting the specimens, there are some breakages of aggregate particles, but the weakness at the interface between the aggregate particles and the cement paste is clearly evident. As one might expect, there were more failures of limestone aggregate particles. At the early

ages of 12 hours and 24 hours, the area of coarse aggregate-cement paste interface failure was almost the same for all four cases considered. Fig. 27 compares the interfacial failures for concrete made with crushed limestone coarse aggregate. The area of interfacial failure was observed to reduce with the increasing age of concrete (from 12 hours to 24 hours). It can be clearly seen that the area of interfacial failure is significantly lower for specimens cured at the higher temperature. The addition of silica fume as a paste additive did not appear to have increased the interfacial strength for limestone concrete within the first 24 hours of age. For concrete made with siliceous river gravel coarse aggregate, Fig. 28 indicates that even though the critical stress intensity factor (K_{IC}) of concrete cured at high temperature increased significantly, the interfacial bond strength does not appear to have increased noticeably with the increase in curing temperature. The effect of silica fume as a paste additive is also not clearly evident, and in fact, the interfacial areas seem to have increased with the addition of silica fume. From Fig. 29, it is clear that for concrete within 24 hours of casting, crushed limestone shows a higher incidence of interfacial failures compared to concrete with siliceous river gravel coarse aggregate. The primary conclusions to be drawn from this analysis of failure planes from indirect tensile fracture tests can be summarized as follows:

1. Limestone coarse aggregate results in better interfacial strength at the aggregate-cement paste interface. However, up to 24 hours after casting, interface in limestone concrete appears to be weaker than for siliceous gravel concrete. This may be because it takes more time for limestone aggregate to develop chemical reactions with the cement.
2. Limestone is more responsive to increases in the curing temperature (from 21.1 °C to 40.5 °C), resulting in a reduction of interfacial failure area of approximately 30%. This is much higher compared to siliceous gravel concrete where the interfacial failures remained almost the same.
3. It has been shown in prior research that the addition of silica fume increases the interfacial bond strength considerably. However, it does not appear to be the case here, at least during the first 24 hours.

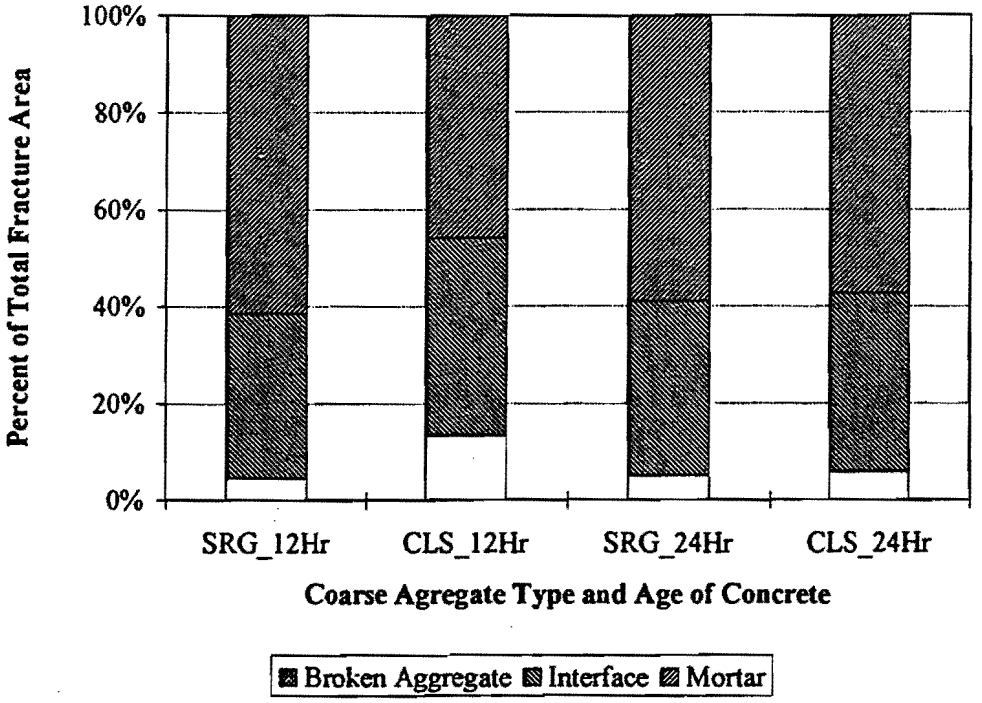

FIG. 26. Comparison of the Distribution of Fracture Surface Areas on Failure Surfaces From Indirect Tensile Fracture Tests

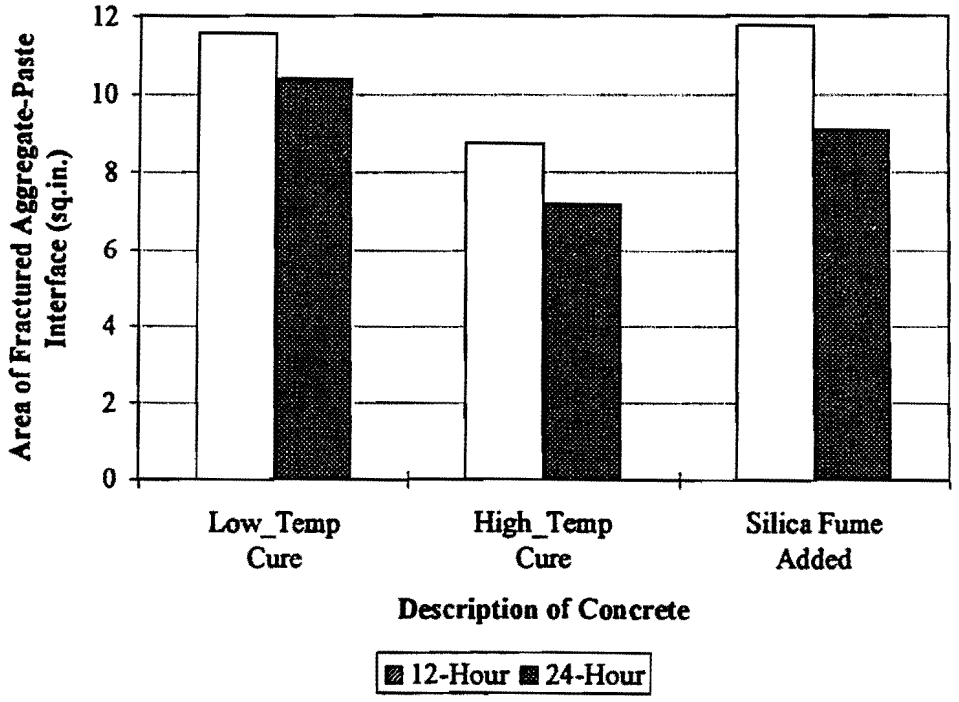

FIG. 27. Comparison of Areas of Interfacial Failure for Three Types of Crushed Limestone Concrete

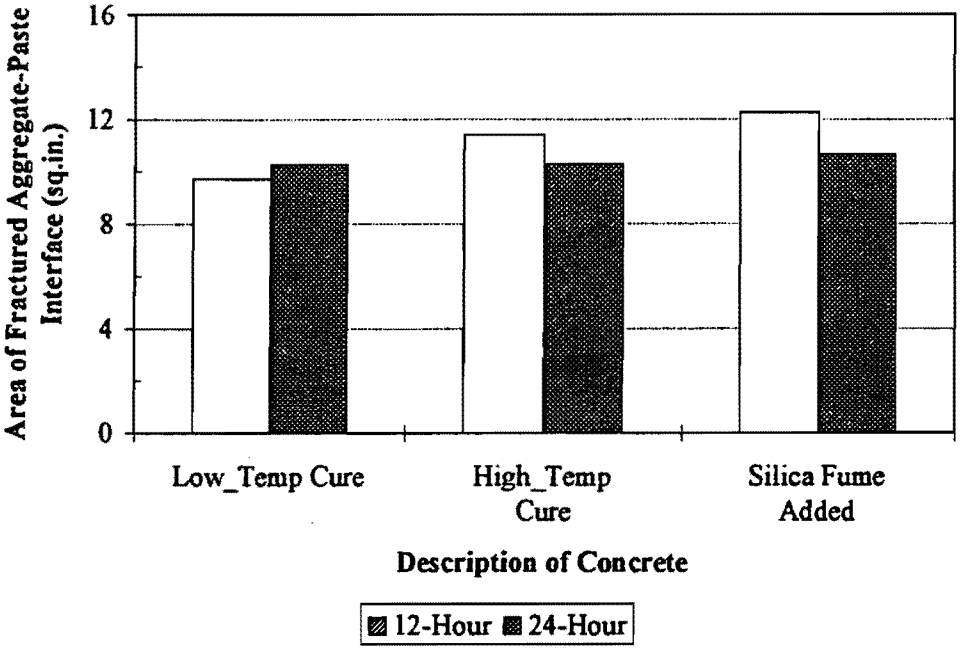

FIG. 28. Comparison of Areas of Interfacial Failure for Three Types of Siliceous River Gravel Concrete

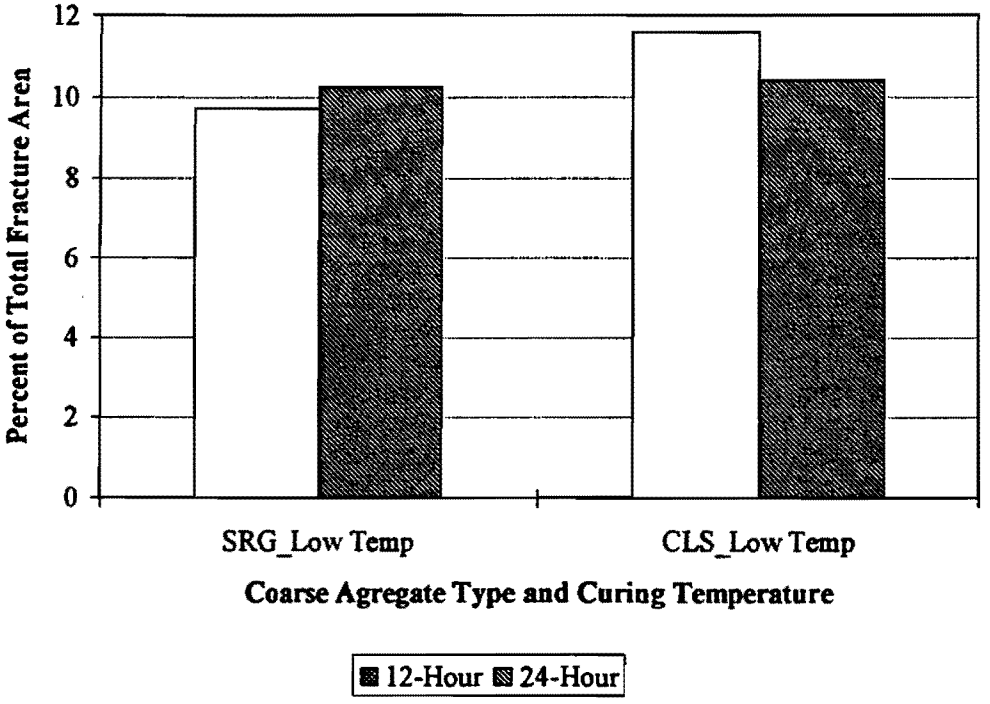

FIG. 29. Comparison of Fractured Interfacial Area of Concrete Cured at 21.1°C

Size-Effect Beam Fracture Test

The size-effect fracture test on notched concrete beams outlined in the RILEM recommendations (RILEM 1990) was used to perform the size-effect beam tests on Portland cement concrete made with different coarse aggregates. The test was performed on three sizes of beams. Test configuration for the size-effect test of notched beams is illustrated in Fig. 30. As discussed earlier, to maintain geometric similarity, the ratios of span/depth, length/depth, and initial crack length/depth for beams of all sizes were maintained the same in specimens of all three sizes.

The following equations represent the calculation procedure for the size-effect beam test as recommended by RILEM. Eq. 17 provides a corrected maximum load allowing for the self-weight of the beam.

$$\Pi_{0_\varphi} = \Pi_\varphi + \frac{2\lambda_\varphi - \Lambda_\varphi}{2\lambda_\varphi}\mu_\varphi\gamma \quad (\varphi = 1,2,...,\nu) \tag{17}$$

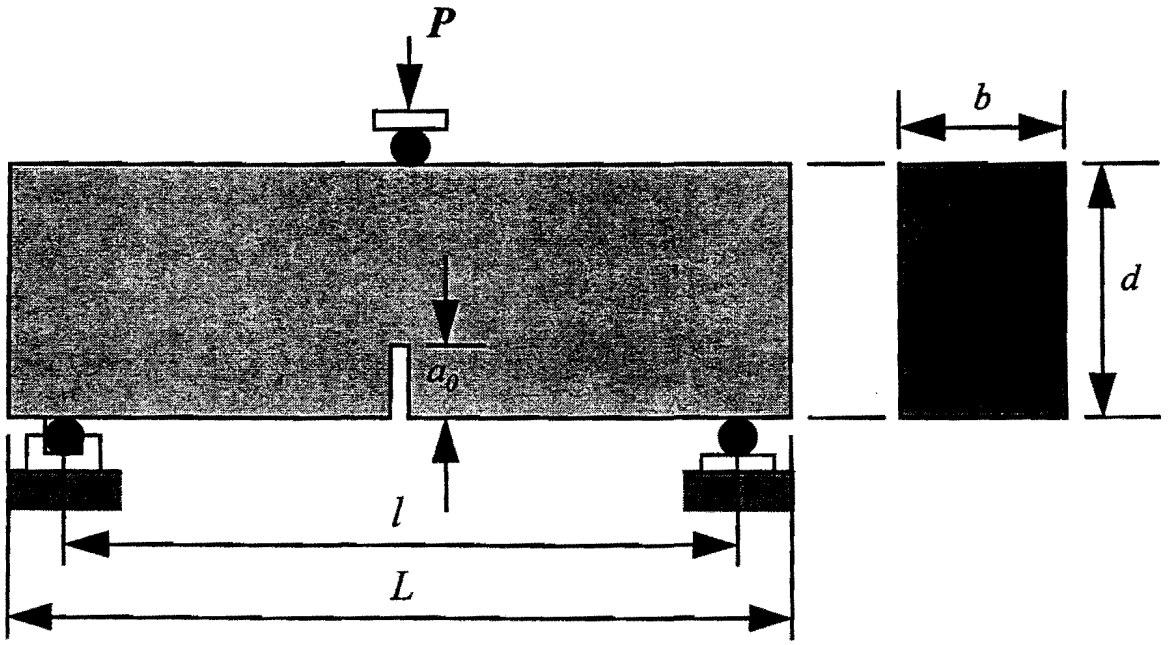

FIG. 30. Schematic Diagram of Size-Effect Beam Test Configuration

In Eq. 17, P = maximum load; P_0 = corrected maximum load; l = test span for the beam; L = length of the beam, m = mass of the beam; and g = gravitational constant. The subscript j is an identifier for the beam size since a number of beam sizes are used. Based on the results from the test, the quantities Y and X, as shown in Eq. 19 are calculated and plotted such that a straight line is obtained. Then A = slope of the straight line; and C = intercept of the straight line on the Y-axis.

$$\Psi_{\varphi} = \left(\frac{\beta \delta_{\varphi}}{\Pi_{0_{\varphi}}} \right)^2 \quad , \quad \Xi_{\varphi} = \delta_{\varphi} \tag{18}$$

$$\Psi = A\Xi + X \tag{19}$$

From the plot between Y and X indicated above, the fracture toughness (K_{If}), brittleness number (β), and the effective length of the fracture process zone (c_f) can be determined by following the analytical procedure indicated below. All three properties mentioned above can be construed as material properties, since a range of specimen sizes have been included in the testing program. As it was shown earlier in this chapter, fracture toughness of the concrete can be calculated with the strain energy release rate (G_f) and the elastic modulus (E) of the material, using the expression given in Eq. 20. To calculate K_{If}, first, G_f is calculated using Eqs. 21 and 22.

$$K_{I\phi} = \sqrt{\frac{\Gamma_{\phi}}{E}} \tag{20}$$

$$\Gamma_{\phi} = \frac{\gamma(\alpha_0)}{E \cdot A} \tag{21}$$

$$\gamma(\alpha_0) = \left(\frac{\lambda}{\delta}\right)^2 \pi \alpha_0 [1.5\ \Phi(\alpha_0)]^2 \tag{22}$$

α_0 is the ratio between the initial crack length (a_0) and the depth (d) of the beam. $F(\alpha_0)$ is calculated using an expression which depends upon the test span/depth ratio (l/d) of the beam. Expressions such as these are derived from analytical methods. In this test, a span/depth ratio of 2.5 was used. Therefore, the expression for $F(\alpha_0)$ is given by:

$$\Phi_{2.5}(\alpha_0) = \frac{1.0 - 2.5\alpha_0 + 4.49\alpha_0^2 - 3.98\alpha_0^3 + 1.33\alpha_0^4}{(1-\alpha_0)^{1.5}} \tag{23}$$

The brittleness number (β) and the effective length of the fracture process zone (c_f) of the concrete is calculated by extending this procedure. In order to characterize the brittleness of structural response, a variety of brittleness numbers have been proposed. In Bazant's size effect law, this brittleness number is defined as the ratio between the depth of the beam (d) and the characteristic structural dimension (d_0). The expression used to calculate the brittleness number is given by Eq. 24. The brittleness number calculated in this fashion is a measure of how brittle the material is. Since the characteristic structural dimension is accounted for in the brittleness number, it is independent of the size and shape of the tested specimen. As indicated in Eq. 24, the brittleness number is a function of the crack size. A low brittleness number would suggest that the material is more ductile in nature.

The effective length of the fracture process zone calculated using this procedure is for a specimen of infinite size. This parameter is an indication of the degree to which micro-cracking ahead of the primary crack can occur in concrete. According to Eq. 24, a larger brittleness number and a smaller effective length of process zone (c_f) are synonymous. A large c_f value would indicate that there is a larger process zone in the

synonymous. A large c_f value would indicate that there is a larger process zone in the material that absorbs more energy which would have otherwise expended to propagate the primary crack. This means that the material would then be less brittle (ductile).

$$\beta = \frac{\gamma(\alpha)\ \delta}{\gamma'(\alpha)\ \chi_\phi} \tag{24}$$

$$\chi_\phi = \frac{\gamma(\alpha)}{\gamma'(\alpha)}\left(\frac{X}{A}\right) \tag{25}$$

Table 19 shows the data on beam sizes and the ultimate load measured on each beam at 24 hours of age. The initial crack length/beam depth ratio (a_0/d) for this test was taken at 0.25. Results from the RILEM procedure are presented in Tables 20, 21, 22, and 23. The same results are illustrated in Fig. 31.

TABLE 19. Data From Size-Effect Beam Test on Concrete

Width of Beam (cm)	Depth of Beam (cm)	Replicate Number	Ultimate Load (lbf)	
			Concrete With Siliceous River Gravel	Concrete With Crushed Limestone
10.2	8.9	1	2757.9	2451.0
10.2	8.9	2	2402.0	2491.0
10.2	14.0	1	4648.4	2999.0
10.2	14.0	2	4946.4	3963.8
10.2	20.7	1	5253.4	4344.6
10.2	20.7	2	5551.4	4541.6

Note: Mass of loading platen = 4.958 kg

TABLE 20. Results From the RILEM Calculation Procedure of Size-Effect Beam Test for Concrete with Siliceous River Gravel Coarse Aggregate

Depth d (mm)	Width b (mm)	Length L (mm)	Test Span ℓ (mm)	Mass of Beam m (kg)	Weight of Beam (N)	Max. Load P (N)	Corrected Load P_0 (N)	$\left(\frac{\beta\delta}{\Pi_o}\right)^2$
76.2	101.6	244.5	222.3	5.31	52.10	3167	3190	8.02
88.9	101.6	384.2	349.3	13.11	128.65	4852	4910	8.36
139.7	101.6	571.9	519.9	29.06	285.06	5458	5586	14.31

TABLE 21. Results From the RILEM Calculation Procedure of Size-Effect Beam Test for Concrete with Crushed Limestone Coarse Aggregate

Depth d (mm)	Width b (mm)	Length L (mm)	Test Span ℓ (mm)	Mass of Beam m (kg)	Weight of Beam (N)	Max. Load P (N)	Corrected Load P_0 (N)	$\left(\frac{\beta\delta}{\Pi_o}\right)^2$
76.2	101.6	244.5	222.3	5.31	52.10	2523	2546	12.58
88.9	101.6	384.2	349.3	13.11	128.65	3534	3592	15.61
139.7	101.6	571.9	519.9	29.06	285.06	4497	4625	20.87

TABLE 22. Statistical Parameters for Size-Effect Beam Test Results

Concrete Made With	Coefficient of Determination (R^2) for Model	SEE for Model	Estimate for Constant	Estimate for X-Coefficient	Std. Error of X-Coefficient
Siliceous River Gravel	0.85	1.91	2.2632	0.0547	0.0226
Crushed Limestone	0.99	1.00	6.1727	0.0700	0.0049

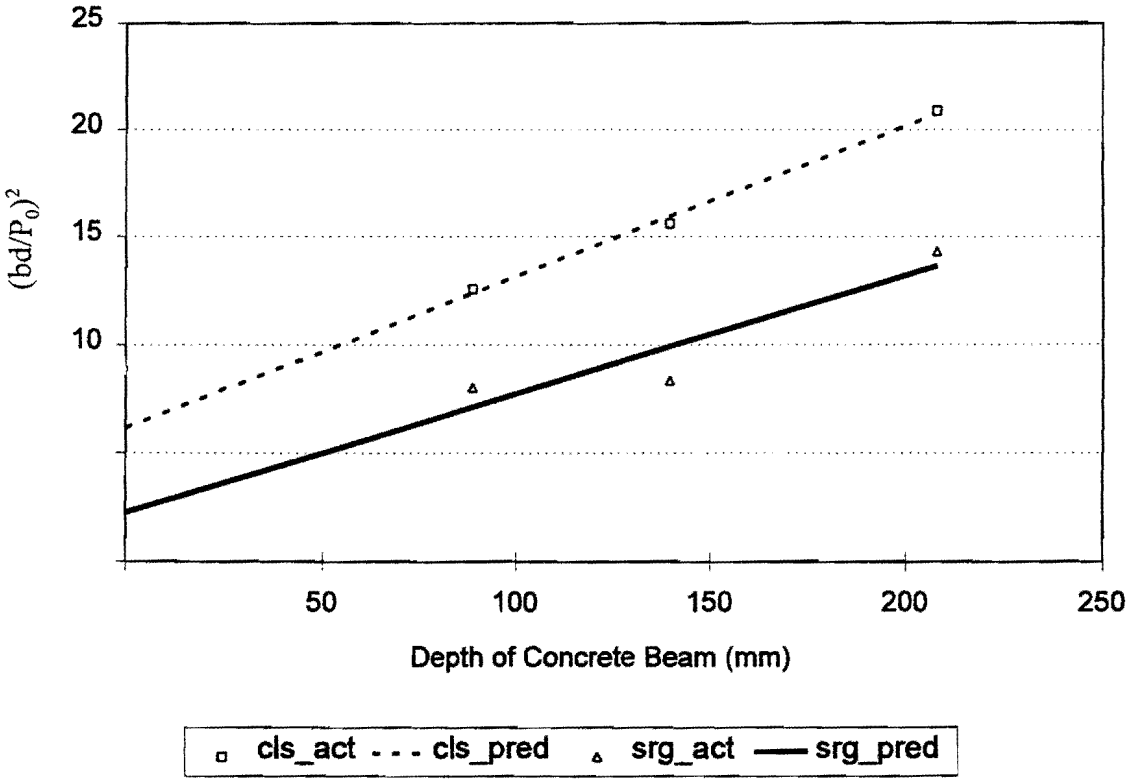

FIG. 31. Results From Size-Effect Beam Test

TABLE 23. Fracture Parameters Obtained From Size-Effect Beam Test at 24 Hours

Parameter	Concrete Made With Siliceous River Gravel	Concrete Made With Crushed Limestone
Fracture toughness, K_{Ip} (MPa √m)	0.41	0.37
Brittleness number, β	3.52	1.65
Effective length of fracture process zone, c_f, (mm)	8.38	17.88

Results given in Table 23 suggest that even though fracture toughness of siliceous gravel concrete and limestone concrete are comparable, significant differences in their

performance may occur due to the differences in the brittleness number and the effective length of the fracture process zone. As shown in Table 23, the brittleness in siliceous gravel concrete is more than twice that of siliceous river gravel, and the effective length of the fracture process zone for limestone concrete is more than twice that for siliceous gravel concrete.

Microscopical Examination of Portland Cement Concrete

Some of the specimens of concrete cylinders used for the split tensile fracture test were subjected to a microscopical examination under the scanning electron microscope (SEM). The scanning electron microscope enables the investigation of concrete microstructure up to magnifications of 5000 and more. Furthermore, these magnified images can be clearly seen, and their most minute details can be recorded. This microscopic examination was undertaken to verify some of the observations made by Graves and Eades (1987) regarding microstructure of Portland cement concrete made using different coarse aggregate types. Due to the solubility of interfacial calcium hydroxide at the aggregate-cement paste interface, no polishing was performed on the samples to be examined. Instead, samples were broken at the interface by manual means such that they would break along the interface.

It was observed that concrete made with siliceous river gravel showed micro-cracks at the aggregate-cement paste interface. No such cracks could be seen for concrete made with crushed limestone. Such micro-cracks were also not visible in concrete made with siliceous river gravel treated with lime. Most importantly, concrete made with siliceous river gravel showed crystallized plates of calcium hydroxide around the aggregate particles at the aggregate-cement paste interface. Fig. 32 is a SEM image of a concrete made with untreated siliceous river gravel under a magnification of 1500. The photograph was taken of the interfacial zone with a coarse aggregate particle (siliceous river gravel) as the backdrop. It can be clearly seen that a very thin layer is present at the interface which has a very distinct morphology from that of the rest of the cement paste. Fig. 33 is a closeup of the interfacial zone (magnification=500) where a

coarse aggregate particle was manually uprooted. The presence of the thin calcium hydroxide shells is quite evident. At some parts of the interface, some of the calcium hydroxide shells have been uprooted, possibly while the aggregate was removed. Fig. 34 is a closeup of the same location as in Fig. 33 but with a higher magnification (x2000).

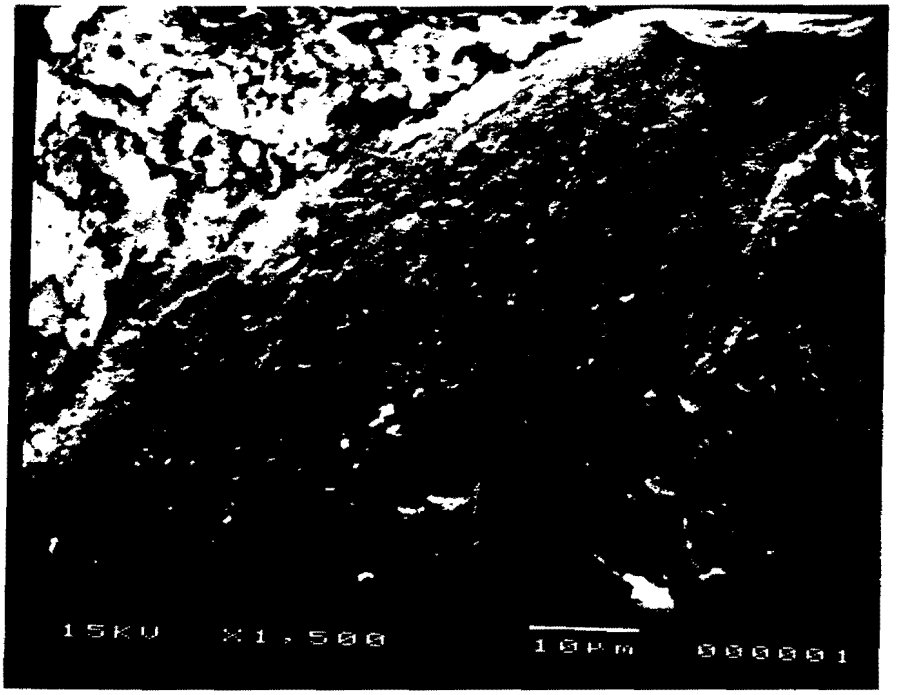

FIG. 32. SEM Image (X1500) Showing Siliceous Gravel Particle and Adjacent Highly Oriented $Ca(OH)_2$ Layer

Fig. 35 is an SEM image (magnification=500) of the surface of a lime treated siliceous river gravel particle. What is very clearly evident in comparing this image with that of Fig. 32 is the smoothness of the untreated siliceous river gravel particle shown in Fig. 32. Fig. 36 shows a crevice where a coarse aggregate particle rested at a magnification of 2000. Even in this instance, it is quite clear when comparing this image with the image in Fig. 34 (same magnification) that the highly oriented calcium hydroxide sheets are not present at the interface. Instead, there appears to be a much rougher irregular texture. Fig. 37 shows the same location as Fig. 36 but at a magnification of 500.

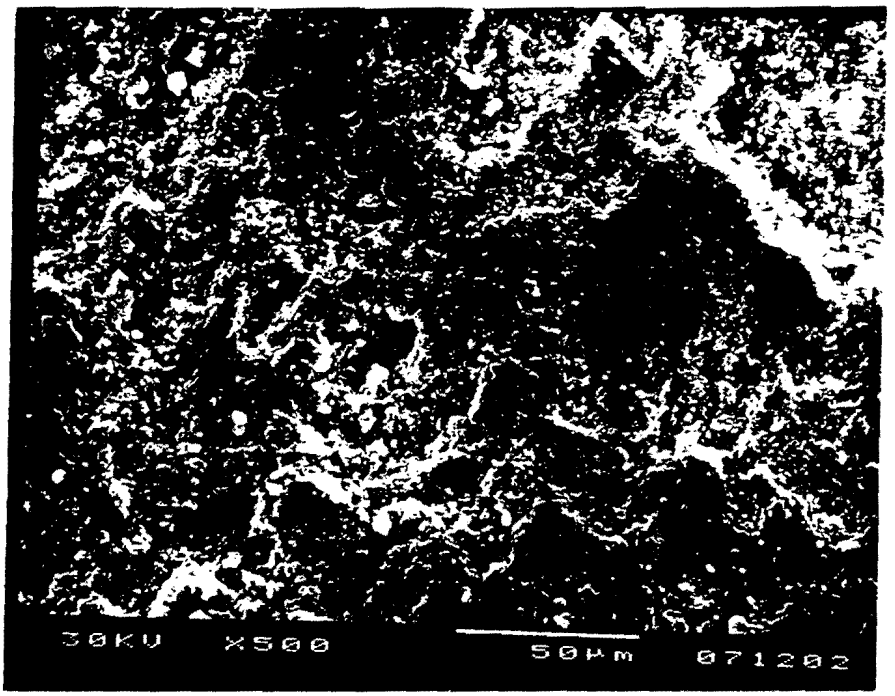

FIG. 33. SEM Image (X500) of Highly Oriented $Ca(OH)_2$ Sheets at the Aggregate-Cement Interface

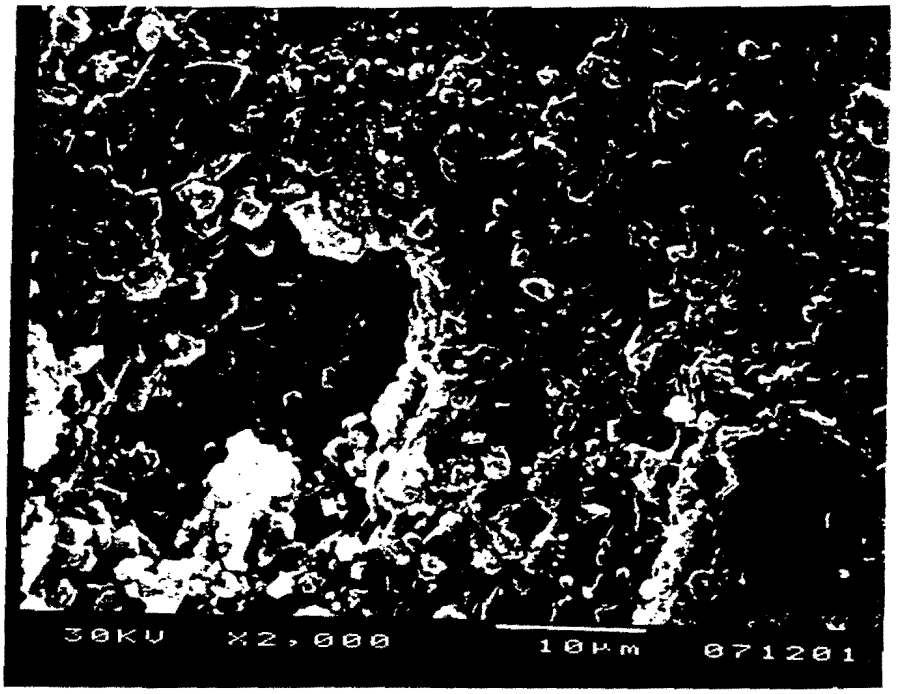

FIG. 34. SEM Image (X2000) of Highly Oriented $Ca(OH)_2$ Sheets at the Same Location as Fig. 33

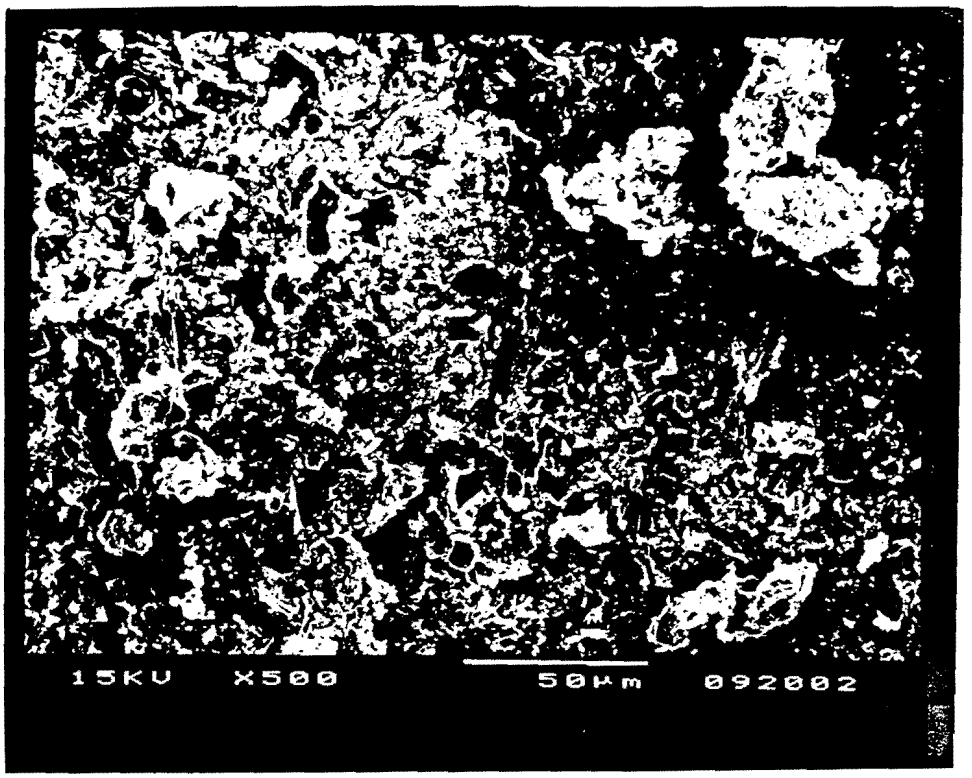

FIG. 35. SEM Image (X500) of the Surface of a Lime Treated Siliceous Gravel Particle

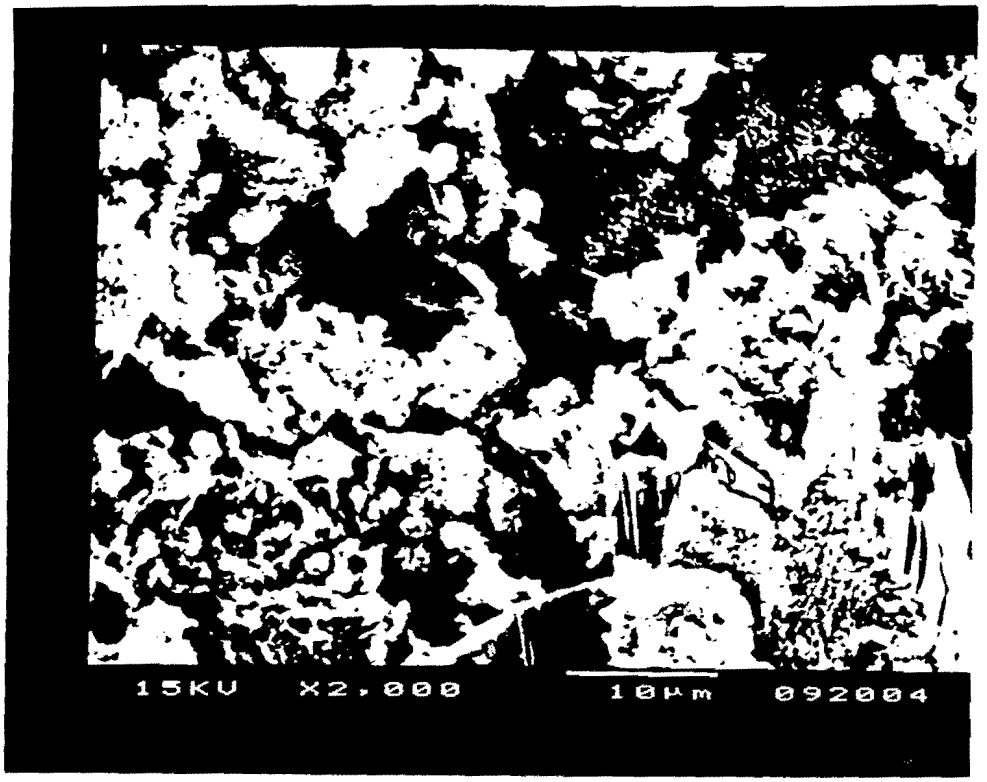

FIG. 36. SEM Image (X2000) of the Same Aggregate Particle Location as in Fig. 35

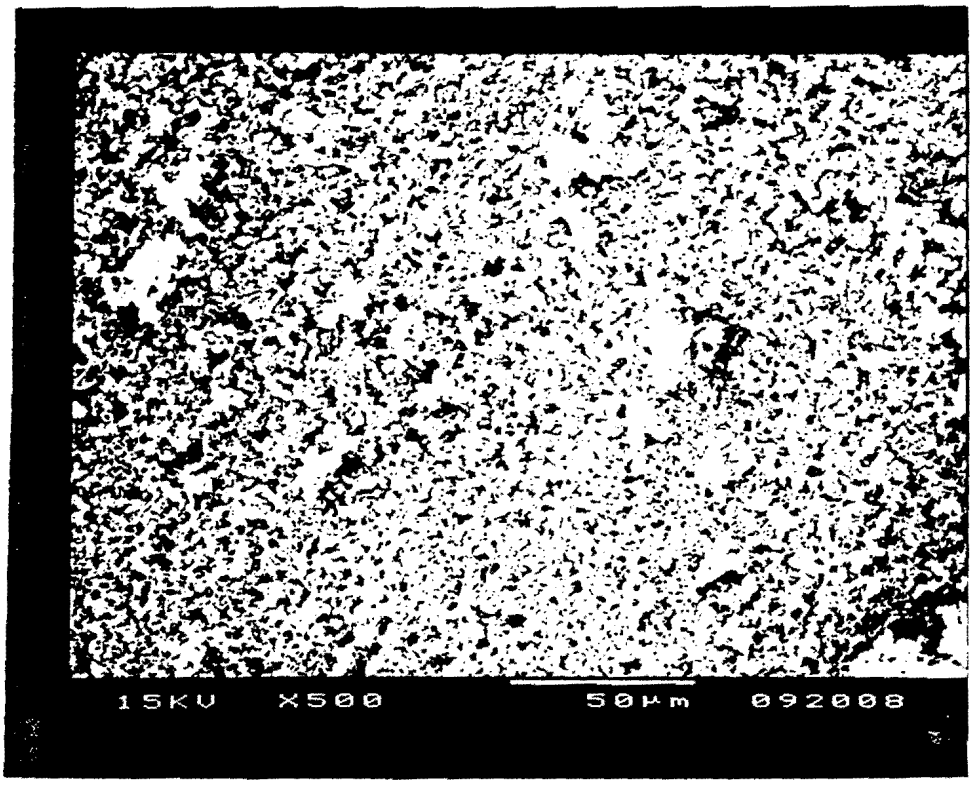

FIG. 37. SEM Image (X500) of the Crevice Where Lime Treated Siliceous Gravel Particle was Located

CHAPTER 5: DELAMINATION OF CONCRETE PAVEMENTS

FACTORS AFFECTING DELAMINATION IN CONCRETE PAVEMENTS

In the discussion of observations from the field survey, it was observed that spalling is the culmination of a form of distress which is initiated very early in the pavement life. This initial form of distress, which is not visible from the pavement surface, was termed a delamination. The occurrence of delaminations is believed to be the result of a number of factors related to both the conditions at the time of paving, as well as conditions afterwards. Field investigation of pavements not yet opened for traffic indicated that initially, these delaminations are present in the form of de-bonding cracks at the interface between aggregates and the cement paste. These de-bonding cracks usually occur near the top of the pavement slab. Eventually, these de-bonding cracks tend to bridge together to form a longer delamination.

The formation of these de-bonding cracks at the interfacial zone between the aggregate particles and the cement paste point to a relationship between the interfacial properties and delaminations. This factor is further accentuated by the high percentage of spall failure along aggregate-cement paste interfaces (Fig. 38). A discussion of the aggregate-cement paste interface was provided in the previous section. It has been shown that there are considerable differences in interfacial properties between siliceous and carbonaceous coarse aggregates. Graves and Eades (1987) showed the presence of micro-cracks at the interface between cement paste and siliceous aggregates such as siliceous sand and granite. They noted that concrete made with carbonaceous aggregates does not show such micro-cracks and attributed the presence of these micro-cracks to the mineralogical nature of these aggregates. Siliceous aggregates have a net negative charge at the surface, and hence, they attract the positively polarized part of the water molecules, thus creating a presence of water around the aggregate particle. Microscopic analysis of concrete undertaken as a part of this study confirmed the presence of sheets of calcium hydroxide around the siliceous aggregate particles. It is believed that these

sheets of calcium hydroxide cause the interfacial zone to be weaker than the rest of the concrete.

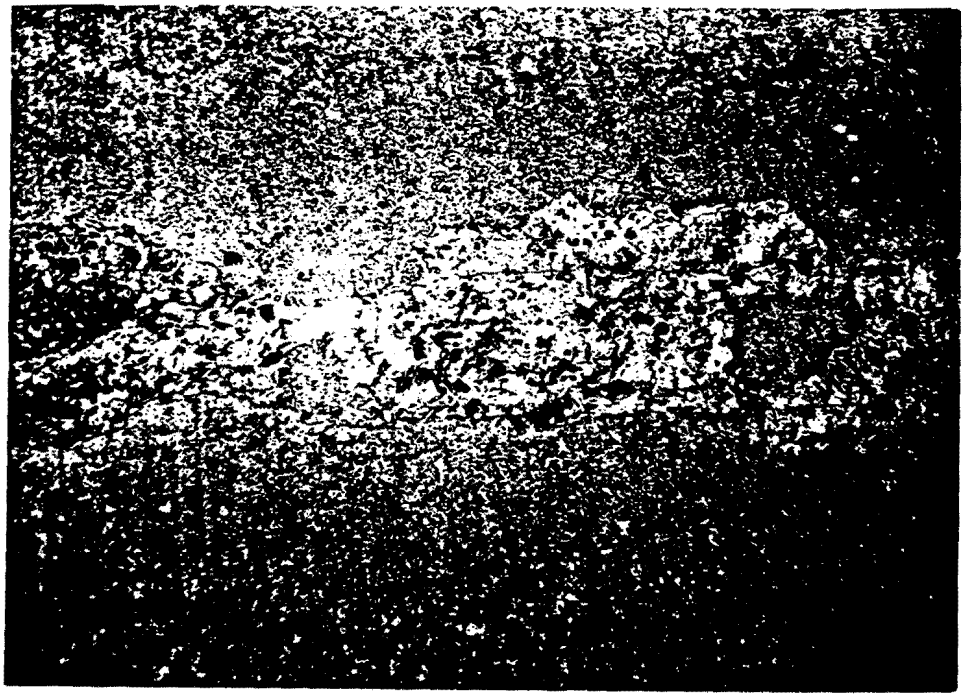

FIG. 38. A Close-Up Look at the Failure Plane of a Spall, Indicating a High Degree of Interfacial Failure

Another factor that may be affecting the delaminations is the anisotropy in concrete. Preliminary fracture tests performed on concrete beams as a part of this study showed evidence of the anisotropic effects of concrete on its strength. It is believed that a primary reason for this anisotropy is the bleeding of concrete. Bleeding is defined as the process of settlement of solids and expulsion of water within fresh concrete (Mindess and Young 1981). When bleeding is mentioned, the common perception is regarding the bleed water collected at the top of a horizontal concrete surface. Hoshino (1989) observed that bleeding water rising to the surface is only a fraction of the amount of water moving inside concrete. Hoshino measured bleeding water according to ASTM

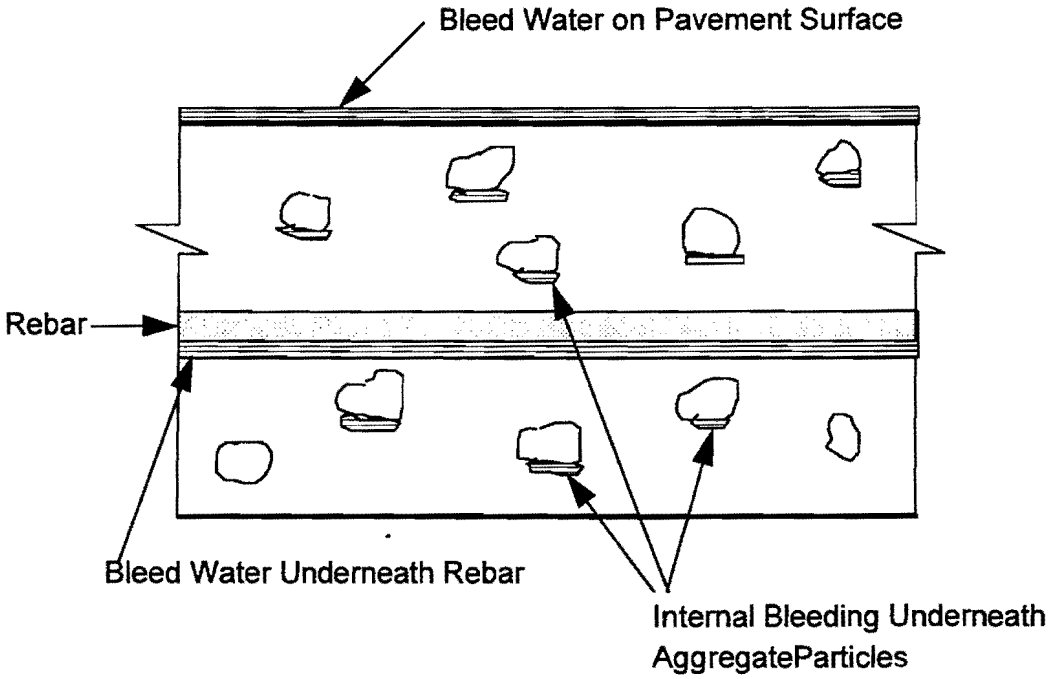

FIG. 39. Different Types of Bleeding in a Concrete Pavement

243-55T. Fig. 39 illustrates different types of bleeding that can occur in a Portland cement concrete pavement slab.

Studies performed by Hoshino (1989) showed how the internal bleeding rate affects the strength of concrete. Hoshino made the following important observations based on his study:

1. With an increase in the size of the coarse aggregate, compressive strength of the concrete decreases.
2. With an increase in the size of the coarse aggregate, the amount of bleeding water decreases.
3. The amount of bleeding water was least in mortar paste containing a cube-shaped special aggregate used in the study. Cube-shaped aggregates caused more seepage water to be retained within the concrete than spherical aggregates did.

The cubic model aggregate was used to investigate the effect aggregate shape has on bleeding.

4. When concrete made with siliceous gravel and crushed stone were compared, crushed stone concrete was found to produce less bleed water.
5. The amount of bleed water increased with increasing height of the specimen.
6. For any water-cement ratio, the strength of concrete specimens in a section closest to the top surface is approximately inversely proportional to the amount of bleed water.
7. When measured at the same horizontal level, the strength of concrete at any water/cement ratio decreased with the increase of bleeding rate.

These observations show very clearly how the strength of concrete close to the surface of the pavement can be affected by the amount of bleed water. Hoshino also observed that the residual water from bleeding tends to stay on the lower surface of the aggregate particles and has a large influence on the strength. Also, siliceous aggregates attract water molecules due to their negative surface polarity. Both these factors may strongly point to the formation of highly oriented calcium hydroxide sheets, particularly underneath the larger aggregate particles in concrete closest to the top surface.

PREDICTION OF THE OCCURRENCE OF DELAMINATIONS BY EARLY-AGE STRESS ANALYSIS OF CONCRETE PAVEMENTS

Field studies undertaken in this research have shown that the formation of de-bonding cracks or delaminations in concrete pavements begin even before the pavement is opened for traffic. Therefore, it is clear that these de-bonding cracks or delaminations may be caused by some means other than traffic. Most likely, such damage is caused by stresses generated due to the environmental conditions the pavement is subjected to, particularly during the early part of its life. Observations made at the CRCP test section in Cypress, Texas, showed that parts of the test section where the curing compound was not applied for up to one hour after paving have signs of spalling earlier than in other areas on which the curing compound was applied immediately after paving. This shows

that the environmental exposure at a very early age of the pavement may be crucial for the subsequent well being of the pavement. If the pavement section can be shielded from extreme environmental conditions such as high temperatures, high wind velocities, and very low relative humidities, it is likely that the pavement will not have as many delaminations, and as a result, will not have as much spalling.

Based on the field observations of this research, spalling is considered as a process where the pavement is first delaminated very close to the surface (a sub-surface flaw), and the delamination eventually propagates to the surface causing a visible spalling distress. These delaminations are believed to occur at a very early-age in the life of the pavement, possibly as early as during the first few days after paving. The depth of these delaminations are approximately 2-4 cm from the pavement surface. Measurement of pore humidity inside the concrete pavement using techniques developed at the Texas Transportation Institute showed that these pore humidities are distributed across the depth of the pavement such that there is a high pore humidity gradient closer to the top of the pavement surface. A schematic diagram of such a distribution is shown in Fig. 40.

It is imperative at this point to investigate whether these moisture gradients near the surface of the pavement slab can actually generate stresses large enough to create flaws (delaminations) in the concrete. There is very little research available at this time regarding methods by which early age analysis of concrete pavements can be achieved. A finite element computer program developed at the Texas Transportation Institute (Kadiyala 1992) based on a moisture diffusion numerical model developed by Gay (1994) has made it possible to analyze early age concrete pavements. This numerical model incorporates both shrinkage and creep of early age concrete pavements. A sensitivity analysis was performed to predict stresses caused by early-age shrinkage and creep in concrete pavements. Results from this analysis were compared with strengths obtained from laboratory data.

Factors Affecting Pore Humidity

There were a number of factors investigated regarding their effects on spalling. Mentioned earlier, a number of factors come into play in the analysis to predict spalling. These factors include the following:

1. design factors such as the pavement thickness, reinforcement and the subbase conditions.
2. materials related factors such as the cement factor, water-cement ratio aggregate properties, moisture diffusivity of concrete, and compressive strength of concrete.
3. construction factors such as the time and season of paving and the type of curing compound used.
4. ambient conditions during the early ages of the pavement.

Design factors such as the reinforcement and subbase primarily govern the restraint in the pavement for shrinkage. Thickness of the pavement slab will affect the pore humidity distribution and, hence, the shrinkage strain. After the delaminations are formed, the subbase type will have an effect on the bending stresses within the pavement caused by traffic loads. As it was suggested by Zollinger and Barenberg (1990), these bending stresses may have an influence on the spalling stresses. Mix design parameters have a direct bearing on the magnitude of the shrinkage strain created in the pavement. When the cement factor is high or when the water/cement ratio is high, the shrinkage also will be high. The coarse aggregate acts as a hindrance to the shrinkage of the concrete. This obstruction to shrinkage will create some stresses within the concrete matrix, but in the absence of the aggregate, larger shrinkage strains will result. The compressive strength of the concrete will determine the elastic deformation allowable in the concrete without incurring damage. Moisture diffusivity, which is the relative ability of moisture to flow through a particular concrete, will govern the rate at which moisture is dissipated from the concrete pavement slab, and hence, it will determine the moisture

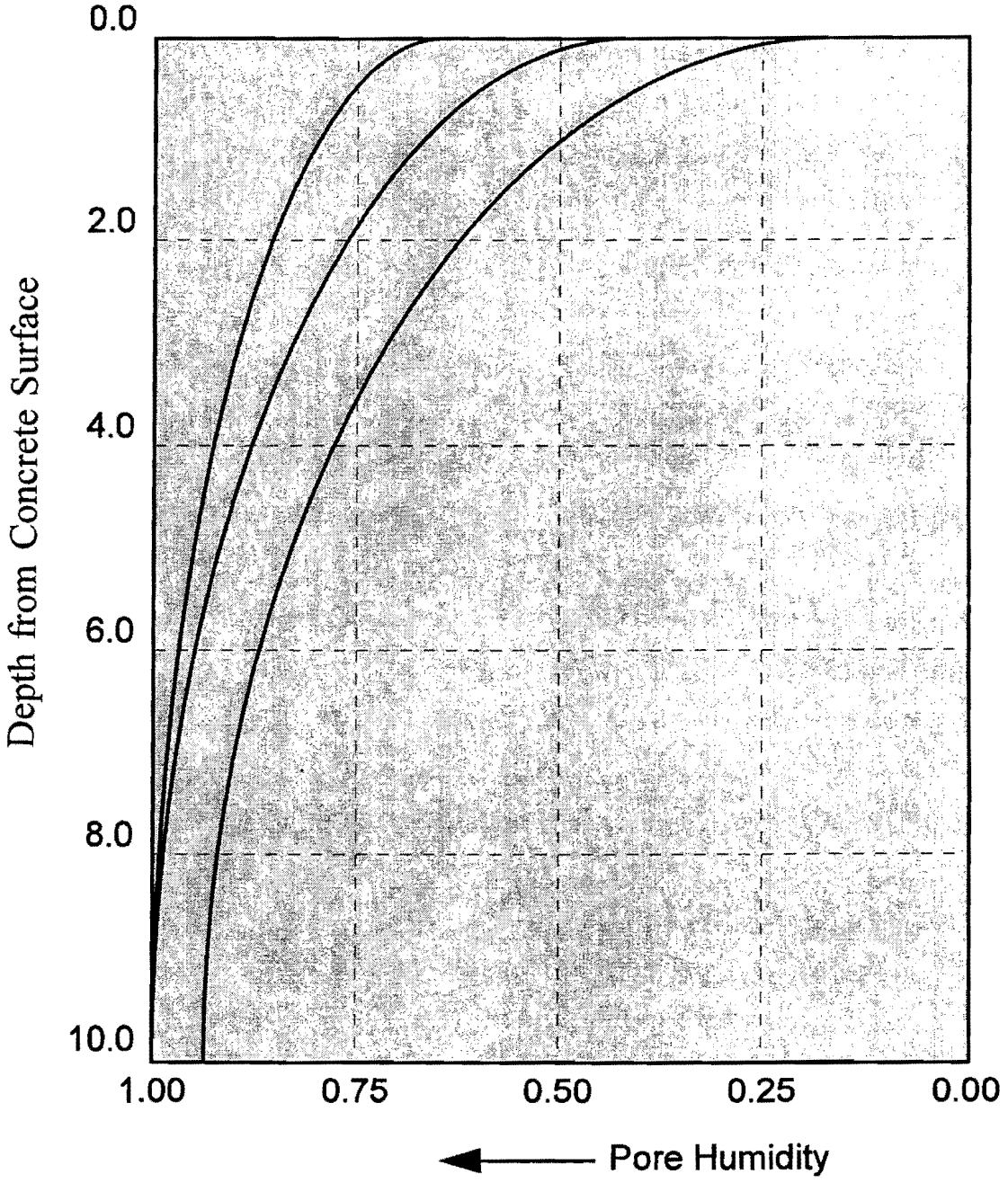

FIG. 40. Schematic Diagram Illustrating Typical Pore Humidity Distribution Measured Across the Depth of Slab (in.) (1 in = 2.54 cm)

gradient generated within the slab. The construction conditions will also affect early-age stresses because initial ambient environmental conditions will dictate the magnitude of shrinkage that can take place in the concrete pavement. In addition, the type of curing compound used has a major bearing on the moisture loss from the pavement.

Finite Element Computer Program

The finite element analysis program developed by Kadiyala (1992) to analyze early-age concrete pavements consisted of two modules (Fig. 41). Module I deals with the shrinkage strain model which predicts the shrinkage strain with time, as a distribution across the depth of concrete based on factors indicated below. These output data from Module I of the computer program also present the temperatures at different depths in the concrete pavement. These output data are fed into Module II which is the stress analysis program where the shrinkage strains and temperature differentials are used to calculate the stresses in the early-age concrete based on both shrinkage and creep. Boundary conditions for Module I are illustrated in Fig. 42. In this scenario, the loss of moisture in the pavement is considered to be only from the top surface of the pavement. Therefore, the moisture loss is one-dimensional.

Fig. 43 illustrates the type of finite element mesh used in the stress analysis (Module II). The boundary conditions at the end of the slab are considered as fully restrained when the cracks are about to be initiated.

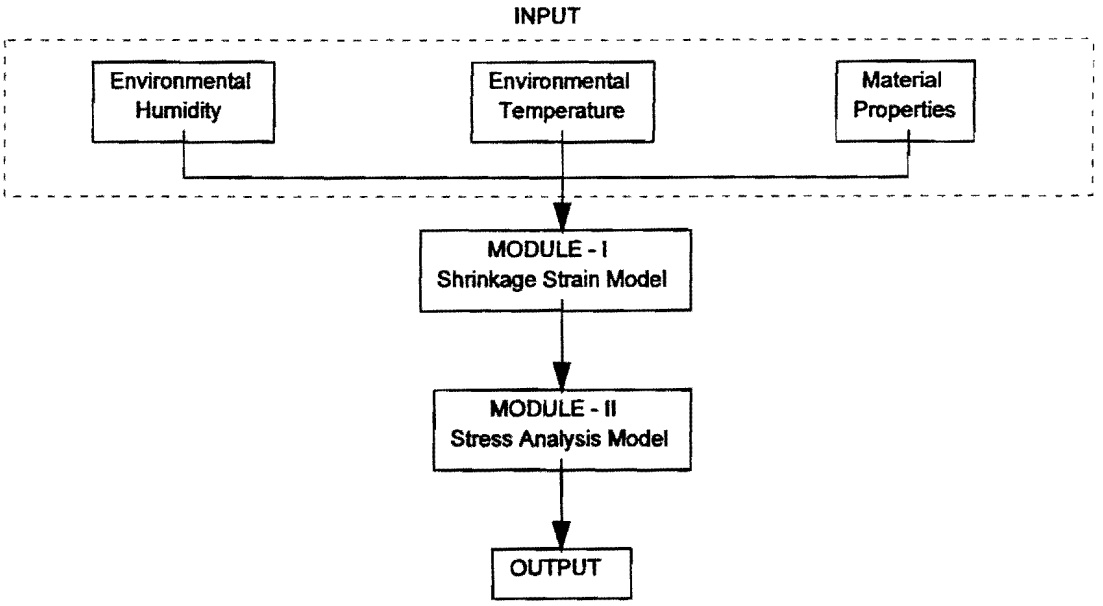

FIG. 41. Computer Program Formulation for Finite Element Analysis of Early-Age Concrete Pavements

Theoretical Aspects of the Analysis

The model used to predict the drying shrinkage was based on the model shown by Eq. 26 as suggested by Bazant and Najjar (1972).

$$\frac{\partial h}{\partial t} = div\ (C\ grad\ h) + \frac{\partial h_h}{\partial t} + K\frac{\partial T}{\partial t} \tag{26}$$

$$\frac{\partial h}{\partial t} = \nabla\left[\ k_h\ \nabla\ (h)\ \right] + \frac{\partial h_h}{\partial t} + K\frac{\partial T}{\partial t} \tag{27}$$

where t = time; h = pore humidity in concrete at time t; T = temperature in concrete; k_h = moisture diffusivity of concrete; h_h = percent moisture content due to self-desiccation of concrete; and K = hygrometric coefficient. The hygrometric coefficient K enables the

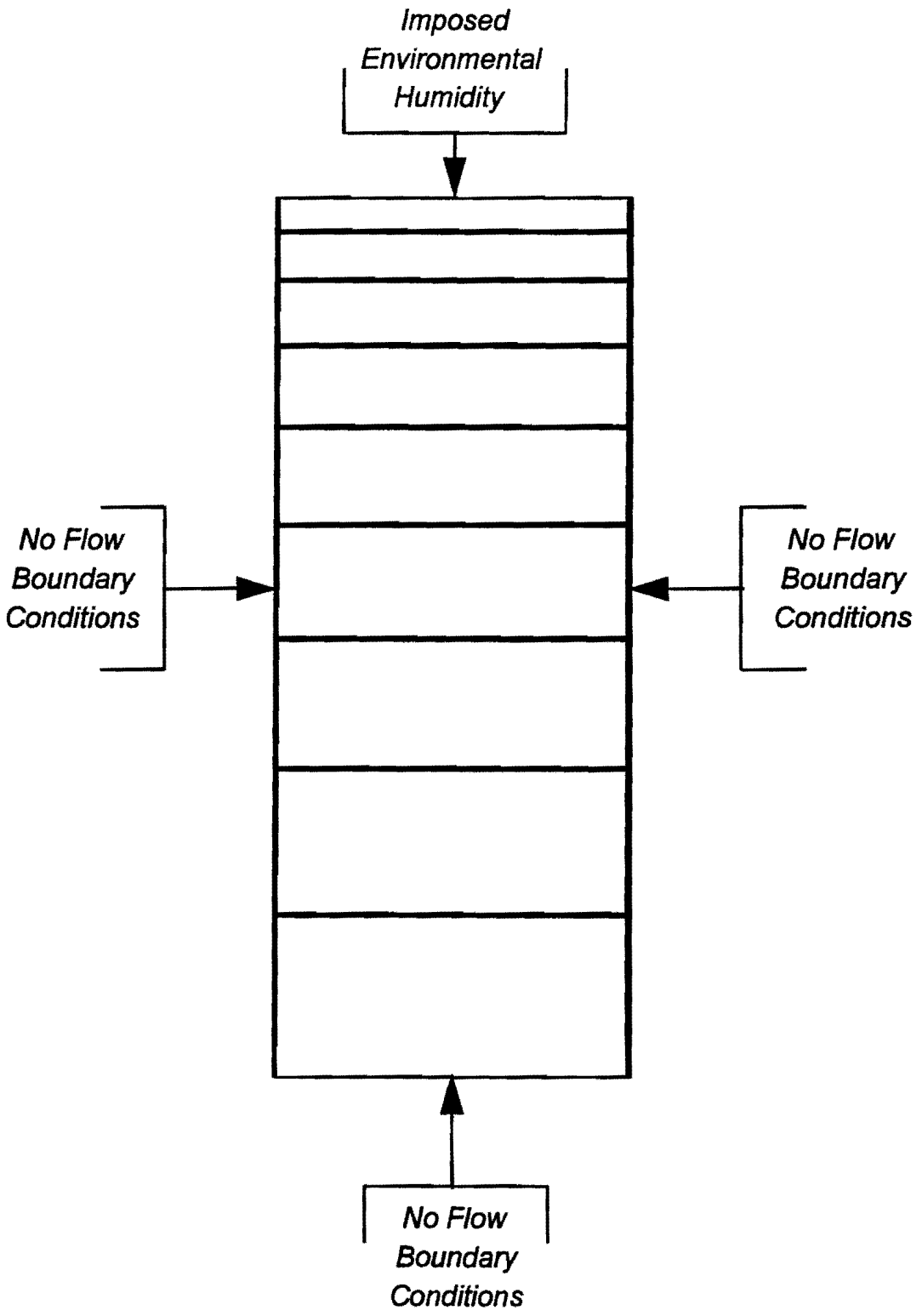

FIG. 42. Boundary Conditions for Finite Element Formulation of One-Dimensional Moisture Diffusion (Module I)

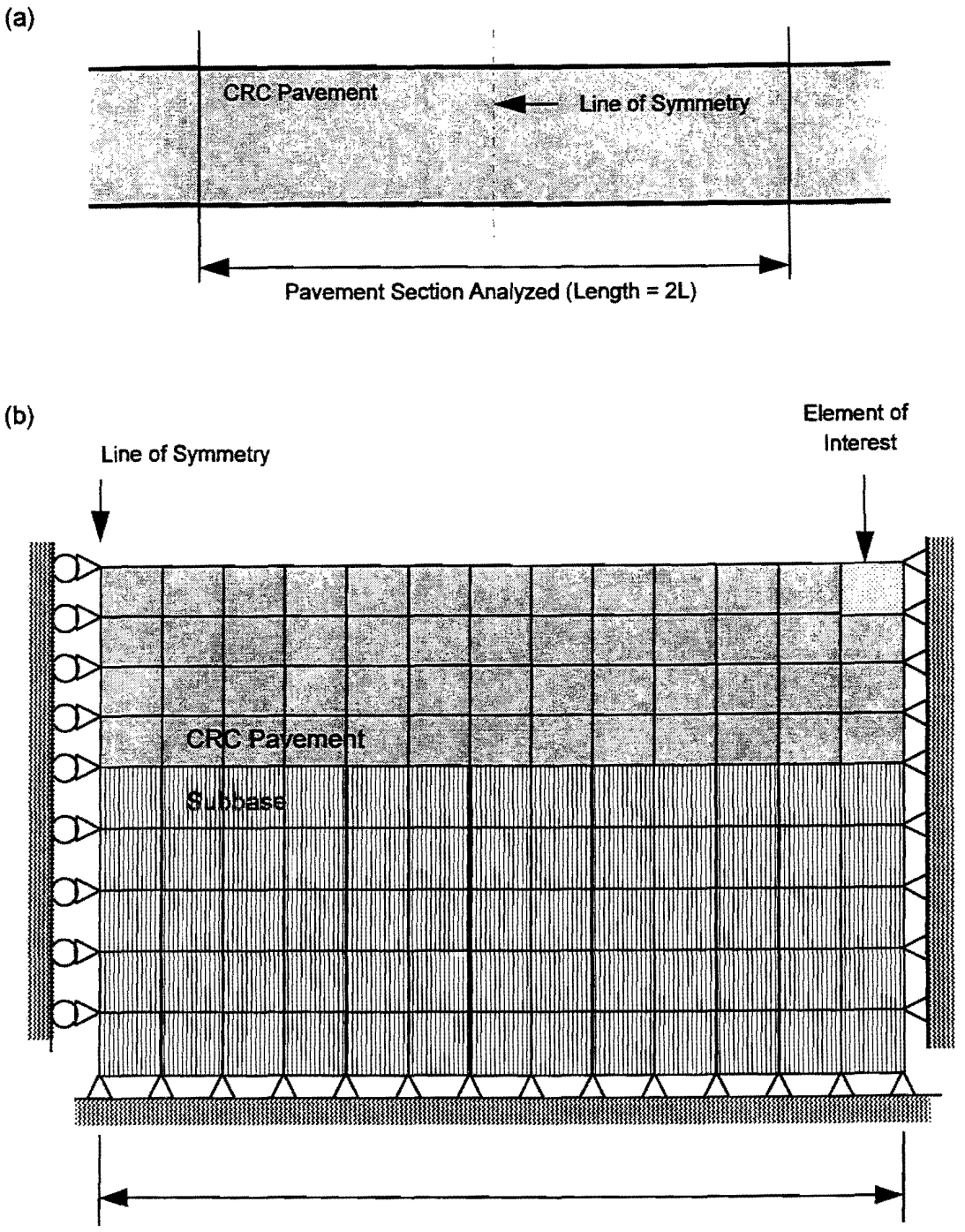

FIG. 43. Finite Element Formulation for Stress Analysis in Module II: (a) Pavement Configuration, and (b) Finite Element Mesh and Boundary Conditions

incorporation of the effect of temperature on the pore humidity. This enables the use of only the moisture diffusivity for the pore humidity prediction. Based on actual data, the following empirical equation was developed by Bazant to calculate K.

$$K = 0.0135\, h_t \frac{\left(1 - h_c\right)}{\left(1.25 - h_t\right)} \tag{28}$$

The diffusivity of concrete $(k_h)_t$ at time t is calculated using the following equation:

$$\left(k_h\right)_t = k_d \left(\alpha_0 + \frac{1-\alpha_0}{1 + \left(\frac{1-h_t}{1-h_c}\right)^n} \right) \tag{29}$$

where k_d = diffusivity of concrete when the pore humidity is 100%; α = ratio of minimum and maximum k_h (a constant for a given concrete mix); n = a constant which characterizes the drop in k_h; h_c = percent moisture content at which k_h is the average of maximum and minimum; and h_t = percent moisture content at time t. The moisture diffusivity at a certain time is calculated using Eq. 29. In Eq. 29, the constant terms α_0, n, and h_c were taken to be 0.05, 10, and 0.75, respectively. The pattern of change for the moisture diffusivity with changing pore humidity, calculated using the above parameters, is shown in Fig. 44. In Fig. 44, the diffusivity is shown in non-dimensional form as a ratio with the moisture diffusivity when the pore humidity is 100%.

Once the pore humidity distribution over a period of time was predicted, Kadiyala (1992) predicted the shrinkage strain (ϵ_{sh}) in the concrete pavement using the Bazant-Panula (B-P) model (Bazant and Panula 1978). Later, a revised version of that model was proposed by Bazant et al. (1991). The analysis to be performed in this study adopted the revised B-P model which the authors named the BP-KX model. The BP-KX

model is concisely outlined below.

The shrinkage strain at any time t is given by:

$$\epsilon_{sh}(t) = \epsilon_{sh\infty} K_h S(t) \tag{30}$$

where $\epsilon_{sh\infty}$ = final shrinkage corrected for the age-dependence; K_h = factor incorporating the dependence of shrinkage strain on relative humidity of the environment; and $S(t)$ = factor incorporating the time dependence of shrinkage strain.

$$S(t) = \tanh\left(\frac{t}{\tau_{sh}}\right)^{1/2} \tag{31}$$

$$\tau_{sh} = \frac{0.32\left(k_s D\right)^2}{C_1\left(t_{0_e}\right)} \tag{32}$$

where k_s = shape factor which is recommended to be 1.0 for an infinite slab; and D = effective cross-section thickness of the concrete structure in millimeters which is equal to twice the volume-to-surface ratio.

$$C_1(t_0) = C_0\left[0.6 + \left(\frac{4.5}{t_{0_e}}\right)^{1/2}\right] \; ; \; C_0=10, \; but \; C_1(t_0) \leq 18 \tag{33}$$

$$\epsilon_{sh\infty} = \frac{\epsilon_{s\infty}}{\left[G\left(17+\frac{\tau_{sh}}{40}\right) G\left(12+t_{0_e}\right)\right]} \tag{34}$$

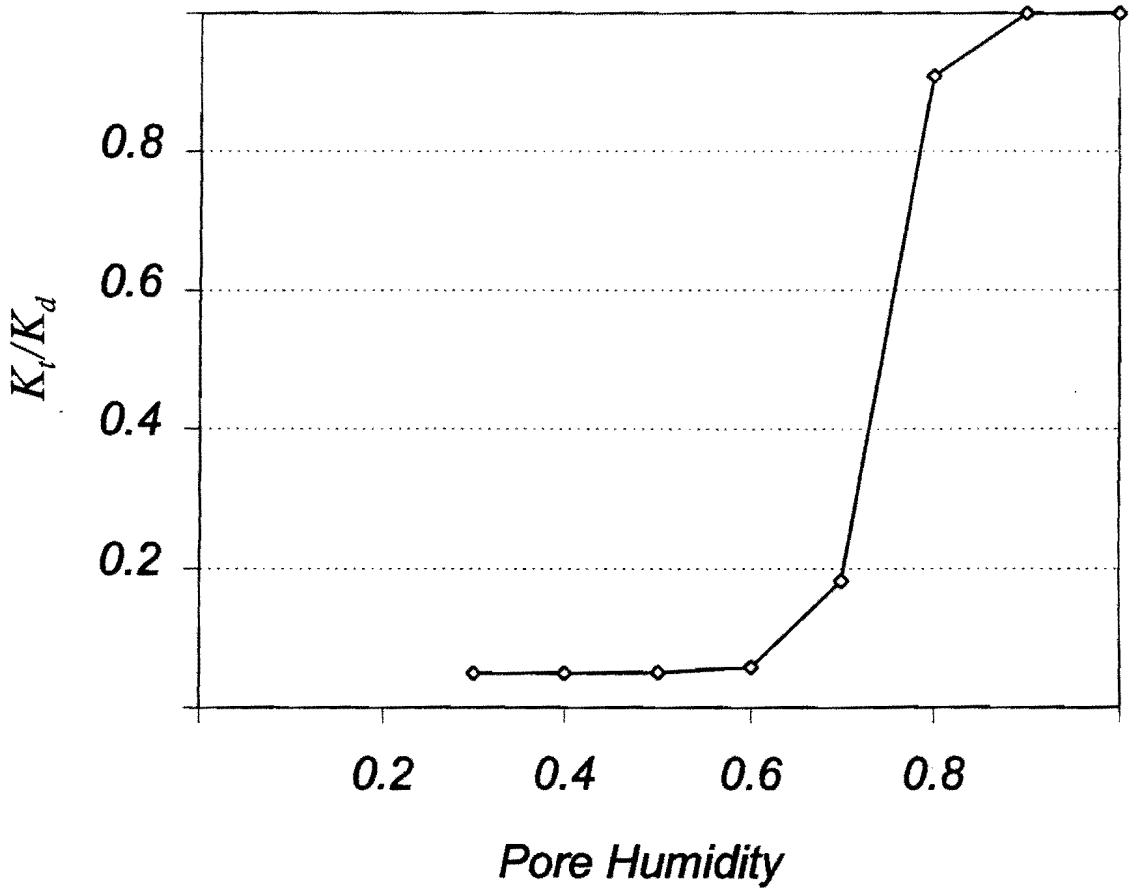

FIG. 44. Variation of Moisture Diffusivity With Pore Humidity (From Eq. 29)

where $\epsilon_{s\infty}$ = final shrinkage in 10^{-3}, and

$$G(x) = \sqrt{\frac{x}{4+0.9x}} \tag{35}$$

$$\epsilon_{s\infty} = \left(1.15\alpha_1 + 0.16 \right)\alpha_2\ \alpha_3 \tag{36}$$

$$\alpha_1 = \left(\frac{w}{c}\right)^{1.5} c^{1.1}\ f_c'^{-0.2} \left(1 - \frac{a}{\rho_c} \right)\ \alpha_4 \tag{37}$$

$$\alpha_4 = 0.7 + \frac{0.3}{\left(\frac{a}{s} - 1.6\right)^3} \quad for \quad \frac{a}{s} > 2.6 \; (\alpha_4 = 1 \; otherwise) \tag{38}$$

α_2 = 1.0 for Type I cement; and α_3 = 1.4 for specimens sealed during curing. Also, c = cement content in lb/ft^3; w/c = water/cement ratio; f_c' = 28-day compressive cylinder strength of concrete in psi; a/c = aggregate/concrete density ratio; and a/s = aggregate/sand ratio.

Sensitivity Analysis of Early-Age Concrete Pavements

The following factors were incorporated in the sensitivity analysis of predicting early-age stresses in the concrete pavement caused by non-load related factors.

Environmental Factors

1. Ambient temperature
2. Ambient relative humidity

Mix Design Factors

1. Cement factor (quantity of cement per unit volume of concrete)
2. Water/cement ratio
3. Ratio of density of aggregates to the density of concrete

Material Properties

1. Moisture diffusivity of concrete
2. 28-day compressive strength of concrete

Design Factors

1. Pavement thickness

Construction Factors

1. Time of paving (hour of day)
2. Season of paving (winter, spring, summer, fall)
3. Curing conditions

In order to incorporate these factors into the analysis, actual weather data had to be used to simulate different paving times and seasons. The most appropriate pattern for both the ambient relative humidity and ambient temperature, which is a periodic (sinusoidal) pattern with amplitude and the mean value, was adopted for this purpose. The pore humidity and shrinkage strain depend on the effectiveness of the curing method. In order to simulate the effect of curing, a modification factor was introduced. These modification factors were calibrated by comparing predicted pore humidity with actual data measured from field studies. The multiplication factor increases with increasing effectiveness of the curing compound. The effect of coarse aggregate type in the analysis was incorporated by way of the ratio between the density of coarse aggregate and the density of concrete. The factorial used in the analysis of concrete pavements at early-ages was in two parts. Table 24 indicates the factorial where weather conditions at the time of paving are incorporated. Table 25 shows the factorial in which factors relating to the concrete mix design were included. The experiments performed are indicated by an 'X' in Tables 24 and 25.

TABLE 24. Factorial Incorporating Weather Conditions at the Time of Paving

Paving Month	Paving Time	Experiment
January	8 AM	x
January	12 Noon	x
January	4 PM	x
July	8 AM	x
July	12 Noon	x
July	4 PM	x

The computer program used for the stress analysis allows the user to change the analysis period. For this analysis, a period of 12 weeks (2016 hours) was considered. The output of stresses were obtained every 7 days (168 hours). Since the analysis was performed over a period of 12 weeks, an average moisture diffusivity of concrete for the first 12 weeks was considered to be 12.9 cm^2/day. Laboratory and field measurement of moisture diffusivity for early-age concrete have given values as high as 38.7 cm^2/day, and it reduces with time to around 6.45 cm^2/day in an exponential fashion (Xin et al. 1995). Fig. 45 shows a schematic diagram indicating how moisture diffusivity changes with age of concrete.

A subbase layer was included in the analysis of stresses. The thicknesses of the slab and subbase were taken at 30.5 and 61 cm, respectively. The boundary conditions in the analysis were set up such that symmetry is taken into account (Fig. 43). An 2.44 m long slab was analyzed. Due to the symmetry, the actual length used in the analysis was 1.22 m. Fig. 46 shows the stresses obtained from the analysis.

TABLE 25. Factorial Incorporating Concrete Mix Design Parameters

Water/Cement Ratio	Cement Factor (sacks/m^3)	Aggregate/Concrete Density Ratio	Experiment
0.3	7.9	0.625	
0.3	7.9	0.729	x
0.3	9.2	0.625	
0.3	9.2	0.729	
0.4	7.9	0.625	
0.4	7.9	0.729	x
0.4	9.2	0.625	x
0.4	9.2	0.729	x

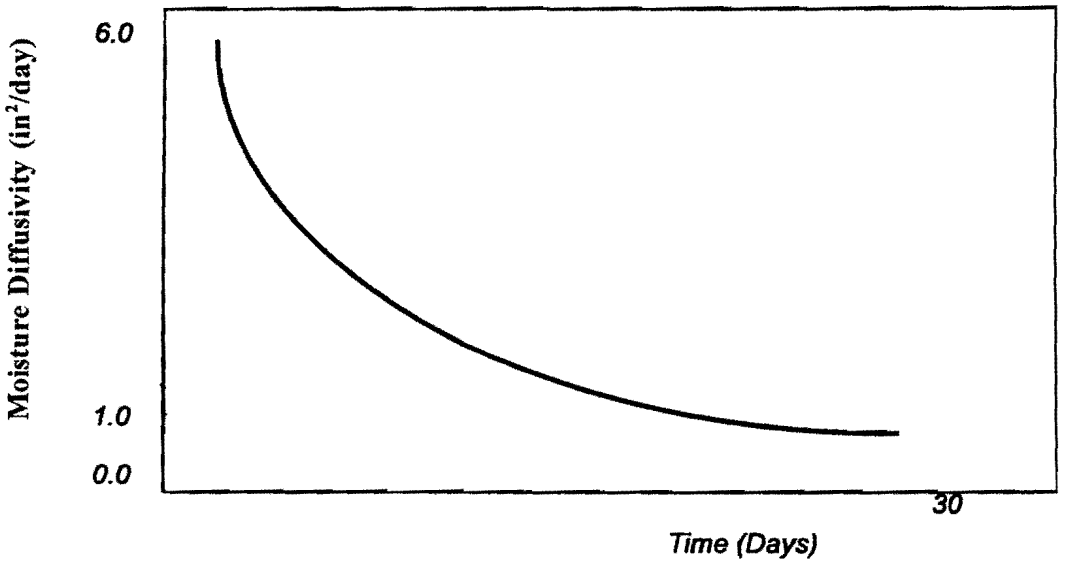

FIG. 45. Schematic Diagram Showing the Change in Moisture Diffusivity With Concrete Age (1 in^2/Day = 6.45 cm^2/Day)

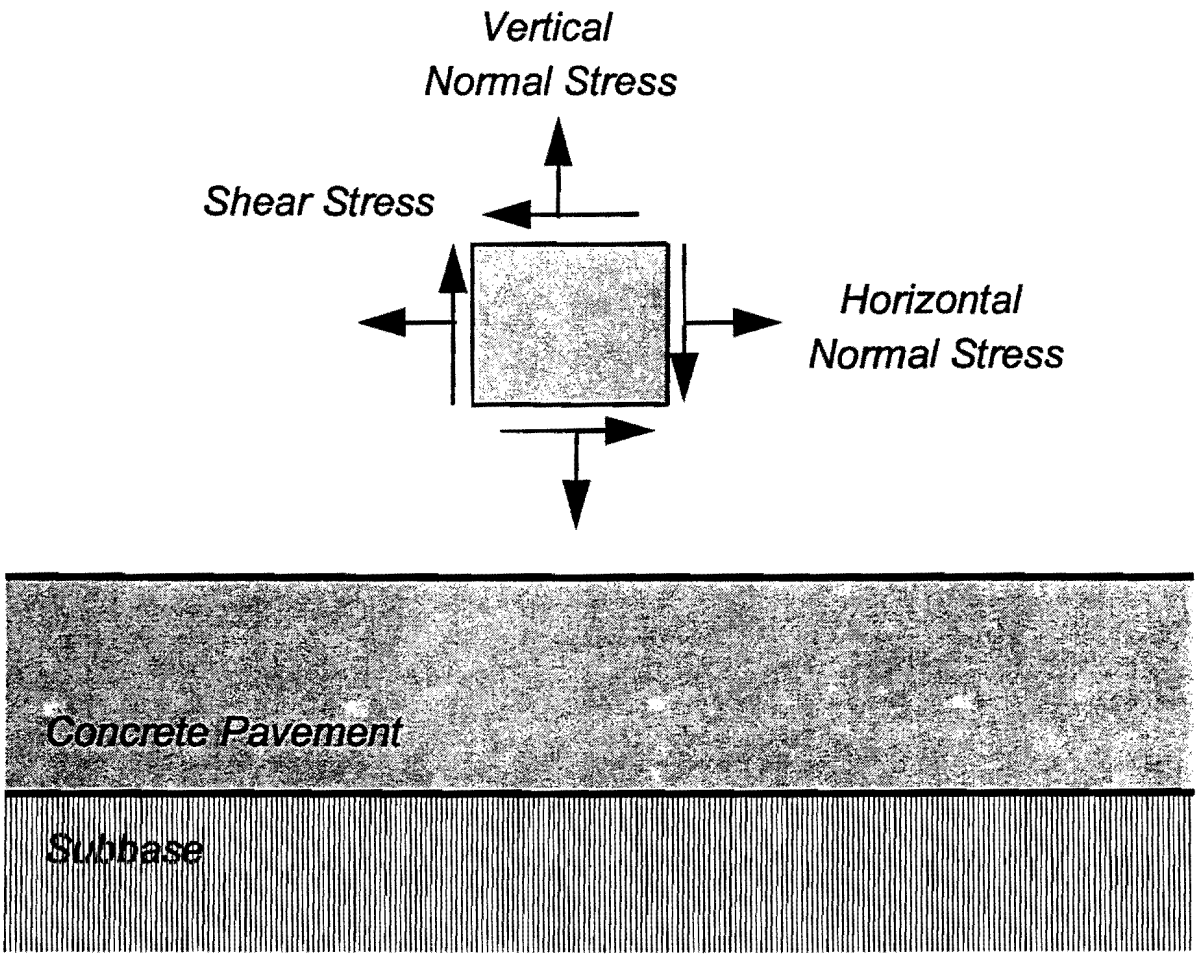

FIG. 46. Schematic Diagram Showing Stress Components Included in the Analysis

Results From the Analysis of Early-Age Concrete Pavements

Results from the analysis described above are presented in the following section. The analysis is performed for average weather conditions for the months of January and July in Houston, Texas. This particular analysis was performed by assuming that no curing compound was applied to the concrete. Fig. 47 illustrates the maximum stress plotted for different paving times of the day during the month of January. All three stress components shown in Fig. 46 are included in the illustration. However, it is the vertical normal stress and the shear stress which are believed to directly affect the formation of the delaminations. It can be seen that of the three times of the day, the 4 PM paving provides the highest shrinkage stress in all three

stress components. 8 AM paving provides the least stress levels for the three paving times adopted.

Fig. 48 illustrates the predicted maximum horizontal normal stress compared between the winter (January) and summer (July) paving conditions. The summer paving conditions are shown to result in higher horizontal normal shrinkage stresses. Even though the difference in shrinkage stress levels is not very high, this may be partly due to the fact that monthly average weather data was used for the analysis. It is expected that the differences in predicted stresses between winter and summer would have been much more significant if actual daily weather data were used. Figs. 49 and 50 show similar results for the vertical normal stress and shear stress. It can be seen that these stress levels, particularly in the case of 4 PM paving, go up to as much as 200 psi which is quite significant, particularly for early age concrete. All these maximum stress values occur at the top right hand corner of the finite element mesh (shaded element in Fig. 43) where the delaminations are most likely to occur.

Figs. 51-53 show the comparison of maximum predicted stress levels in pavements under different curing conditions. The curing conditions were simulated by the use of calibrated data from pore humidity field measurements. A correction factor was calculated for each curing method/compound by taking the ratio between the measured pore humidity and the predicted pore humidity (without curing) for those pavements in which pore humidities were measured. It is believed that the difference in stress values would have been higher if the diffusivity was taken as non-linear (i.e., diffusivity changing with the pore humidity in the pavement).

Figs 54-56 illustrate the effect of mix design parameters in the predicted shrinkage stresses. Fig. 54 shows the difference in the vertical normal stress for water cement ratios of 0.3 and 0.4. As expected, the concrete with the higher water-cement ratio provided a much higher shrinkage stress level. Fig. 55 compares the case of two cement factors (number of cement bags used to make 1 cubic yard of concrete). There is a 10-15% difference between maximum vertical stress values for the cement

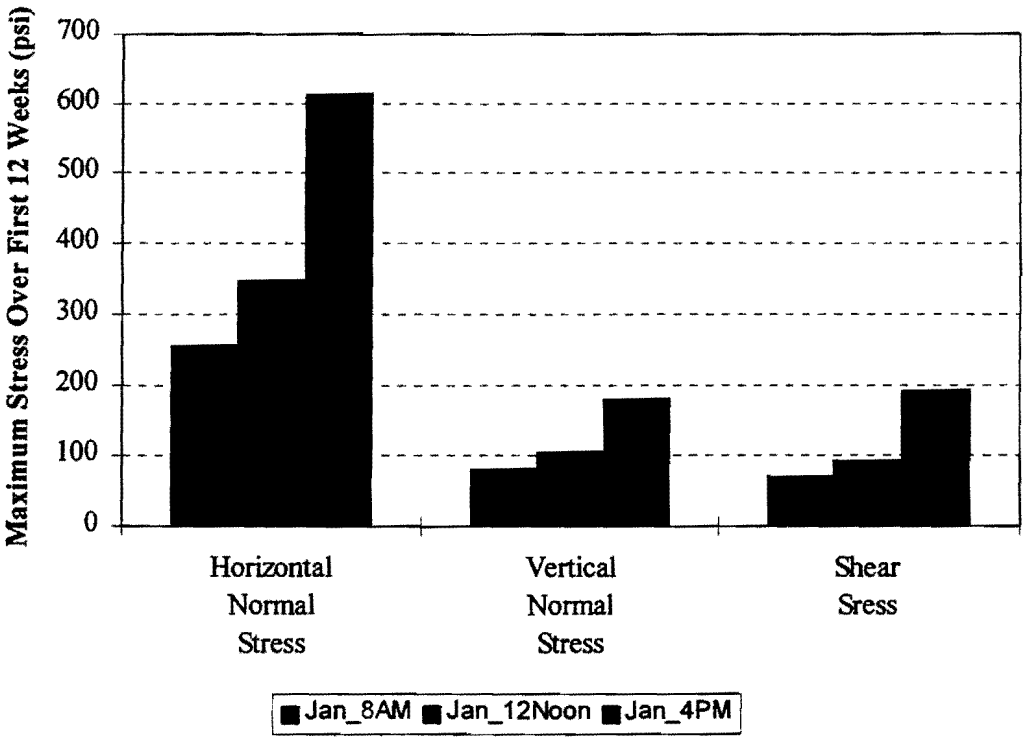

FIG. 47. Maximum Stress in the Pavement Section During the First 12 Weeks After Paving (1 psi = 6.89 MPa)

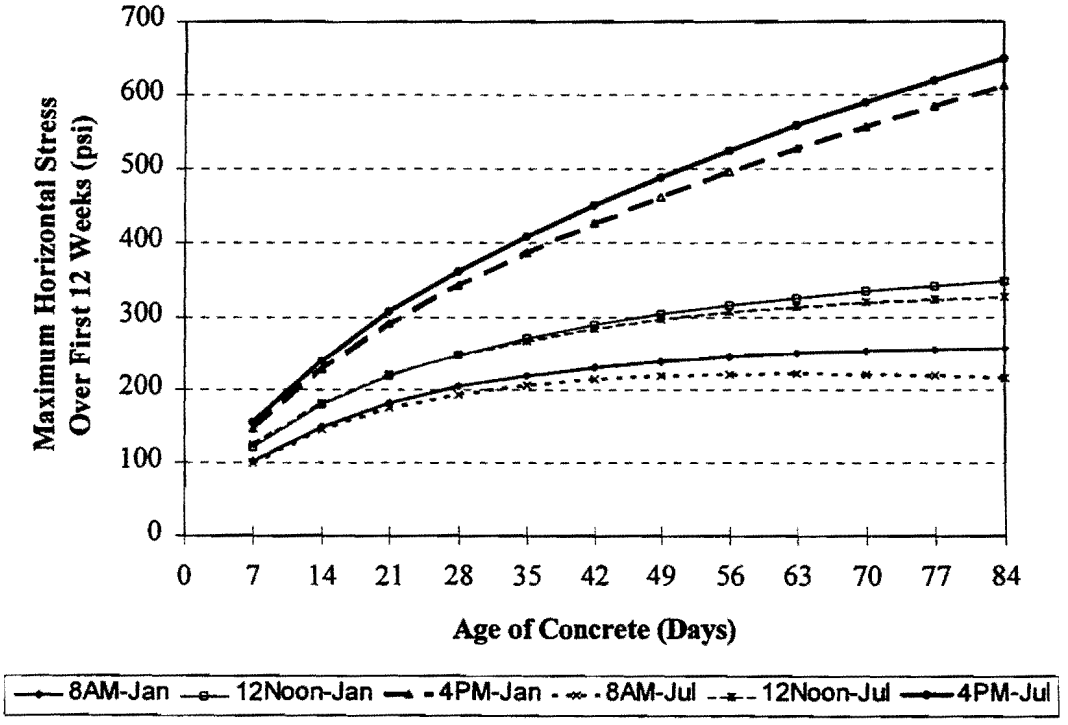

FIG. 48. Predicted Maximum Horizontal Normal Stress in the Pavement Section During the First 12 Weeks (1 psi = 6.89 MPa)

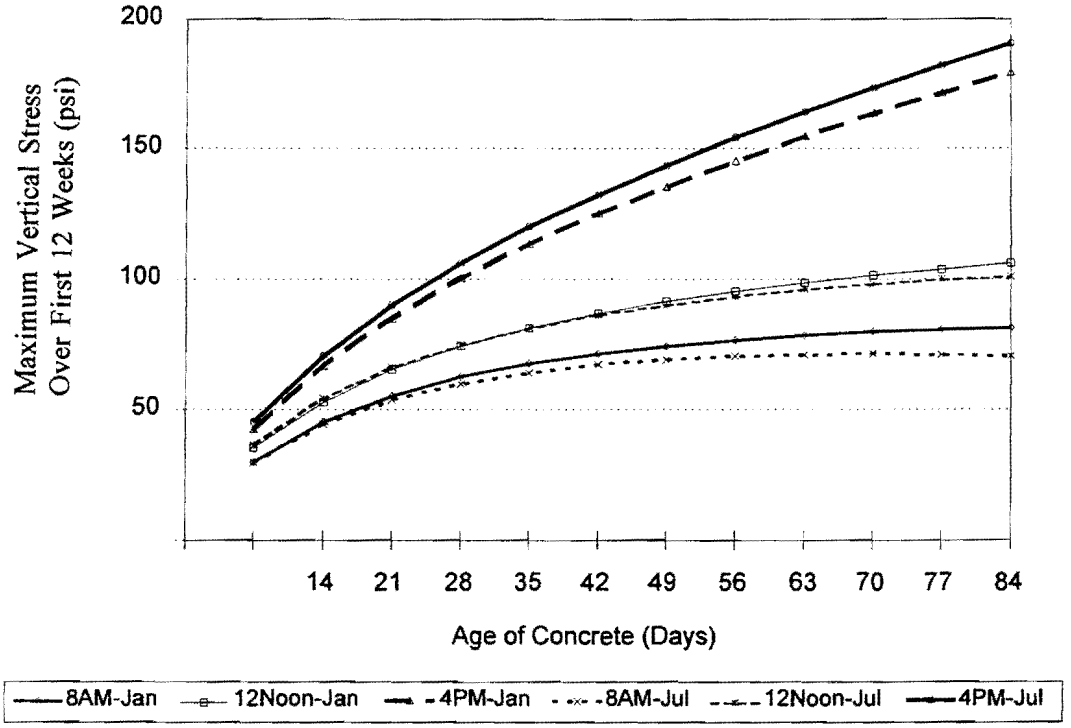

FIG. 49. Predicted Maximum Vertical Normal Stress in the Pavement Section During the First 12 Weeks (1 psi = 6.89 MPa)

factors of 6 and 7, with the higher cement factor providing a higher shrinkage stress level. Fig. 56 shows the effect on shrinkage stress from the other mix design factor, the density of the coarse aggregate used. A significant difference is shown for two aggregate types with densities of 1442 and 1682 kg/m^3.

Discussion of Results

The stress analysis of early-age concrete pavements indicated significantly high stresses for all three stress components of stress, namely, the horizontal normal stress, vertical normal stress, and the shear stress. Fig. 46 indicated how these three stress components act on a pavement section. It is clear that for delaminations to occur, the critical stresses would be the vertical normal stress and the shear stress. One of the shortcomings in the BP-KX model (Bazant et al. 1991) is that the model can only predict mean shrinkage across a cross section. In this scenario, the ultimate

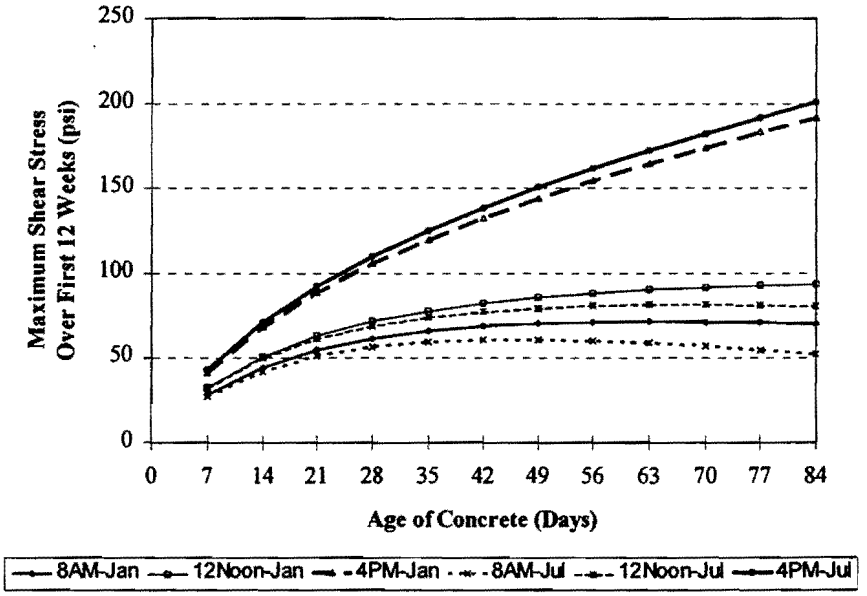

FIG. 50. Predicted Maximum Shear Stress in the Pavement Section During the First 12 Weeks (1 psi = 6.89 MPa)

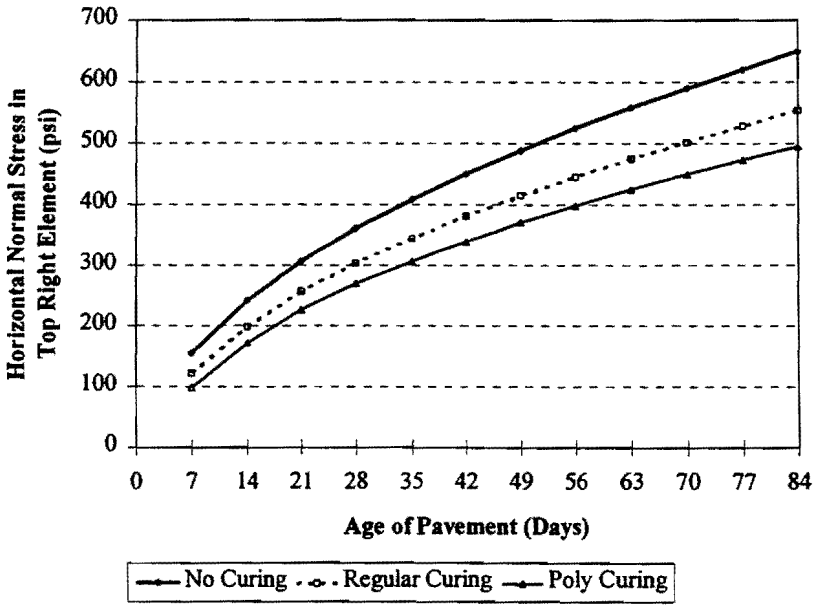

FIG. 51. Comparison of Horizontal Normal Stress in the Pavement Section Under Different Curing Conditions (1 psi = 6.89 MPa)

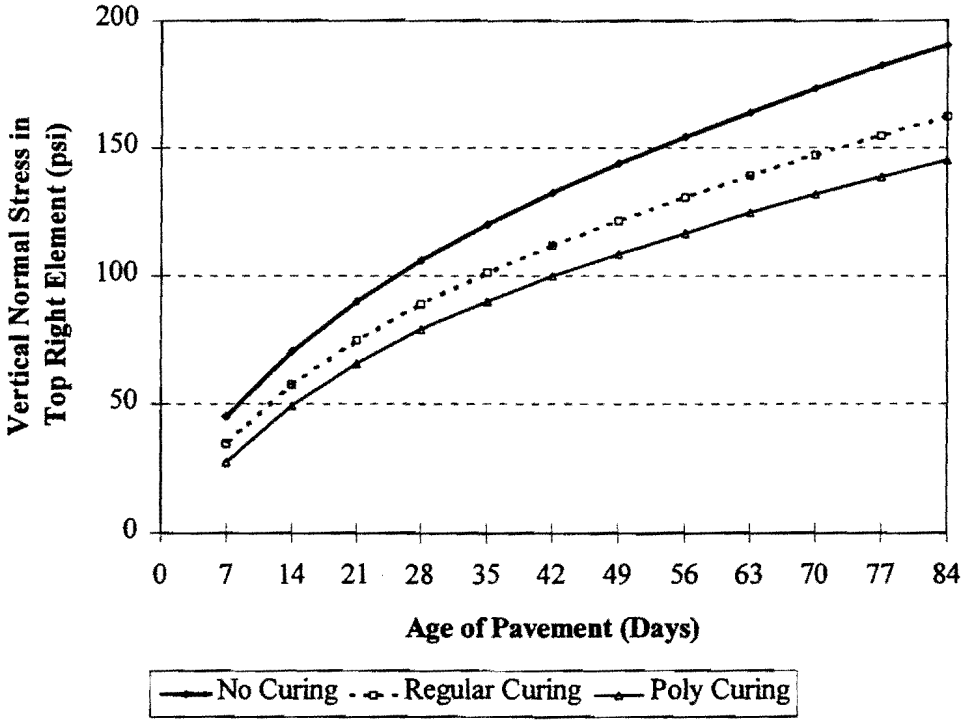

FIG. 52. Comparison of Vertical Normal Stress in the Pavement Section Under Different Curing Conditions (1 psi = 6.89 MPa)

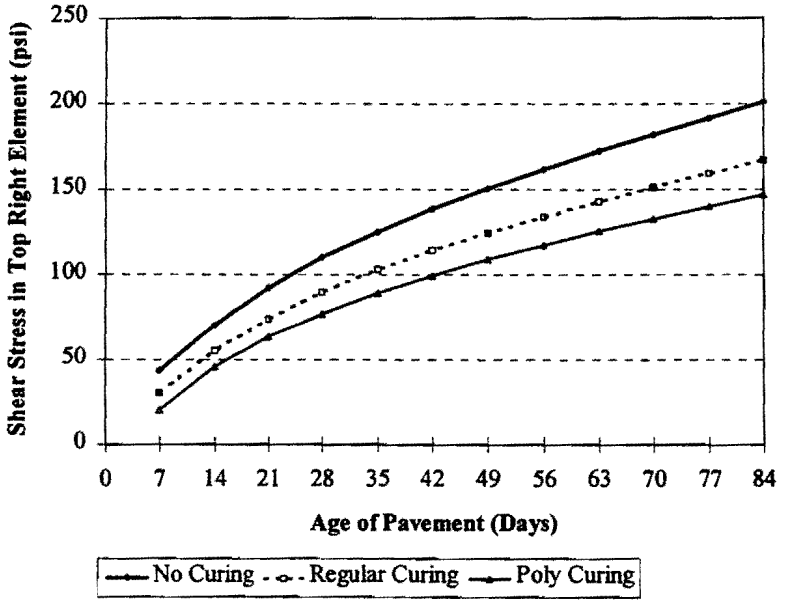

FIG. 53. Comparison of Shear Stress in the Pavement Section Under Different Curing Conditions (1 psi = 6.89 Mpa)

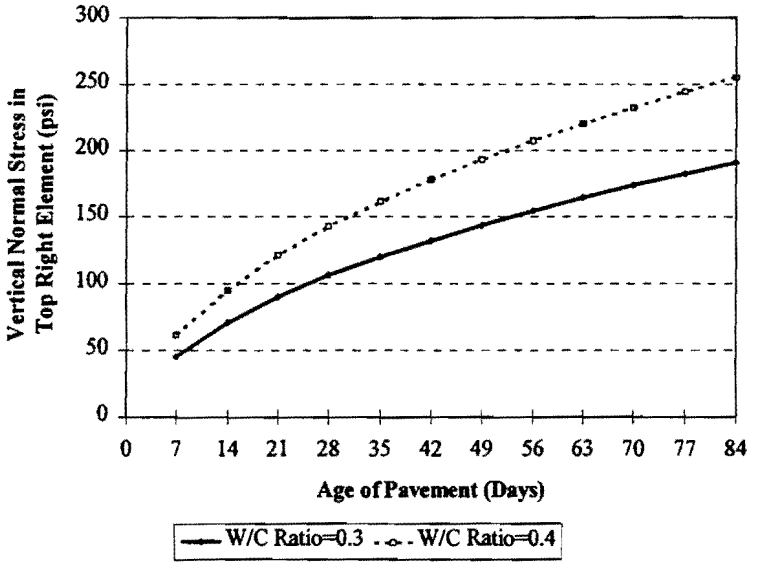

FIG. 54. Comparison of Maximum Vertical Normal Stress in the Pavement Section Under Different Water/Cement Ratios (1 psi = 6.89 MPa)

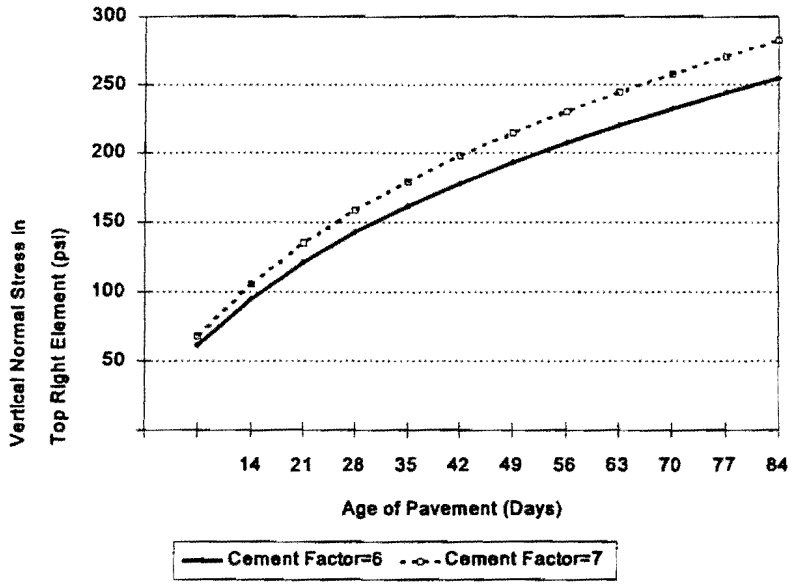

FIG. 55. Comparison of Maximum Vertical Normal Stress in the Pavement Section Under Different Cement Factors

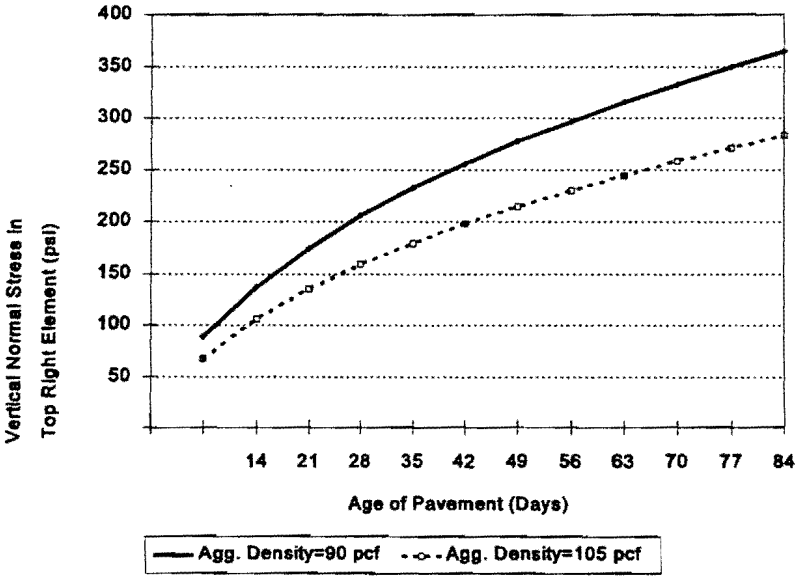

FIG. 56. Comparison of Maximum Vertical Normal Stress in the Pavement Section Using Coarse Aggregates With Different Densities

shrinkage that is being calculated using Eq. 30 is an average ultimate shrinkage strain for the slab thickness. It is known from field measurements of pore humidity that the pore humidity, and hence, the shrinkage, is non-uniform across the pavement

thickness with the shrinkage strains at the top of the slab being much higher than at other locations along the depth. This means that the shrinkage strain calculated using the BP-KX model underestimates the shrinkage at the top of the slab. This shows that in the actual scenario, the stresses at the top of the slab would be even higher than those predicted. However, since free shrinkage, which provides a more accurate representation of the shrinkage in a concrete pavement, is very difficult to measure, the BP-KX model is the best available model for the prediction of shrinkage at this time.

Field studies on spalling indicated that spalling takes place predominantly in concrete pavements with siliceous aggregates as the coarse aggregate. Further studies indicate that in many concrete pavements with crushed limestone as coarse aggregates, the presence of very little spalling is due to the absence of de-bonding cracks at the aggregate-cement paste interface. Microscopical studies of laboratory concrete samples indicate the presence of micro-cracks at the aggregate-cement paste interface for concrete with siliceous aggregates, but such cracks are rarely found in concrete with crushed limestone as coarse aggregate. This shows that in the case of concrete made with these two commonly used coarse aggregates, there is a difference in the initial state of the concrete. In siliceous river gravel, there is likely to be a number of micro-cracks at the aggregate-cement paste interface whereas in most crushed limestone concretes, there are no such initial flaws even prior to the application of the load.

Fig. 19 showed a plate with an elliptical flaw in the middle. It was shown earlier that when there is no flaw in the plate, the curvature is infinite, and σ_A is equal to σ. In the case of a fairly wide crack ($2a$=38 mm and b=2.5 mm), σ_A is equal to sixteen times the applied stress σ. It appears that this is the reason for the discrepancy in the spalling levels between concrete made with siliceous gravel and crushed limestone. Since there are stress concentrations present in concrete with siliceous gravel, the likelihood of delaminations would be much higher. As a result, the likelihood of spalling would be much higher as well. In fracture mechanics, the stress intensity factor (K_I) in a body subjected to an external stress of σ due to an elliptical

embedded flaw similar to that shown in Fig. 19 is given by:

$$K_I = \frac{\sigma \sqrt{\pi b}}{\psi} g(\phi) \tag{39}$$

$$\psi = \frac{3\pi}{8} + \frac{\pi}{8}\frac{b^2}{a^2} \tag{40}$$

$$g(\phi) = \left(\sin^2\phi + \frac{b^2}{a^2}\cos^2\phi \right)^{1/4} \tag{41}$$

If we assume a circular flaw in concrete, a is equal to c, and therefore,

$$K_I = 2\ \sigma \sqrt{\frac{b}{\pi}} \tag{42}$$

From the size-effect fracture tests, the fracture toughness of concrete at 24 hours was found to be 400 MPa √m. Thus, the corresponding critical stress can be calculated for a flaw size equal to the maximum aggregate size. If the maximum aggregate size is 38 mm, the critical nominal stress value would be 289 MPa √m. This value applies for just one crack, and there may be a number of such cracks. Therefore, we can see that the delaminations due to a Mode I fracture alone, are feasible.

Fig. 57 shows the effect of a satisfactory curing method such as polyethylene curing has on the pavement. Fig. 57 compares the stresses predicted from the early-age stress analysis program for different curing methods, with the strength of concrete measured in the laboratory. It can be seen that when there is no curing, the stress is higher than the strength of concrete; whereas, the situation improves when a more effective curing method such as polyethylene sheets is used.

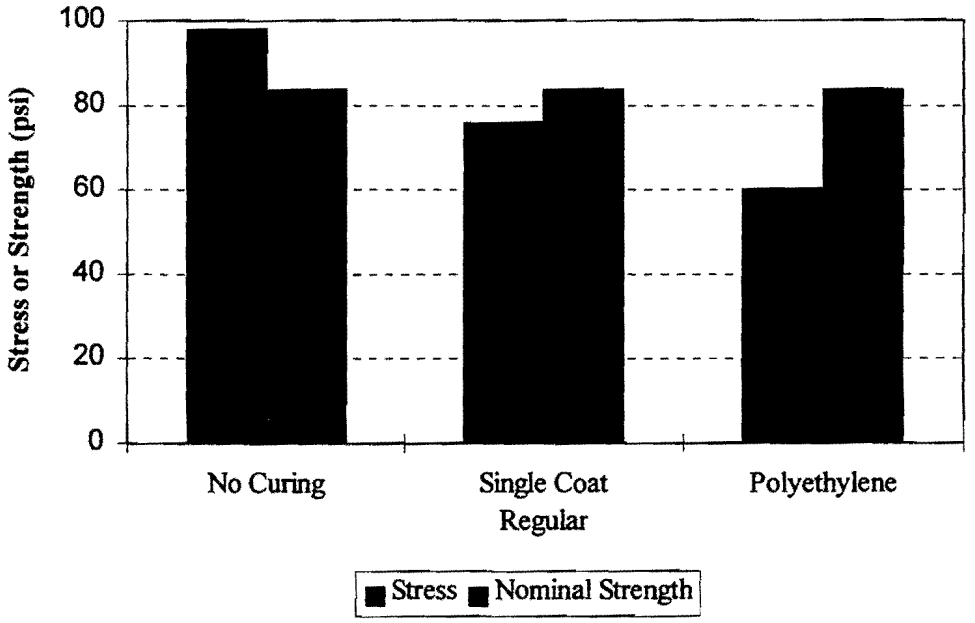

FIG. 57. Comparison of Laboratory Measured Concrete Strength With Stresses Predicted for Different Curing Conditions (1 psi = 6.89 MPa)

CHAPTER 6: SPALLING AS A DESIGN CRITERION

As indicated earlier, delaminations occur near the transverse cracks and/or joints in concrete pavements very early in the pavement life. Results from the field surveys indicated that the delaminations may occur prior to the pavement being open for traffic. This points to the fact that the delaminations are a result of factors other than traffic loading. Based on results from the analysis of early-age concrete pavements, it can be seen that significantly high stresses can develop in pavements due to shrinkage and temperature change. The delaminations which develop early in pavement life will develop into spalls due to the fatigue action induced by traffic loads and temperature fluctuations. One important factor which influences the extension of these delamination cracks into spalls is the level of friction at the crack faces of the delamination. Results from an analysis where this factor was investigated are given below.

INFLUENCE OF INTERFACE FRICTION AT DELAMINATIONS FACES ON SPALLING

A spall model based on the tensile mode of failure that may be applied to CRC or jointed pavements based on the mechanism is illustrated in Fig. 58 for the general case of a jointed concrete pavement. In this mechanism, the extension of delaminations into spalls is presented in the case of traffic loads. The delamination is considered to be a continuous flaw parallel to the pavement surface at a depth of a few cm. This mechanism was shown to be applicable to the situation indicated by Fig. 7 of this report, where it was shown that the delamination can extend beyond the spall area. An analytical solution to the spall stresses was derived by taking the following factors into account:

1. Degree of friction at the delamination faces.
2. Normal and shear stresses created by the traffic load.
3. Properties of the joint filler material.

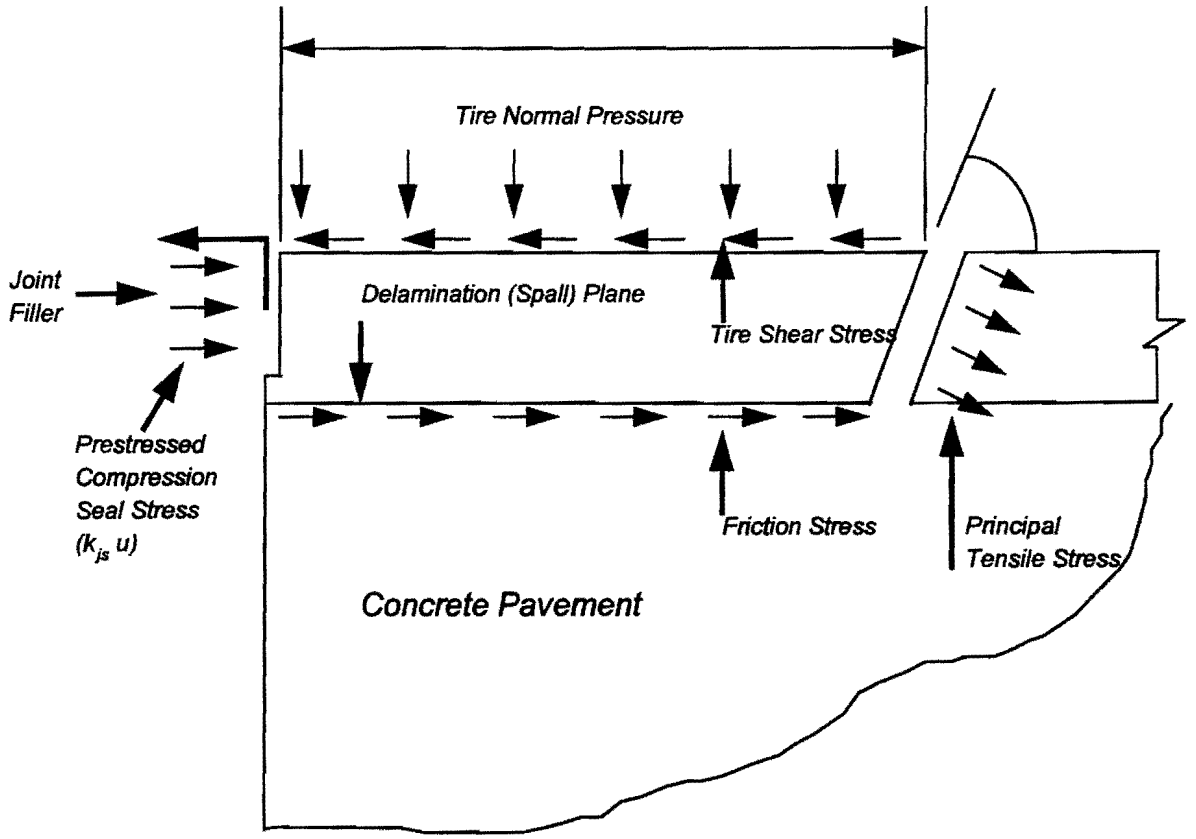

FIG. 58. Schematic Diagram of Spalling Mechanism for Tensile Mode of Failure in Jointed Concrete Pavement

Resolving all forces for equilibrium in the horizontal direction:

$$\overset{+}{-}\sum F_W = 0 = k_{js}\, u - \tau\, \ell + \left\{\sigma_t \cdot \frac{t}{\sin\theta}\right\}\sin\theta + q\mu\left(\ell - \frac{t}{\tan\theta}\right) \tag{43}$$

and solving for the concrete tensile stress or spall stress (σ_t):

$$\sigma_t = (\tau - q\mu)\,\frac{\ell}{t} + \frac{q\mu}{\tan\theta} - \frac{k_{js}u}{t} \tag{44}$$

where τ = vehicle tire shear stress; q = normal tire pressure; μ = concrete friction coefficient on the spalled plane; ℓ = tire pressure load length; t = depth of spall delamination; θ = orientation of principle stresses; k_{js} = spring coefficient for joint sealant; and u = displacement of spalled concrete. The quantity $q\mu$ constitutes the friction stress (τ_f). It is assumed that quantity $q\mu$ is not fully mobilized until $u \geq \delta$ such

that δ_f represents the threshold displacement where $\tau_f = q\mu$ (Fig. 59). At values of $u < \delta_f$, τ_f may be defined as a function of u. Therefore:

$$\tau_f = k_f \quad \text{if} \quad 0 \leq u \leq \delta_f \tag{45}$$

and,

$$\tau_f = C_2 \quad \text{if} \quad u \geq \delta_f \tag{46}$$

where C_2 is equal to $q\mu$.

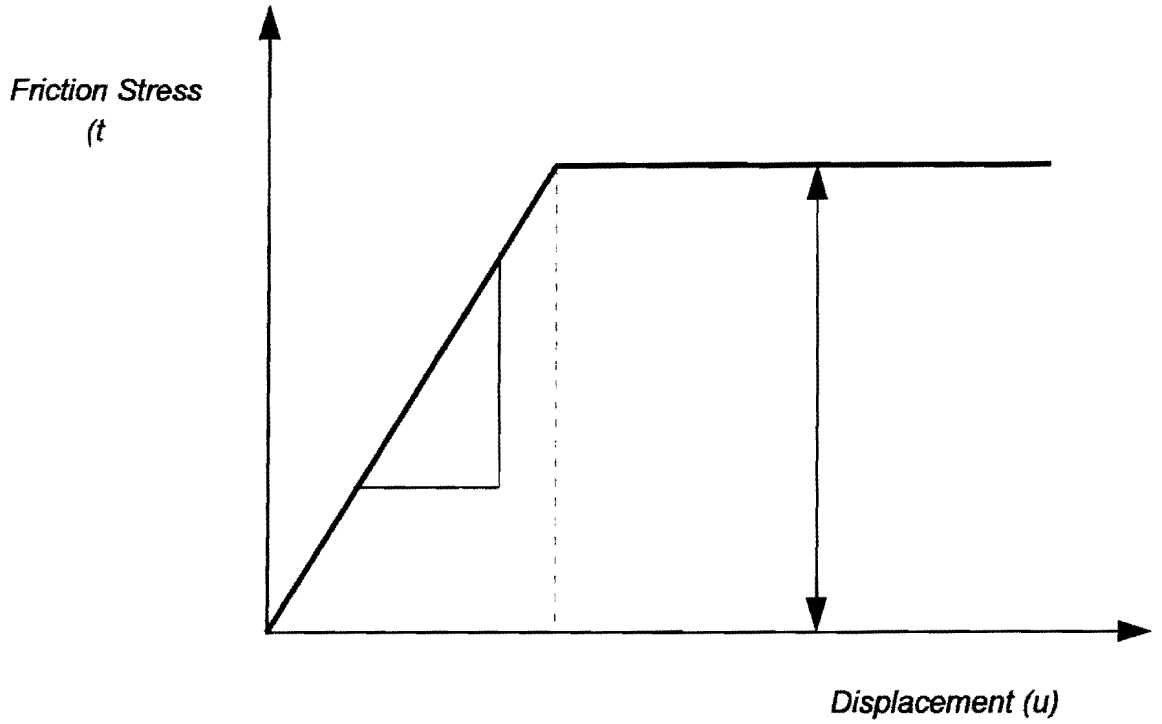

FIG. 59. Mobilization of Frictional Stress at the Delamination

Substituting τ_f for $q\mu$ and σ_{js} for $k_{js}\,u$:

$$\sigma_t = (\tau - \tau_f)\frac{\ell}{t} + \frac{\tau_f}{\tan\theta} - \frac{\sigma_{js}}{t} \quad \text{for} \quad \tau > \tau_f \tag{47}$$

where $\sigma_{js} = k_{js}\,(u \pm u_{temp})$; q_s = stress in joint sealant; $u_{temp} = \Delta L/2$; $\Delta L = C\,L\,(\alpha\Delta T + e)$; C = subbase friction factor; L = crack of joint spacing; α = concrete thermal

coefficient of expansion; ΔT = temperature change in concrete pavement; and e = concrete drying shrinkage.

The term σ_{js} may be either positive or negative depending on the pavement temperature conditions and joint sealant type, which means the stress σ_{js} may be partially due to a temperature related residual stress in the joint sealant. Therefore, the displacement u_{temp} is referenced to the position where the stress (due to temperature change only) is equal to zero. The stress σ_{js} is positive if the joint sealant maintains a compressive stress (such as a preformed compression seal) against the edge of the sealant reservoir. This effect will decrease the concrete spall stress (σ_t) as shown in Eq. 47. For other types of sealants, σ_{js} may only be zero or negative which will increase φ in comparison to the stress resulting with preformed type of joint sealants.

Stress from a vehicle tire is just one mode from which fatigue failure of a pavement could occur. The objective of this analysis is to predict spall stresses acting on a delaminated portion of the concrete slab as a result of stresses induced by a vehicle tire. Stresses from this static analysis can be used to predict the fatigue life of a spall under this mode of failure. Such an analysis is also helpful in estimating some of the parameters such as deformation of the joint filler and the spall angle, which are included in the mechanistic spall model. In this analysis, it is assumed that there is a thin delaminated layer on the top part of the pavement slab. Work of several researchers has indicated the presence of a 2.5 to 5.1 cm thick laminate in a pavement slab surface created as a result of environmental factors, primarily differential shrinkage (NCHRP 1979; Emborg 1989). It is also assumed in this analysis that the bottom portion of the concrete slab is rigid, and only the delaminated top portion is subject to deformation under the wheel load. Also, the delaminated layer is treated as a continuum.

As indicated in Fig. 60, depending on the level of friction between the delaminated layer and the rigid concrete portion, only horizontal displacement is possible in the delaminated layer. The friction effects at the interface were modeled using forces acting in a direction opposite to that of the possible movement. The analysis was performed for conditions similar to Eq. 47, which is for cases where the shear stress

applied by the tire is greater than the friction force generated at the delamination boundary under threshold friction conditions when the joint displacement u is equal to the threshold slip δ_f.

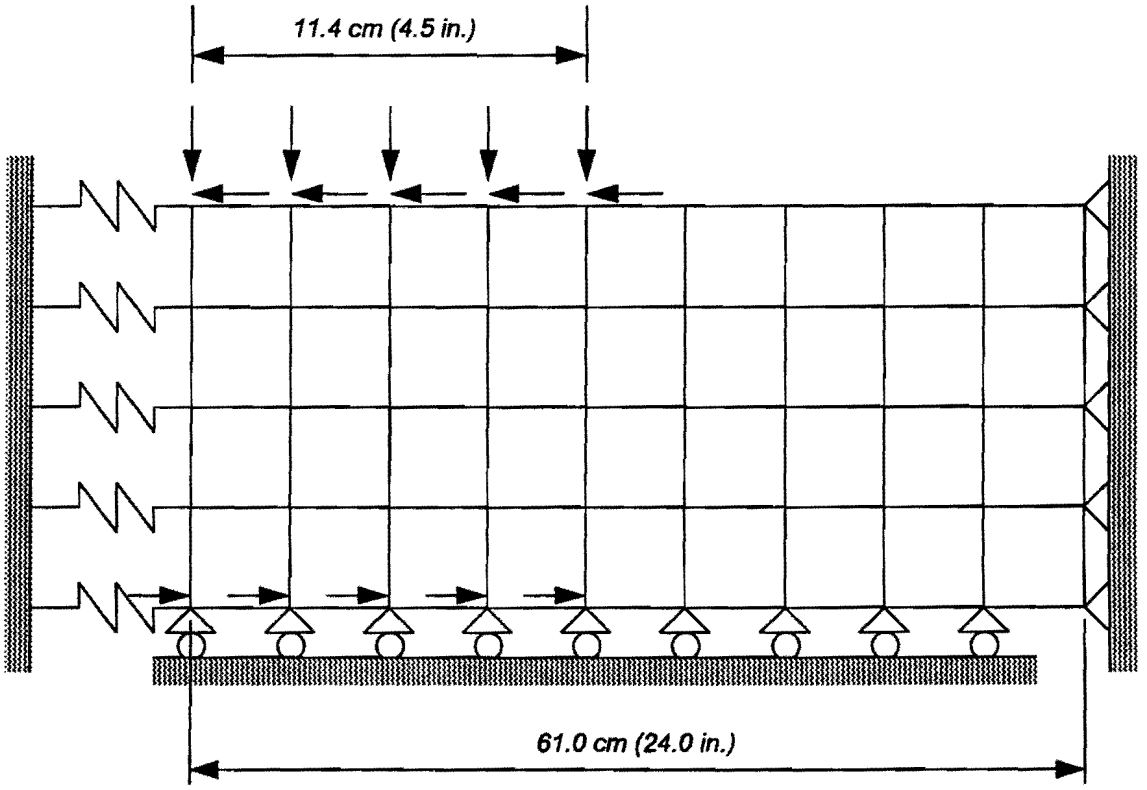

FIG. 60. Finite Element Formulation for the Analysis of Tensile Mode of Spalling

Finite Element Model

A two-dimensional finite element analysis (assuming plane strain conditions) was performed on this laminate (Fig. 60) to examine its stress distribution. The finite element configuration consisted of 245 nodes and 192 elements, and the analyzed section was taken as 61 cm long. Three values for the depth of delamination were considered at 1.3, 2.5, and 5.1 cm. Boundary conditions used in the finite element analysis are shown in Fig. 60. The joint filler was modeled as an elastic foundation, and the far end of the laminate was considered as fixed.

Loading Conditions

As previously mentioned, field investigations indicated that spalling near transverse cracks (or joints) shows a tendency to spall on the downstream side of the crack. Also, most of these spalls were located along the crack in such a way to indicate that they may have been caused by the traffic load. With this in mind, a loading configuration as shown in Fig. 60 was applied with concentrated forces at nodal points. The loading from the tire was treated as uniform in both normal and shear directions. The normal pressure of 689 kPa, and a longitudinal shear stress of 172 kPa were considered (Tielking and Roberts 1987; Tielking 1991). The loads along the lower horizontal boundary in Fig. 60 are applied to represent the frictional forces induced by the normal traffic load as a result of bond friction at the delamination face. The other nodes along the bottom boundary are free of frictional forces because the normal pressure at these nodes are negligible.

Material Characterization

Concrete was characterized as linearly elastic. For concrete, an elastic modulus of 27,560 MPa and a Poisson's Ratio of 0.15 were assumed. For the elastic foundation representing the joint filler, a spring coefficient (k_{js}) of 27 MN/m^3 was used. The analysis was conducted for three friction coefficients (0.0, 0.2, and 0.5) and three depths of delamination of 1.3 cm, 2.5 cm, and 5.1 cm. The friction stress C_2 is calculated by multiplying the normal tire pressure q with friction coefficient μ. The range of friction coefficients was selected based on field observations of spalled pavements which showed the greatest amount of distress in the least traveled lanes. It is assumed, given this evidence, that low values of friction resulted due to an accumulation of moisture (for short durations) on the interface of the delamination near the transverse crack faces.

Results

Fig. 61 shows how the maximum principal tensile stress in the analyzed section changes with both the friction coefficient denoted as f_c and the depth of delamination. It shows a decreasing trend for this tensile stress with increasing delamination depth, and a decreasing trend with increasing friction coefficient. This indicates that a shallow delamination is likely to develop into a spall much earlier than a deeper delamination because of much higher stress levels. Fig. 61 also compares the maximum principal tensile stress values obtained from the finite element analysis with those calculated using Eq. 47, which is applicable when the shear stress applied by the tire is greater than the friction force generated at the delamination boundary under threshold friction conditions where $u=\delta_f$. These values seem to compare well.

Fig. 62 illustrates the angle of principal stress for elements in the zone of maximum stress location below the edge of the load away from the transverse crack when $u = \delta_f$. This angle is defined as the counter-clockwise angle between the horizontal x-axis and the principal stress direction. The average value of this angle is seen to vary between 10 and 15 degrees. The average value of the angle for each friction coefficient is used in the calculation of maximum principal tensile stress from Eq. 47. It can be seen from Fig. 62 that this angle is dependent upon the depth of delamination and the coefficient of friction. The angle of inclination of the principal planes can be estimated from Fig. 62 to be used in Eq. 47.

DEVELOPMENT OF A SPALLING MODEL BASED ON AVAILABLE DATA

In order to establish good design practices and maintenance strategies for spalling, it is important to estimate the time at which spalling first takes place and the level of spalling at different times during a pavements service life. In order to eliminate spalling from concrete pavements, it would be necessary to make sure that no delaminations occur in the first place. This calls for extremely effective curing practices based on the ambient temperature and humidity profiles at the time of paving and immediately afterwards.

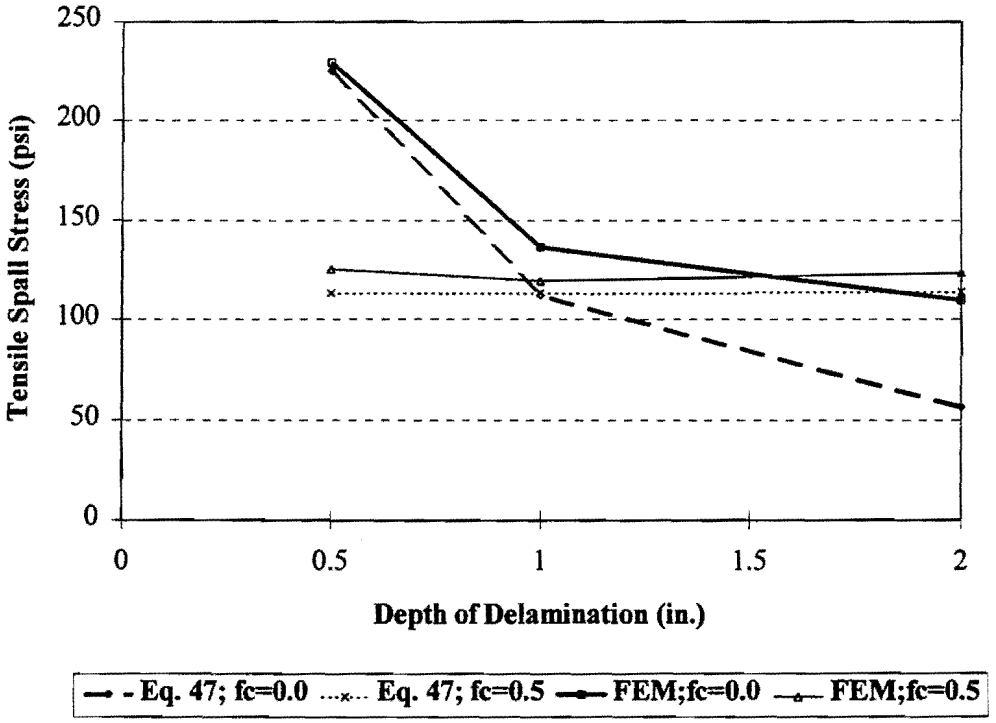

FIG. 61. Comparison of Calculated Spall Stress (Eq. 47) With Finite Element Analysis Results (1 psi = 6.89 Mpa ; 1 in = 2.54 cm)

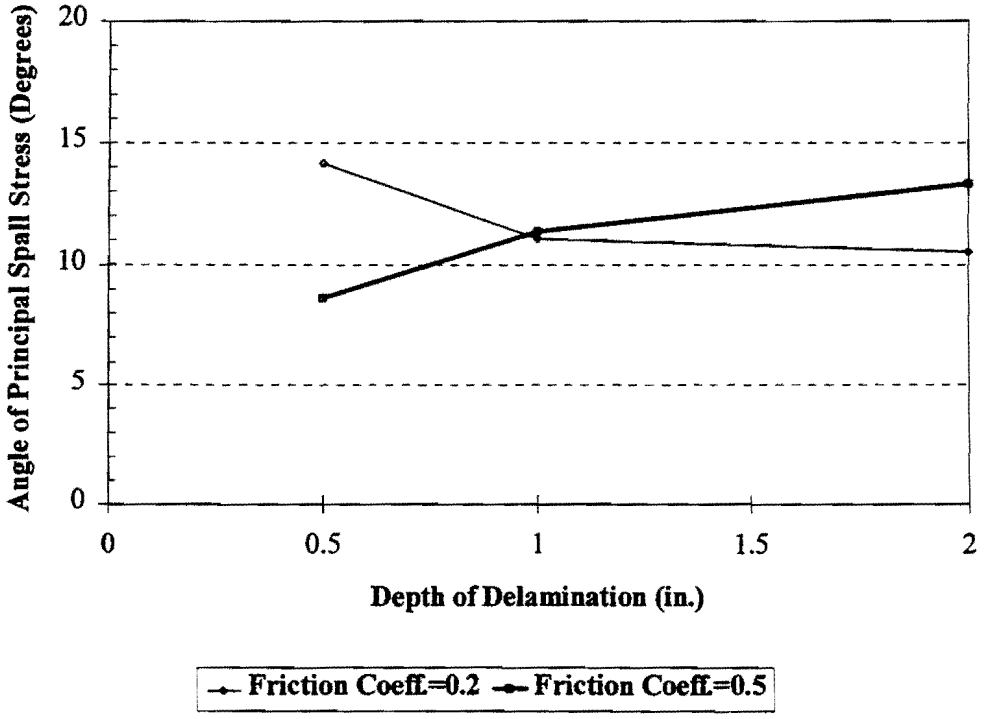

FIG. 62. Variation of Principal Stress Direction With Depth of Delamination (1 in = 2.54 cm)

However, further study is required to assess the economic feasibility of such considerations associated with highway construction. In the meantime, it may be important to predict the occurrence of spalling and its development with time, based on factors identified as the best predictors of spalling.

A design framework for spalling is proposed in this paper, based on a statistical method for determining prediction models from field data obtained from pavement condition surveys. This statistical method is referred to as the failure-time theory (Kalbfleisch and Prentice 1980). In this method, the failure-time is a random variable, and the dependence of failure-time is assessed using explanatory variables (co-variates).

For pavements under the same conditions, the time it takes for it to spall will vary from one section of pavement to the other due to the random nature of spalling. Therefore, this time to failure (spalling) can be represented by a probability density function. This is a situation where extreme values of such a random variable (largest or smallest value, but in this case, the smallest value for failure time) is of interest. These extreme values from samples of different numbers of data points are also random variables and have probability distributions of their own. These extreme values may be derived from the distribution of the initial variate.

Failure Time Theory and Concept of Survivability

Let T be a non-negative random variable representing failure time of a pavement section from a homogeneous population. The probability distribution of the failure time T can be specified using one of three different functions, namely the survivor function, the probability density function, and the hazard function. The survivor function $S(t)$ is defined as:

$$S(t) = P\left(T \geq t \right), \; 0 < t < \infty \tag{48}$$

The survivor function is a monotonic non-increasing left-continuous function with $S(0) = 1$ and $\lim_{t\to\infty} S(t) = 0$.

The survivor function can be described as the probability of failure at time t provided that the pavement did not fail up to that time. Due to aging of pavement, the survivability of pavement should gradually decrease with time. If the failure time T is a continuous variable, the probability density function $f(t)$ of the failure time T is given by:

$$f(t) = \lim_{\Delta t \to 0} \frac{P\ (\ t \le T \le t+\Delta t\ )}{\Delta t} = -\frac{dS(t)}{dt} \tag{49}$$

In other words, it is the proportion of pavements failing near time t within a very small time interval per unit time. $f(t)$ is a non-negative function. From the definition of the cumulative probability distribution function $F(t)$ of the failure time T,

$$F(t) = P\ (\textit{the pavement section fails before time } t) = \int_0^t f\ (\ T\ )\ dT \tag{50}$$

Then,

$$S(t) = 1\ - F(t) \tag{51}$$

The hazard function $h(t)$ of the failure time is defined as the probability of failure during a small time interval Δt assuming that the pavement has survived up to the beginning of the time interval. Therefore, this gives the conditional failure rate.

$$h(t) = \lim_{\Delta t \to 0} \frac{P(t \le T \le t+\Delta t \mid T \ge t)}{\Delta t} = \frac{f(t)}{S(t)} = -\frac{d \ln S(t)}{dt} \tag{52}$$

The hazard function for a pavement is positive and monotonically increases with time.

The selection of a theoretical mathematical distribution to represent failure data is an important step in the survival analysis. There can be many different causes that lead to the failure of a pavement at a particular time. It would be very difficult, if not impossible, to isolate all these causes and mathematically account for all of them. Therefore, choosing a theoretical distribution to approximate failure data needs to be made carefully by considering the type of hazard or survival function characteristics for the application at hand.

There are several candidate distributions commonly used in failure-time theory. These are the exponential distribution, the log-normal distribution, and the Weibull distribution. The simplest of these, the exponential distribution, provides a constant rate of hazard where no aging effects are involved (i.e., it has no memory, and hence the age of pavement does not affect its future survival). If the exponential distribution were to be used, failure (spalling) would be a random event which is independent of time. This is not suitable to represent spalling in a pavement where the hazard should monotonically increase with time (or damage) thus displaying the aging effect. The log-normal distribution is a distribution of a variable whose logarithm follows the normal distribution. It shows an initially increasing and then decreasing hazard rate. This decrease takes place almost as soon as the median is passed and approaches zero as time approaches infinity. This is also not suitable for pavements where there is accumulation of damage and an ever increasing rate of hazard.

The two parameter Weibull distribution is a generalized form of the exponential distribution. Unlike the exponential distribution, however, the Weibull distribution does not assume a constant rate of hazard. It is characterized by two parameters, the shape parameter and the scale parameter. By changing the values of these parameters, this

distribution may be used to model survival distribution of a population with increasing, decreasing, or constant risk. It can provide a monotonically increasing hazard and have a Type-III extreme value distribution. A Type-III extreme value distribution is one where its largest value has a finite upper bound and the smallest value has a finite lower bound. Therefore, this is suitable for determining the minimum of a series of minima (i.e., failure times). The probability density function $f(t)$ of the two parameter Weibull distribution is given by:

$$f(t) = \lambda \gamma (\lambda t)^{\gamma-1} e^{-(\lambda t)^{\gamma}} \qquad t \geq 0,\ \gamma, \lambda > 0 \tag{53}$$

where γ is the shape parameter and λ is the scale parameter. The survivor function $S(t)$ is therefore:

$$S(t) = e^{-(\lambda t)^{\gamma}} \tag{54}$$

and the hazard function, which is the ratio between $f(t)$ and $S(t)$ is given by:

$$h(t) = \lambda \gamma (\lambda t)^{\gamma-1} \tag{55}$$

These distributions can be generalized to incorporate the effect of a number of co-variates. For illustrative purposes, the case of a single co-variate represented by Z is considered. Usually, the scale function selected is $exp(Z \beta)$, where β is an unknown parameter. If the effect of co-variates is to act multiplicative on the Weibull hazard, the conditional hazard may be taken as:

$$h(t ; Z) = \lambda\gamma (\lambda t)^{\gamma-1} \exp(Z\beta) \tag{56}$$

A characteristic feature of the failure time data is that the response variable (such as the failure time) cannot be negative. This enables the use of a transformation, such as the log transformation, before standard statistical methods can be applied. Log

transformation is advantageous because it will reduce the presence of extremely large values in the distribution which can otherwise have a strong influence on the final fitting of the extreme value. The probability density function of the natural logarithm of the failure time Y ($Y = ln\ T$) is given by:

$$f(Y) = \frac{1}{\sigma} \exp\left[\frac{Y-\alpha}{\sigma} - \exp\left(\frac{Y-\alpha}{\sigma}\right)\right] \tag{57}$$

where $\sigma = 1/\gamma$ and $\alpha = -\ ln\ \lambda$. Also, the survival function $S(Y)$ and the hazard function $h(Y)$ for the natural logarithm of failure time are given by:

$$S(Y) = \exp\left[-\exp\left(\frac{Y-\alpha}{\sigma}\right)\right] \tag{58}$$

and

$$h(Y) = \frac{1}{\sigma} \exp\left(\frac{Y-\alpha}{\sigma}\right) \tag{59}$$

With the addition of the co-variates, the survival function $S(Y)$ is given by:

$$S(Y) = \exp\left[-\exp\left(\frac{Y-\alpha}{\sigma}+Z\beta\right)\right] \tag{60}$$

From Equation 60, we can obtain the linear model:

$$Y = \alpha - (\sigma\beta)Z + \sigma \ln\left[\ln\left\{\frac{1}{1-F(y)}\right\}\right] \tag{61}$$

which can also be represented for n number of co-variates $Z_1, Z_2, \ldots\ldots Z_n$ as the linear

regression model:

$$Y = \alpha + \sum_{i=1}^{n} Z_i \beta_i^* + \sigma W_p \tag{62}$$

where n = number of co-variates, $\alpha = - ln \lambda$, $\sigma = 1/\gamma$, $\beta^* = - \sigma \beta$, and W_p represents the p^{th} percentile of the extreme value distribution, i.e.,

$$p = \int_{-\infty}^{W_p} e^{w - e^w} dW \tag{63}$$

and therefore,

$$W_p = \ln \left[\ln \left(\frac{1}{1-p} \right) \right]; \qquad 0 \le p \le 1 \tag{64}$$

Although the failure time theory and the survivability concept were explained above in terms of the actual time response of failure time, often, other variables can be used as the response variable. For instance in spalling, we can use the number of spalled cracks as the response variable. This would enable the pavement engineer to perform the analysis without really defining what level of failure a pavement is in. A prediction equation can be developed which includes both the level of spalling as well as the reliability level, and the failure level need only be decided upon prior to the use of this equation for the prediction of spalling or to obtain the probability of survival. Since we are considering the spalling distress in this paper, the response variable would be the natural logarithm of the number of spalled cracks. The *LIFEREG* procedure of the statistical analysis package SAS® (SAS 1988) can be used to obtain the regression parameters described in Eq. 62.

Spalling Model Based on Available Data

All this information is not available in the current pavement condition survey database. Only the cumulative traffic volume, cumulative rainfall, and the minimum average low temperature at the time of each condition survey can be calculated from the available data. Since these three factors show a high correlation with the spalling data, and also since the mechanisms of spalling identify these as three primary factors affecting spalling, a satisfactory spalling model can still be obtained by using them.

The importance of rainfall in this model is reflected in two ways. First, as it was mentioned earlier, in rural highways, debris inside cracks on the outside lane can get splashed with rainwater onto the outside lane. This will make spalling in the outside lane subject only to stresses from the vehicle tires. Now, with more debris inside cracks in the inside lane, it can be subject to both the traffic induced stresses and temperature change induced stresses. Secondly, rainfall provides lubrication at the crack faces inside transverse cracks and delaminations. This will reduce or eliminate the cohesion between the crack faces which plays an important role in reducing the stresses. When friction across the delamination faces are low, it results in higher stresses (Fig. 61). The spalling model can be presented in the form of Eq. 65:

$$\log_e(\textit{No of Spalled Cracks}) = \alpha + \beta_1^* \, \textit{CUMTR} + \beta_2^* \, C_i \qquad (65)$$

where *CUMTR* = cumulative traffic in millions, and *CRAIN* = cumulative rainfall in centimeters, at the time of condition survey. Using the *LIFEREG* procedure in the SAS statistical analysis package, the following linear regression models were obtained for pavements made with siliceous river gravel and crushed limestone separately (Eqs. 66 and 67). Since the natural logarithm of the number of spalled cracks per survey section (Y) was considered as the response variable, to validate the model, left censoring was performed on the large number of sections which had not spalled at the time of the

survey. For pavements with siliceous river gravel coarse aggregate:

$$Y = 2.01 = 0.027\ CUMTR - 5.3E - 04\ CRAIN + 1.34\ Log_e\left[Log_e\left\{\frac{1}{1-p}\right\}\right] \qquad (66)$$

For pavements with crushed limestone coarse aggregate:

$$Y = 0.31 = 0.009\ CUMTR - 2.31E - 04\ CRAIN + 0.85\ Log_e\left[Log_e\left\{\frac{1}{1-p}\right\}\right] \qquad (67)$$

In Eqs. 66 and 67, p is the reliability level to be selected for the spalling data. Table 26 provides statistical data for spalling models in Equations 66 and 67. Fig. 63 illustrates the actual and predicted levels of spalling for pavements made with siliceous river gravel coarse aggregate. The scatter in Fig. 63 may be a result of different initial conditions at the time of paving, variations in aggregate properties, and differences in temperature changes between pavements.

Results From the Proposed Spalling Model

The results from the models in Eqs. 66 and 67 are illustrated in Figs. 64-67. These illustrations are given for a specific case of average daily traffic (ADT) of 20,000, annual traffic growth rate of 1%, and an average annual rainfall of 100 cm. Figs. 64 and 65 illustrate how the survivability (probability of survival) changes with time for pavements made with siliceous river gravel and crushed limestone coarse aggregates, respectively. As expected, they display the aging effect of the pavement by giving probabilities of survival decreasing with time. It can be clearly seen from these curves how the probability of survival would change depending on the failure criterion selected. The failure criterion is the number of spalled cracks per survey section (304 m long) that the pavement engineer would consider as failure. This provides the pavement engineer with sufficient flexibility with regard to deciding on which failure criterion to use. As shown in Figs. 64-67, different design curves can be developed for different failure

criteria. Or else, the probability of survival can be directly calculated using the model for each failure criterion. A survivability curve over the lifetime of a pavement which has a steep drop during the first few years would be inappropriate since it is an indication of possible fast deterioration (spalling) of the pavement.

TABLE 26. Statistical Parameters Pertaining to Model Development

Statistical Parameter		Siliceous Gravel	Crushed Limestone
Log Likelihood		2241	1019
α	Parameter Estimate	2.01	0.31
	Standard Error	0.14	0.12
	Chi-Square	201.0	6.3
	Pr>Chi	0.0001	0.0121
β_1	Parameter Estimate	0.027	0.009
	Standard Error	0.002	0.0046
	Chi-Square	176.7	3.39
	Pr>Chi	0.0001	0.0655
β_2	Parameter Estimate	-0.00053	0.000231
	Standard Error	0.0001	0.00027
	Chi-Square	15.73	0.75
	Pr>Chi	0.0001	0.39
σ	Parameter Estimate	1.34	0.85
	Standard Error	0.029	0.02

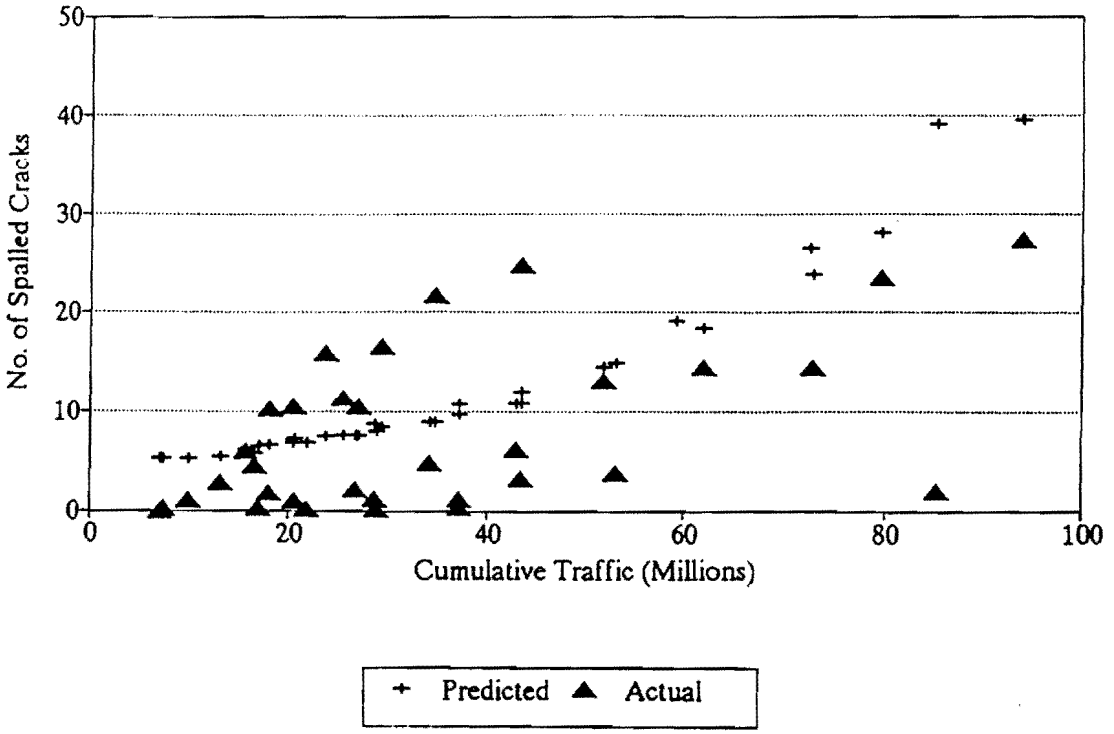

FIG. 63. Comparison of Spalling Predicted Using Eq. 66 With Actual Spalling Data for Siliceous Gravel Pavements

Figs. 66 and 67 show the predicted number of spalls per survey section for pavements with siliceous river gravel and crushed limestone coarse aggregate types respectively. Different curves are provided for three levels of reliability (50, 90, and 99%). The level of reliability in this situation is the level of reliability for the spalling data distribution at any given time. The LIFEREG procedure of SAS will take into account the fact that at each pavement condition survey, the spalling database provides a population of spalling data for each pavement master section. A level of reliability, p, is then assigned to the model such that the users of the model are able to specify their own reliability levels. As an example, a 90% reliability would mean that 90% of the original field data would fall below this level.

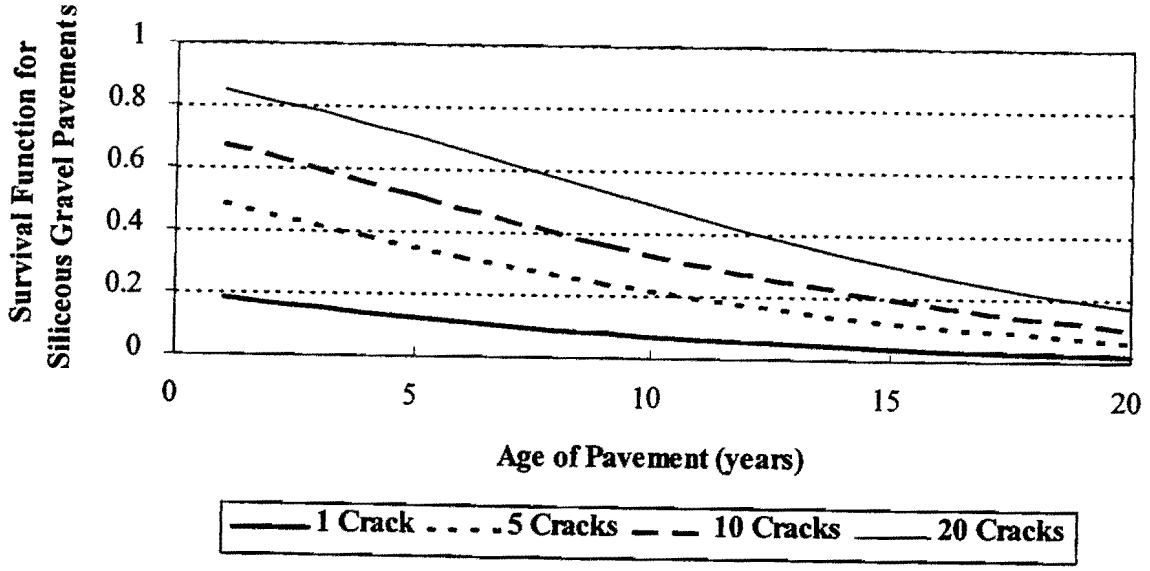

FIG. 64. Survivability of Pavements With Siliceous Gravel as Coarse Aggregate, for Different Spalling Failure Criteria

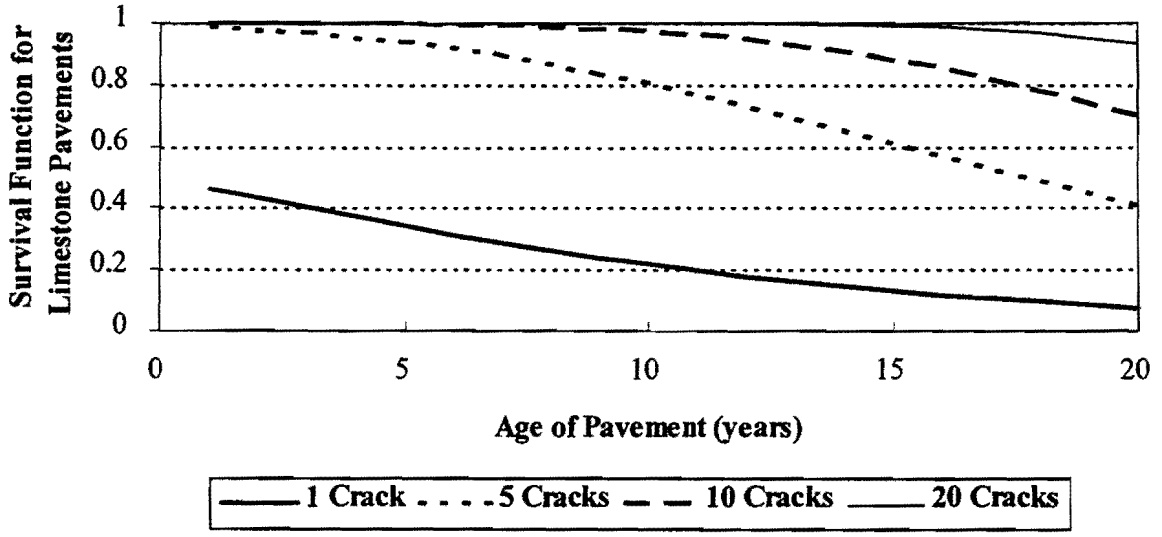

FIG. 65. Survivability of Pavements With Crushed Limestone as Coarse Aggregate, for Different Spalling Failure Criteria

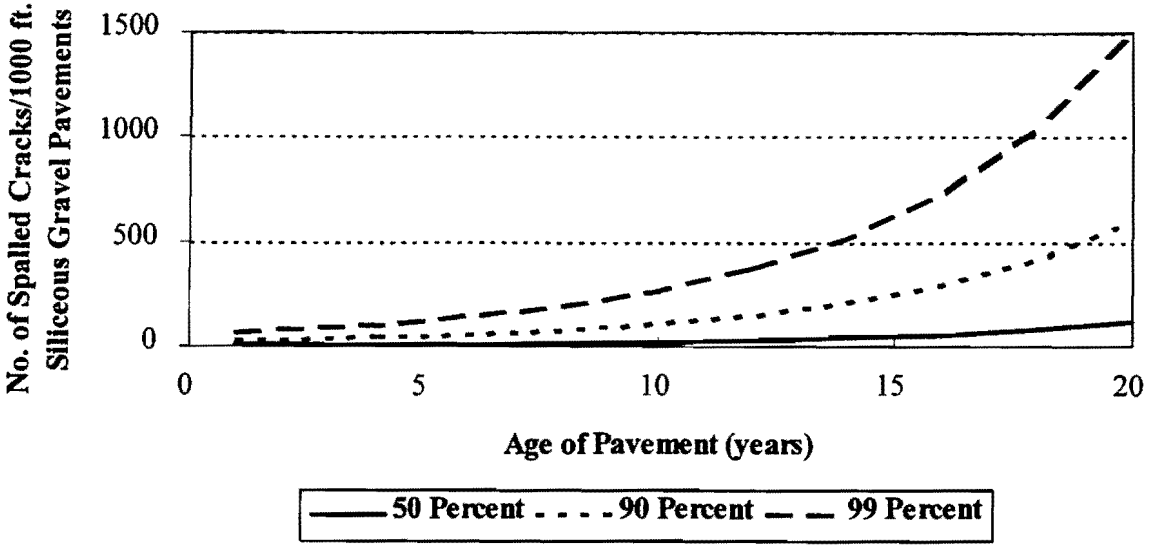

FIG. 66. Predicted Level of Spalling for Pavements With Siliceous Gravel as Coarse Aggregate, for Different Levels of Reliability

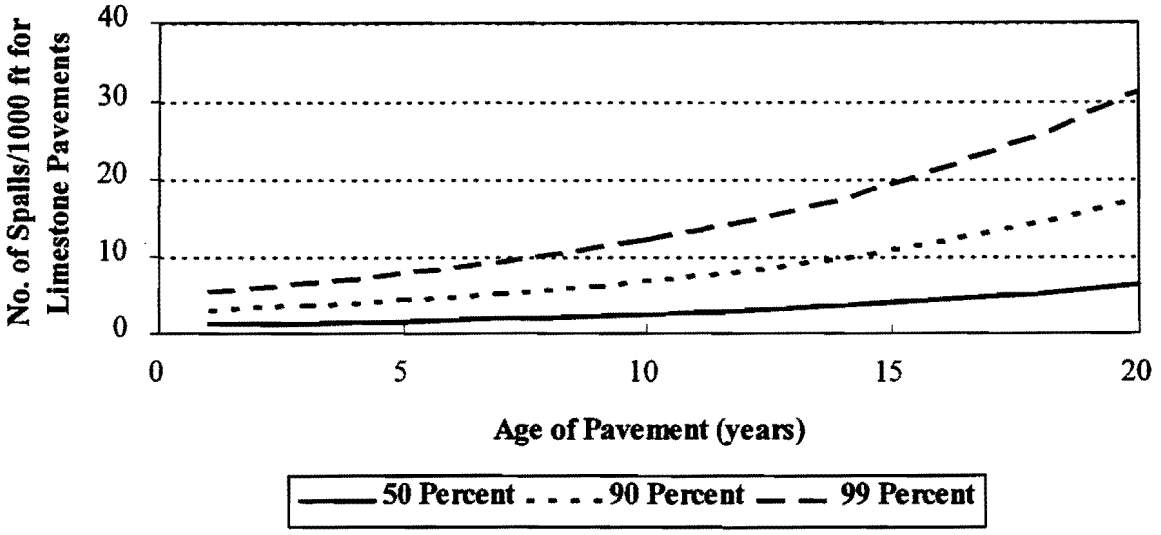

FIG. 67. Predicted Level of Spalling for Pavements With Crushed Limestone as Coarse Aggregate, for Different Levels of Reliability

Framework for an Improved Spalling Model

In order to develop a framework to incorporate spalling in the design of concrete pavements, factors identified in this study to influence spalling can be considered. The important observations from the studies described in previous chapters are summarized below:

1. Spalling originates (and is concentrated) near the transverse cracks or joints in concrete pavements in the form of either de-bonding cracks at the aggregate cement paste interface or delaminations.
2. These de-bonding cracks or delaminations are formed horizontally at a depth of 2-5 cm (1 to 2 inches) from the pavement surface.
3. These de-bonding cracks or delaminations most likely take place prior to the opening of the pavement for traffic.
4. Prediction of shrinkage stresses in early-age pavements based on finite element analysis indicates the feasibility of developing significant stress levels in the pavement that may be sufficiently high to create delamination.
5. These early developments of delaminations are governed by the ambient environmental conditions at the time of paving, the curing method adopted, and concrete mix design parameters such as water/cement ratio, cement factor, and the density of the aggregate.
6. The development of delaminations into spalls is a fatigue phenomenon, primarily dependent upon the level of traffic and temperature fluctuations.
7. Degree of restraint at the transverse crack/joint is a governing criterion on the development of spalls.
8. The degree of restraint point to the crack width and the rainfall are two factors that influence spalling.

Fig. 68 provides a schematic representation of the stages involved in the spall development process.

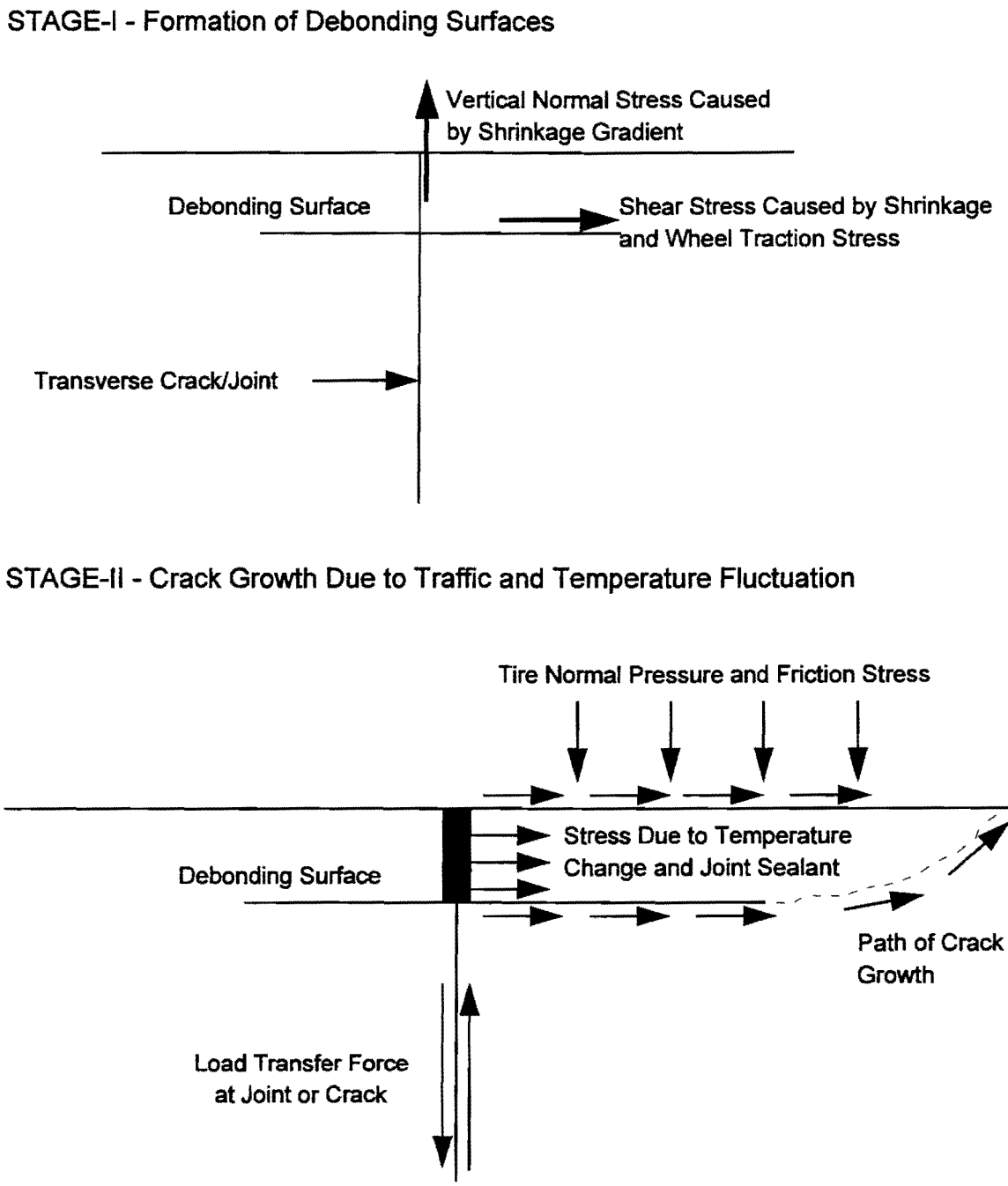

FIG. 68. Schematic Diagram Showing the Mechanism for Spall Development

In Stage-I, the vertical normal stress and the shear stress as shown in Fig. 68 contribute to the formation of delaminations or de-bonding surface formation. The vertical normal stress is generated by the action of the wheel load and the load transfer at the

transverse crack or joint faces. The shear stress is generated by shrinkage in concrete and the traction between the wheel and the pavement surface. In Stage-I, both Type-I (crack opening) and Type-II (in-plane shear) fracture are applicable, and, therefore, this can be treated as a mixed mode fracture. In Stage-II, the delaminations grow due to the action of traffic and temperature fluctuations. From a purely mechanistic standpoint, the spall model can be explained in the manner shown below:

1. Prediction of early-age concrete stresses generated due to shrinkage and temperature change. The factors to be considered are ambient environmental conditions, curing method, and material properties such as mix design parameters and moisture diffusivity.
2. Assessment of the likelihood of delamination by comparing early-age stresses with the interfacial strength at the aggregate-cement paste interface.
3. Calculation of the pavement fatigue life by incorporating fatigue damage due to traffic and temperature change.
4. Estimation of the number of load cycles to failure.

It is not feasible to incorporate all these factors into the spalling model at this point because all the data needed for that exercise are not available in existing databases. It is recommended that the following data pertaining to the pavement should be considered in future data collection efforts aimed at spalling model development:

Factors Relating to the Initial Condition

1. Ambient relative humidity and temperature during the first few days after paving
2. Method of curing
3. Aggregate-cement paste interfacial strength (represented by either the tensile strength of concrete, fracture toughness of concrete, or fracture energy at the aggregate-cement paste interface)

Factors Relating to Fatigue Damage

1. Fatigue stresses caused by traffic loads
2. Fatigue stresses caused by periodic fluctuation of temperature
3. A model developed in the laboratory to predict the fatigue fracture life of concrete

Factors Affecting Restraint Necessary for Generation of Stresses

1. Rainfall at the time of condition survey
2. Aggregate type which influences the level of cohesion between the delamination faces
3. Type of subbase which influences restraint to slab movement

Spalling prediction models from existing literature, which were described earlier, modeled spalling primarily as an age dependent phenomenon. Other factors included in these models were freezing index, freeze-thaw cycles, joint sealant type, and joint spacing. The validity of some of these factors in the spalling process was questioned in previous sections based on observations made in this research. None of these models have taken into account the obviously apparent relationship of spalling on concrete material properties. These material properties include:

1. Coarse aggregate type in concrete and properties of aggregates
2. Strength of the aggregate-cement paste interface
3. Mix design factors such as water/cement ratio and cement factor

Based on the observations made on spalling in this study, it is considered that the above-mentioned factors related to materials need to be included in some form in a spalling prediction model. In the spalling model developed based on available data, one of the materials related to parameters, the coarse aggregate type, was taken into account. One promising method to improve on the model is to use the calibration methodology for the development of a spalling model. What is most commonly used in calibration is to obtain

regression parameters for each individual pavement master section, and then relate these regression parameters to appropriate design factors.

Design Framework for Spalling Based on the Calibration Method

In addition to the factors identified in the spalling model proposed in Eqs. 66 and 67, it is imperative that the local conditions are taken into consideration since spall development appears to be strongly influenced by them. One promising way to do this is to use the method of calibration. The application of calibration methods to pavement distress prediction models was adopted by Zollinger and McCullough (1993). The significance of using the design method based on calibration can be summarized as follows:

1. The calibration method allows for the incorporation of local field conditions that affect pavement performance.
2. Material properties such as the Critical Stress Intensity Factor (K_{IC}) for fracture can be incorporated in the prediction model.
3. Predicted pavement life with regard to spalling is calculated based on the pavement engineer's definition of failure.
4. Use of survival analysis enables the incorporation of the level of reliability with the baseline distribution.

In this design method proposed by Zollinger and McCullough (1993), the number of load cycles to failure (N_f) is predicted based on:

1. Laboratory Testing ($N_{f\text{-}LAB}$),
2. Calibration with Field Conditions ($N_{f\text{-}C}$), and
3. Design Criteria ($N_{f\text{-}D}$).

A laboratory-based model to predict fatigue life ($N_{f\text{-}LAB}$) is needed. Since the fatigue in the case of spalling is a fracture phenomenon, a laboratory based fatigue fracture model is appropriate. A comprehensive search of available literature on fatigue fracture of concrete

revealed two such models. One model was proposed by Ramsamooj (1994), and he predicted the laboratory fatigue life ($N_{f\text{-}LAB}$) using Eq. 68.

$$N_{f\text{-}LAB} = \frac{30\, f_r^2}{K_{IC}^2} \int_{c_0}^{c_f} \frac{dc}{-\ln\left[1 - \left(\frac{K_I - K_{IOP}}{K_{IC}}\right)^2\right] - \left(\frac{K_1 - K_{IOP}}{K_{IC}}\right)^2 \left(1 - \frac{2C_t}{f}\right)} \tag{68}$$

where f_r = modulus of rupture of concrete; K_{IC} = critical stress intensity factor in concrete; K_{IOP} = stress intensity factor at the endurance stress limit of concrete usually taken at 50 to 55% of the modulus of rupture; c_0 = initial crack length (maximum aggregate size); c_f = final crack length (when spall distress is visible); and C_t = rate of change of the compliance of concrete with time.

In the above laboratory-based fatigue model, the fatigue life is expressed as a function of the critical stress intensity factor (K_{IC}) of concrete. As indicated in our laboratory data, the fracture toughness of Portland cement concrete is sensitive to a number of factors including the curing temperature, aggregate treatment methods, and paste additives in the concrete (such as silica fume). In this proposed framework for an improved spalling model, the effect of these factors (vis-a-vis: aggregate properties) can be included.

A second model for the prediction of fatigue fracture life was proposed by Bazant and Xu (1991). This model is a modified version of Paris' Law, and it is shown in Eq. 69.

$$\frac{da}{dn} = C\left(\frac{\Delta K_I}{K_{IM}}\right)^m \tag{69}$$

The calibration of the estimate of the load cycles to failure ($N_{f\text{-}C}$) can be obtained from field data as long as the appropriate type of data has been collected and tabulated within the database. However, past calibration efforts have indicated that weather conditions at the time of construction can be very important in the calibration of performance models. Previous descriptions of the spalling mechanism also strongly suggest the possible influence that construction conditions may have in the prediction process. Pavement sections subjected to greater drying potential and moisture loss may have a greater tendency to develop delaminations. In light of this evidence, it is reasonable to use a measure of drying potential during the construction period as characterized by the cooling degree days. This data is available in the national weather database and is determined as a function of the temperature below 65°F. Therefore, the higher the temperatures throughout a 24 hour period, the smaller the recorded cooling degree days. Another factor that may also be important is the amount of annual rainfall the pavement section was subjected to. Accumulated rainwater may infiltrate the interface of the delamination and reduce the frictional resistence along the interface and increase the stress intensity at the tip of the delamination thus promoting the development of spalling.

A spalling model for CRC pavement was developed relating the percent cracks spalled (in terms of the total number of surveyed transverse cracks) with the cumulative traffic. This spalling prediction model is of the form:

$$Ln[-Ln\ (\%\ Cracks\ Spalled)\ ] = \gamma Ln\lambda + \gamma.\ Ln(CUMTR)$$

or

$$y = a + mx$$

where

y = Ln (-Ln (% Cracks Spalled))

x = Ln (CUMTR)

$a = \gamma Ln\lambda$

$b = \gamma$

$\lambda = \exp(a/b)$

where CUMTR = cumulative traffic in millions at the time of condition survey. The database contained information with regard to either the percent of spalled cracks (% cracks spalled) or the number of transverse cracks that were spalled. Not all of the sections contained information with regard to the crack spacing or the total number of cracks surveyed. Therefore, to maintain consistency, the percent of cracks spalled was computed by assuming a crack spacing of 1.22 m.

The coefficients of the linear regression model (a, b, and λ) shown above were obtained for each section that was extracted from the Texas Rigid Pavement Database. Therefore, a set of the regression parameters were calculated for each pavement project. Cooling degree days, obtained from the climatological data records for the month and year of construction of each pavement project, were plotted versus *lambda* (where $lambda = e^{a/b}$) for crushed limestone pavements (Fig. 69) and for siliceous gravel pavements (Fig. 70). The graphs indicate that bands of relationships exist between degree days and lambda. These bands of data suggest that there is something common in the banded pavement sections. It was observed that pavement sections from the same county or from nearby counties tended to fall in the same band. This may be due to similarities among sections with respect to humidity, temperature, or moisture conditions of the counties or in the aggregate sources used for the pavement sections. However, this could not be verified in terms of the currently available data; the specific differences for these bands could not be accurately established. However, it is expected that further investigation in this area will throw light upon the reasons for these pavements falling in the same band.

It is clear from Figs. 69 and 70 that a good possibility exists that a relationship can be established among the coefficients in the regression analysis. However, it is expected that with the availability of more data as suggested in the spalling mechanism proposed here, such relationships could be developed. Once the fatigue life based on field calibration ($N_{f\text{-}C}$) is obtained from such relationships, fatigue life used for design ($N_{f\text{-}D}$) is calculated based on $N_{f\text{-}LAB}$ and $N_{f\text{-}C}$ using the following modification factors:

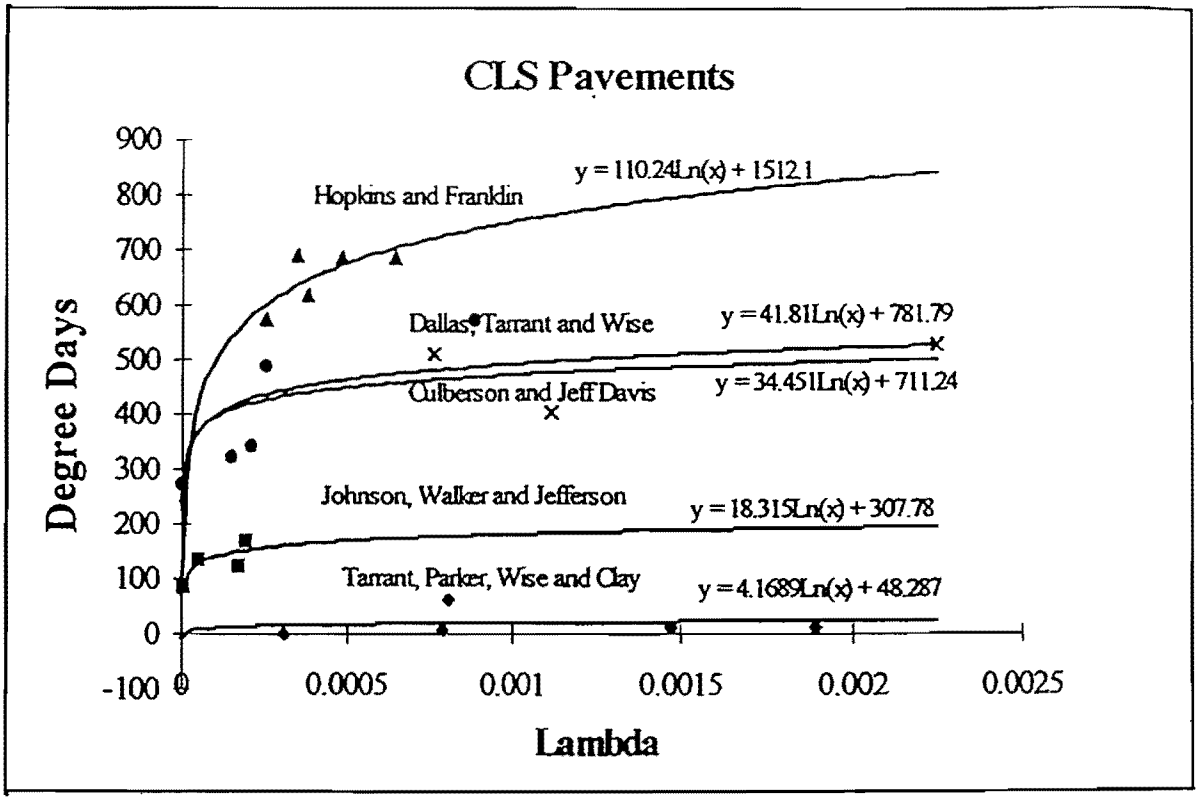

FIG. 69. Correlation between Degree Days and Lambda for Limestone Aggregate Pavements

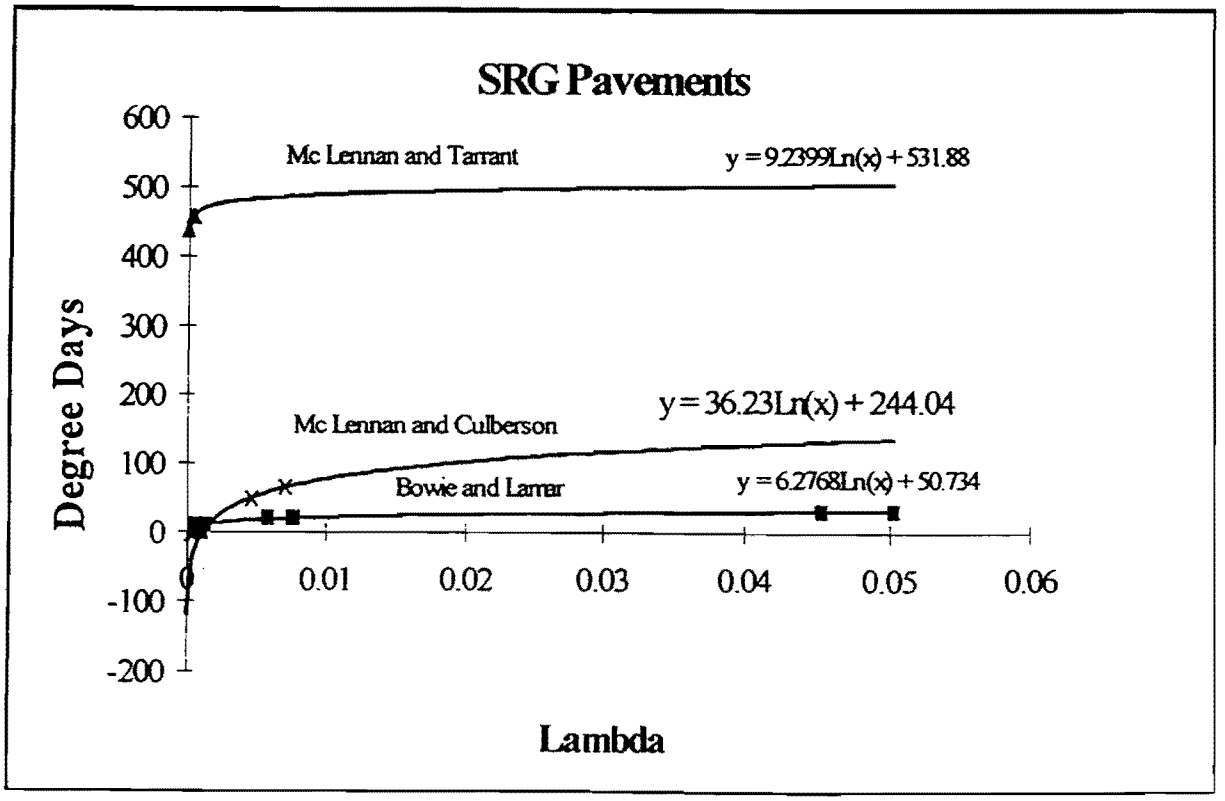

FIG. 70. Correlation between Degree Days and Lambda for SRG Aggregate Pavements

Modification Factors Used in the Design Process

1. MF_C - $N_{f\text{-}LAB}$ in terms of the fatigue stress / $N_{f\text{-}C}$
2. MF_D - $N_{f\text{-}LAB}$ in terms of the design stress / $N_{f\text{-}D}$

Proposed Improved Design Framework

Stage I: Prediction of the Occurrence of Delaminations

The design factors applicable to Stage I are:

1. Ambient relative humidity and temperature
2. Method of curing
3. Aggregate type and blend
4. Mix design factors (water/cement ratio, cement factor)
5. Early-age saw-cutting
6. Strength of concrete and aggregate-cement paste interface

Stage II: Prediction of Spalling

Spalling is expressed as a function of fatigue damage. Fatigue damage may be due to a combination of traffic loading and temperature fluctuations. The coefficients in the design equation (Eq. 72) can be related to the rainfall and aggregate fractal dimension since both of these factors affect the restraint at the delamination faces. The design factors applicable to Stage II are:

1. Laboratory based prediction model for fatigue life based on fracture
2. Prediction model for fatigue life based on fracture using field calibration parameters

3. Modification factors for design from which the fatigue fracture life for design can be calculated.

Therefore, it is important that in order to obtain a good spalling prediction model, the above mentioned data need to be collected in the future.

CHAPTER 7: CONCLUSIONS AND RECOMMENDATIONS

CONCLUSIONS

Spalling in concrete pavements is a very important distress which causes roughness in the ride and a reduction in the load transfer efficiency at both joints and cracks in Portland cement concrete pavements. Spalling also creates a negative perception regarding the structural integrity of the pavement to the road user. Therefore, it is imperative that spalling be incorporated as a design criterion for all types of Portland cement concrete pavements. To incorporate spalling in concrete pavement design, a spalling prediction model based on a sound mechanistic approach is a necessity.

Available literature on spalling provides some information on the factors that affect spalling. None of these studies appear to have looked at spalling from a mechanistic standpoint. Several spalling prediction models are also available in the literature. However, these models are not based on a sound mechanism of spalling. These spalling prediction models treat spalling primarily as an age-dependent phenomenon. It is clear from the findings of this research that spalling is not just an age-dependent phenomenon, but it has implications from the properties of materials in concrete, construction conditions, and environmental conditions a pavement has to undergo in its lifetime. Therefore, a sound spalling prediction model should include all of the factors indicated above. As an example, it is clear from the findings of this research that spalling has a strong influence on the type of coarse aggregate used in concrete. Therefore, if one were to model spalling as just an age-dependent phenomenon and the influence of aggregate type is disregarded, it will obviously lead to large discrepancies in the actual and predicted spalling levels as seen from previous spalling predictions.

Some of the spalling models published in the literature suggest that spalling is primarily caused by D-cracking and freeze-thaw of the concrete. However, concrete pavements in south Texas, which undergo very few freeze-thaw cycles every year, have shown significant spalling. Also, field studies undertaken in this research showed that

there is very little, if any, D-cracking in the pavements surveyed. Such evidence tends to disprove the theory that D-cracking and freeze-thaw are the primary factors affecting spalling in concrete pavements.

Based on the results of this study, it is believed that the development of spalling in a Portland cement concrete pavement involves several stages. In Stage I, de-bonding cracks appear at the interfacial region between the aggregate particles and the cement paste. These de-bonding cracks are generally found at a depth of 2-4 cm below the pavement surface. Based on the mechanism proposed in this research for spalling, these de-bonding cracks are developed as a result of stresses exerted by early-age shrinkage in concrete pavement slabs. In Stage II, these de-bonding cracks will be bridged with more applications of shrinkage stresses and stresses imposed by traffic loads and temperature fluctuations in the pavement. This bridging of the de-bonding cracks results in a continuous flaw in a horizontal plane, and it is referred to as delamination in this research. Evidence from field studies undertaken in this research suggest that both the de-bonding cracks and the delaminations occur very early in the life of a pavement, possibly as early as during the first few days after paving. Sensitivity analysis of very early-age concrete pavements for stresses due to shrinkage and creep indicated that sufficiently high stresses can be developed in early-age concrete pavements resulting in delaminations. Available computer analysis tools at the Texas Transportation Institute using the finite element method were used for this analysis. These delaminations are probably caused by stresses induced due to the differential shrinkage in the pavement slab. These stresses are a function of the ambient environmental conditions at the time of paving, the method of curing, concrete mix design parameters, and moisture diffusivity of concrete.

Once these delaminations are created in a concrete pavement, in Stage III of the spall development process, fatigue action due to stresses caused by wheel loads and temperature fluctuations in the pavement result in extending these delaminations into visible spalling distresses. Based on the observations made by engineers of the Texas Department of Transportation (TxDOT), the appearance of spalling at the pavement surface may take anywhere between one year and ten years of pavement life. Some

pavements never spall. What is important to understand here is that the nucleus for the spalling distress is originated almost as soon as that pavement slab is paved. Therefore, any attempts to remedy the situation need to be addressed at that stage.

It was observed from this research that there is a vast difference in the spalling potential of concrete pavements made with different aggregate types. Concrete pavements with crushed limestone aggregate appear to have a resistance to spalling. On the other hand, concrete pavements made with siliceous gravel as the coarse aggregate show a greater likelihood to spall. However, based on the results from the size-effect fracture tests on Portland cement concrete made using crushed limestone and siliceous gravel coarse aggregate, it was observed that the fracture toughness of concrete made with these two aggregate types appears to have comparable values. Therefore, the difference in their influence on spalling may be due to other factors.

Scanning electron microscopy (SEM) of Portland cement concrete samples indicated that there were cracks present at the interface between siliceous gravel aggregate and cement paste. These observations were in agreement with observations made by other researchers. Such micro-cracks were not observed in concrete made with crushed limestone. Since there are cracks present in the siliceous gravel concrete, it is more likely to propagate due to the stress concentrations at the crack tip, as compared to the limestone concrete which does not have a crack present.

Most existing databases do not appear to have all the information pertinent to the spalling prediction model proposed in this research. Therefore, a preliminary spalling prediction model developed from available data using regression analysis combined with survival analysis is proposed. Once a full spectrum of data related to variables affecting spalling is available in the databases, an improved spalling prediction model can be developed.

RECOMMENDATIONS

The development of a comprehensive spalling prediction model would require the availability of data such as the ambient conditions at the time of paving, type and properties of the aggregate, concrete mix design, interfacial strength of the aggregate-cement paste interface, traffic history, and temperature history. Such data has not been collected in the past, and changes in data collection procedures to accommodate these variables would facilitate the development of a more comprehensive spalling model. This needs to be addressed in the development of new databases or expansion of available databases.

Another important factor in the spalling mechanism is the interfacial bond strength at the aggregate-cement paste interface. At this point, several properties such as the tensile strength of concrete and the fracture toughness of concrete can be construed as providing a reasonably accurate reflection of the interfacial bond strength. However, it is necessary to have a parameter that would adequately represent the interfacial strength of the aggregate-cement paste interface by considering the properties of aggregates such as the shape, surface texture, and mineralogy.

REFERENCES

Alexander, K. M., Wardlaw, J., and Gilbert, D. J. (1968). "Aggregate-cement bond, cement paste strength and the strength of concrete." *Proceedings, International Conference on the Structure of Concrete*, London, 59-81.

Alford, N. McN., and Poole, A. B. (1979). "The effect of shape and surface texture on the fracture toughness of mortars." *Cement and Concrete Research*, Vol. 9, No. 5, 583-589.

Atkinson, C., Smelser, R. E., and Sanchez, J. (1982). "Combined mode fracture via the cracked Brazilian disc test." *International Journal of Fracture*, Vol. 18, No. 4, 279-291.

Bazant, Z. P., and Najjar, L. J. (1972). "Nonlinear water diffusion in non-saturated concrete." *Materials and Structures*, RILEM, Paris, Vol. 5, 3-20.

Bazant, Z. P. and Panula, L. (1978). "Practical prediction of time-dependent deformation of concrete - Part I: Shrinkage." *Materials and Structures*, RILEM, Paris, Vol. 11, No. 65, 307-316.

Bazant, Z. P. (1984). "Size effect in blunt fracture." *Journal of Transportation Engineering*, ASCE, Vol. 110, No. 4, 518-535.

Bazant, Z. P., Kim, J.-K., and Panula, L. (1991). "Improved prediction model for time-dependent deformations of concrete: Part I - Shrinkage." *Materials and Structures*, RILEM, Paris, Vol. 24, 327-345.

Bazant, Z. P., and Xu, K. (1991). "Size effect in fatigue fracture of concrete." *ACI Materials Journal*, Vol. 88, No. 4, 390-399.

Bertacchi, P. (1970). "Adherence entre aggregates et ciment et son influence surles caracteristiques des betons." *Rev. Mater. Constr. Trav. Publics.*, 659-660.

Buck, A. D., and Dolch, W. L. (1966). "Investigation of a reaction involving non-dolomitic limestone aggregate in concrete." *Journal of the American Concrete Institute*, Vol. 63, No. 7, 755-763.

Diamond, S., Mindess, S., and Lovell, J. (1982). "On the spacing between aggregate grains in concrete and the dimension of the aureole de transition." *RILEM Colloquium*, Liaisons Pates de Ciment Materiaux Asoces, Toulouse, France, C42-C46.

Dossey, T., and Weissmann, A. (1989). "A continuously reinforced concrete database." *Research Report 472-6*, Center for Transportation Research, The University of Texas at Austin, Austin, Texas.

Dossey, T., and Hudson, W. R. (1993). "Distress curves for CRCP crack spalling." *Technical Memorandum No. 1908-12*, Center for Transportation Research, The University of Texas at Austin, Austin, Texas.

Emborg, M. (1989). "Thermal stresses in concrete structures at early ages." *Doctoral Thesis*, Division of Structural Engineering, Lulea University of Technology, Sweden.

Epps, J.A., Meyer, A.H., Larrimore, I.E., and Jones, H.L. (1974). "Roadway maintenance evaluation user's manual." *Research Report 151-2*, Texas Highway Department, Texas Transportation Institute, College Station, Texas.

Farran, J. (1956). "Contribution mineralogique a l'etude de l'adherence entre les constituants hydrates des ciments et les materiaux enrobes." *Rev. Mater. Constr. Trav. Publics*, Ed. C., 490-491:155-172; 492:191-209.

Farran, J., Jarelas, R., Maso, J. C., and Perrin, B. (1972). "Existence d' une aureole de transition entre les granulats d'un mortier, ou d'un beton, et la masse de la pate de ciment hydrate." *Consequences Sur les Proprietes Mecaniques*, C. R. Acad. Sc. Ser. D. 275, 1467-1469.

Folk, R. L. (1968). *Petrology of Sedimentary Rocks*, Hemphill's, Drawer M, University Station, Austin, Texas.

Gay, D. A. (1994). "Development of a prediction model for pavement roughness on expansive clay." *Ph.D. Dissertation*, Department of Civil Engineering, Texas A&M University, College Station, Texas.

Gillott, J. E. (1975). "Practical implications of the mechanisms of alkali-aggregate reactions." *Proceedings, Symposium on Alkali-Aggregate Reaction - Preventive Measures*, Reykjavik, Iceland, 213-230.

Glucklich, J. (1968). "The effect of micro-cracking in time dependent deformations and the long-term strength of concrete." *Proceedings, International Conference on the Structure of Concrete*, Cement and Concrete Association, London, 82-92.

Graves, R. E., and Eades, J. L. (1987). "Strength developed from carbonate cementation in silica/carbonate systems." *Final Report*, Department of Geology, University of Florida, Gainesville.

Griffith, A. A. (1920). "The phenomena of rupture and flow of solids." *Philosophical Transactions, Series A*, Vol. 221, 163-198.

Gutierriz de Velasco, M., and McCullough, B.F. (1981). "Summary report for 1978 CRCP condition survey in Texas." *Research Report 177-20*, Center for Transportation Research, University of Texas at Austin, Austin, Texas.

Hayakawa, M., and Itoh, Y. (1982). "A new concrete mixing method for improving bond mechanisms." *Bond in Concrete*, Edited by P. Bartos, Applied Science Publishers, London, 282-288.

Hillemeier, B., and Hilsdorf, H. K. (1977). "Fracture mechanics studies on concrete compounds." *Cement and Concrete Research*, Vol. 7, No. 5, 523-536.

Hoshino, M. (1989). "Relationship between bleeding, coarse aggregate, and specimen height of concrete." *ACI Materials Journal*, Vol. 86, No. 2, 185-190.

Hsu, T. T. C., and Slate, F. O. (1963). "Tensile bond strength between aggregate and cement paste or mortar." *ACI Journal, Proceedings*, Vol. 60, No. 4, 465-485.

Inglis, C. E. (1913). "Stresses in a plate due to the presence of cracks and sharp corners." *Transactions of the Institute of Naval Architects*, Vol. 55, 219-241.

Irwin, G. R. (1948). "Fracture dynamics." *Fracturing of Metals*, American Society for Metals, Cleveland, Ohio, 147-166.

Irwin, G. R. (1956). "Onset of fast crack propagation in high strength steel and aluminum alloys." *Proceedings, Sagamore Research Conference*, Vol. 2, 289-305.

Irwin, G. R. (1957). "Analysis of stresses and strains near the end of a crack traversing a plate." *Journal of Applied Mechanics*, Vol. 24, 361-364.

Kadiyala, S. M. (1992). "Study of factors affecting the formation of cracks in continuously reinforced concrete pavements." *M.S. Thesis*, Department of Civil Engineering, Texas A&M University, College Station, Texas.

Kalbfleisch, J. D., and Prentice, R. L. (1980). *The Statistical Analysis of Failure Time Data*, John Wiley and Sons, Inc. New York.

Kaplan, M. F. (1961). "Crack propagation and the fracture of concrete." *American Concrete Institute Journal*, Vol. 58, 591-610.

Kopperman, S., Tiller, G., and Tseng, M. (1986). "Interactive microcomputer version, user's manual: IBM-PC compatible version." *Research Report FHWA/TS-87/205*, Federal Highway Administration, Washington, D. C.

Lerch, W. (1956). "Chemical reactions." *Significance of Tests and Properties of Concrete and Concrete Making Materials*, American Society for Testing and Materials, STP 169, 334-345.

Li, L., Chan, P., Zollinger, D. G., and Lytton R. L., (1993). "Quantitative analysis of aggregate based on fractals." Paper presented at the 72nd Annual Meeting of the Transportation Research Board, Washington, D. C.

Lyubimova, T. Y., and Pinus, E. R. (1962). "Crystallization structure in the contact zone between aggregate and cement in concrete." *Colloid Journal*, USSR, Vol. 24, No. 5, 491-498.

Mather, K, and Mielenz, R. C. (1960). "Cooperative examination of cores from the McPherson test road." *Proceedings, Highway Research Board*, Vol. 39, National Research Council, Washington, D. C., 205-216.

McCullough, B. F., Abou-Ayyash, A., Hudson, W. R., and Randall, J. P. (1975). "Design of continuously reinforced concrete pavements for highways." *NCHRP Report 1-15*, Center for Highway Research, The University of Texas at Austin, Austin, Texas.

McCullough, B.F., Ma, J.C.M., and Noble, C.S. (1979). "Limiting criteria for the design of CRCP." *Research Report 177-17*, Center for Transportation Research, The University of Texas at Austin, Austin, Texas.

Mehta, P. K. (1986). "Hardened cement paste-microstructure and its relationship to properties of concrete." *Proceedings, 8th International Congress on the Chemistry of Cement*, Vol. I, Finep, Rio de Janeiro, Brazil, 113-121.

Mindess, S., and Young, F. J. (1981). *Concrete*, Prentice Hall Inc., Englewood Cliffs, New Jersey.

Monteiro, P. J. M., and Mehta, P. K. (1986). "Improvement of the aggregate-cement paste transition zone by grain refinement of hydration products." *Proceedings, 8th International Congress on the Chemistry of Cement*, Vol. III, Finep, Rio de Janeiro, Brazil, 433-437.

NCHRP (1979). "Failure and repair of continuously reinforced concrete pavement." *NCHRP Synthesis 60*, National Cooperative Highway Research Program, National Research Council, Washington, D. C.

Neville, A. M., and Brooks, J. J. (1987). *Concrete Technology*, Longman Scientific and Technical Publishers, London, and John Wiley and Sons, New York.

Ojdrovic, R., and Petroski, H. J. (1985). "The cracked Brazilian specimen for fracture toughness testing of concrete." *International Journal of Fracture*, Vol. 27, R75-R80.

Orowan, E. (1948). "Fracture and strength of solids." *Report on Progress in Physics*, Vol. XII, 185.

Ozol, M. A. (1978). "Shape, surface texture, surface area, and coatings." *Significance of Tests and Properties of Concrete and Concrete-Making Materials*, American Society for Testing and Materials, STP 169B, 584-628.

Peleg, M., and Normand, M. D. (1941). "Characterization of the ruggedness of instant coffee particle shape by natural fractals." *Journal of Sedimentary Petrology*, Vol. 13, No. 2, 79-81.

Ramsamooj, D. V. (1994). "Prediction of fatigue life of plain concrete beams from fracture tests." *Journal of Testing and Evaluation*, ASTM, Vol. 22, No. 3, 183-194.

RILEM Committee on Fracture Mechanics of Concrete - Test Methods (1990). "Size-effect method for determining fracture energy and process zone size of concrete." *Materials and Structures*, RILEM, Paris, Vol. 23, 461-465.

SAS/STAT User's Guide. (1988). Release 6.03 Edition, SAS Institute, Inc., Cary, North Carolina.

Scholer, C. F. (1967). "The role of mortar-aggregate bond in the strength of concrete." *Highway Research Record 210*, Highway Research Board, National Research Council, Washington, D. C., 108-117.

Schwiete, H. E., Ludwig, U., and Albeck, J. (1968). "Die bindung von zuschlagstoffen an zementstein." *Wiss. Z. Tech. Univ. Desden.*, Vol. 17, No. 6, 1587-1590.

Scrivener, K. L., and Pratt, P. L. (1986). "A preliminary study of the microstructure of the cement/sand bond in mortars." *Proceedings, 8th International Congress on the Chemistry of Cement*, Vol. III, Finep, Rio de Janeiro, Brazil, 466-471.

Scrivener, K. L. (1989). "The microstructure of concrete." *Materials Science of Concrete*, Edited by Jan P. Skalny, The American Ceramic Society, 127-162.

Shah, S. P. (1979). "Whither fracture mechanics in concrete design ?" *Proceedings, Engineering Foundation Conference on Cement Production and Use*, Franklin Pierce College, Rindge, New Hampshire, 187-199.

Shelby, M.D., and McCullough, B.F. (1960). "Experience in Texas with continuously reinforced concrete pavement." *Highway Research Board Bulletin 274*, Highway Research Board, National Research Council, Washington, D. C., 1-29.

Sherwood, W. C., and Newlon, H. H., Jr. (1964). "A survey for reactive carbonate aggregates in Virginia." *Highway Research Record 45*, Highway Research Board, National Research Council, Washington, D. C., 222-234.

SHRP (1994). "Sensitivity analysis for selected pavement distresses." *Research Report*, Strategic Highway Research Program, National Research Council, Washington, D. C.

Smith, K.D., Mueller, A.L., Darter, M.I., and Peshkin, D.G. (1990). "Performance of jointed concrete pavements volume II - evaluation and modification of concrete pavement design and analysis models." *Research Report FHWA-RD-89-137*, ERES Consultants, Savoy, Illinois.

Sneddon, I. N. (1946). "The distribution of stress in the neighborhood of a crack in an elastic solid." *Proceedings*, Royal Society of London, Vol. A-187, 229-260.

Strubl, L., Skalny, J., and Mindess, S. (1980). "A review of cement-aggregate bond." *Cement and Concrete Research*, Vol. 10, 277-286.

Suzuki, M., and Mizumaki, K. (1975). "Bond strength between cement paste and aggregates." *Proceedings, Rev. 29th General Meeting, Cement Association of Japan*, 94-96.

Suzuki, M., and Mizumaki, K. (1976). "Bond strength between cement paste and aggregates." *Proceedings, Rev. 30th General Meeting, Cement Association of Japan*, 211-213.

Tayabji, S.D., and Colley, B.E. (1986). "Improved rigid pavement joints." *Research Report FHWA/RD-86/040*, Construction Technology Laboratories, A Division of Portland Cement Association, Skokie, Illinois.

Texas State Department of Highways and Public Transportation. (1985). *Rater's Manual*, Austin, Texas.

Tielking, J.T., and Roberts, F.L. (1987). "Tire contact pressure and its effect on pavement strain." *Journal of Transportation Engineering*, ASCE, Vol. 113, No. 1, 56-71.

Tielking, J.T. (1991). "Pavement shear forces produced by truck tires." *Memorandum*, Department of Civil Engineering, Texas A&M University, College Station, Texas.

Tracy, R. G. (1978). "Deterioration of continuously reinforced concrete pavement in Minnesota - An overview." *Research Report*, Research and Development Section, Minnesota Department of Transportation, Minneapolis, Minnesota.

Valenta, O. (1961). "The significance of the aggregate-cement bond for durability of concrete," *Preliminary Report*, International Symposium on the Durability of Concrete, RILEM, Prague, 55-87.

van Wijk, A. J. (1985). "Purdue economic analysis of rehabilitation and design alternatives for rigid pavements: A user's manual for PEARDARP." *Final Report*, FHWA Contract Number DTFH61-82-C-00035, Federal Highway Administration, Washington, D. C.

Walker, H. N. (1974). "Reaction products in expansion test specimens of carbonate aggregates." *Cement-Aggregate Reactions*, Transportation Research Record 525, Transportation Research Board, National Research Council, Washington, D. C., 28-37.

Walsh, P. F. (1972). "Fracture of plain concrete." *Indian Concrete Journal*, Vol. 46, No. 11, 469-471.

Westergaard, H. M. (1939). "Bearing pressures and cracks." *Journal of Applied Mechanics*, Vol. 6, 49-53.

Williams, M. L. (1957). "On the stress distribution at the base of a stationary crack." *Journal of Applied Mechanics*, Vol. 24, 109-114.

Wright, C. C. (1981). "Experimental continuously reinforced Portland cement concrete pavement - Interstate 95, Cumberland, Maine, final report digest." *Technical Paper 81-4*, Materials and Research Division, Maine Department of Transportation, Portland, Maine.

Xin, D., Zollinger, D. G., and Allen, G. D. (1995). "An approach to determine diffusivity in hardening concrete based on measured humidity profiles." *Advanced Cement Based Materials*, Vol. 2, 1-7.

Yuan, C. Z., and Guo, W. J. (1987). "Bond between marble and cement paste." *Cement and Concrete Research*, Vol. 17, 544-552.

Yuan, C. Z., and Odler, I. (1987). "The interfacial zone between marble and tricalcium silicate paste." *Cement and Concrete Research*, Vol. 17, 784-792.

Zollinger, D.G., and Barenberg, E.J. (1990). "Continuously reinforced pavements: punchouts and other distresses and implications for design." *Research Report No. FHWA/IL/UI 227*, Illinois Department of Transportation, Department of Civil Engineering, Engineering Experiment Station, University of Illinois, Urbana, Illinois.

Zollinger, D. G., and McCullough, B. F. (1993). "Development of Weibull reliability factors and analysis for the calibration of pavement design models using field data." Paper presented at the 72nd Annual Meeting of the Transportation Research Board, Washington, D. C.

APPENDIX A

RAW FIELD SURVEY DATA

2.54 cm = 1 in

0.77 m^3 = 1 yd

1.31 sk/m^3 = 1 sk/yd^3

3.79 liter = 1 gal

0.305 m = 1 ft

16.02 Kg/m^3 = 1 pcF

DATA PERTAINING TO THE FIELD SURVEY

Details Pertaining to Field Survey Sections

SH-6 Bypass in Bryan/College Station

Construction year:	1972.		
Location :	East bypass of SH-6, Bryan-College Station		
Pavement:	20 cm CRCP, 10 cm asphalt stabilized base, 20 cm lime stabilized subbase, natural clay subgrade.		
Mix design :	Cement content	-	6.5 sacks/m^3
	Water content	-	22.7 l/sack (W/C Ratio=0.53)
	Coarse Aggregate Factor	-	0.76
	Air factor	-	4 percent
	Slump	-	6.4 to 7.6 cm
Aggregates :	No records are available which indicate the source (pit) of the aggregate. However, there are notes to indicate that river gravel from the OSR aggregate stockpiles of Gifford Hill have supplied aggregates to this project. This information matched with the information provided by a supervisor of the project. Further details on aggregates are indicated in Table A-1.		

TABLE A-1. Details on Aggregates for SH-6 Bypass

Aggregate	Source	Aggregate Type	Specific Gravity	SSD Unit Wt.(pcf)	% Solid
Coarse Aggregate	Gifford Hill	River Gravel	2.65	105.8	63.9
Fine Aggregate	Gifford Hill	River Sand	2.66	106.5	64.1

Other Information : Cement - Gifford Hill Company, Dallas.

Water - City of Bryan

Construction: Longitudinal rebar - 39 Nos. 16 mm ribbed steel bars.

Transverse rebar - 13 mm dia. bars @ 61 cm

Curing - Membrane curing

Surfacing - Burlap sack drag

Paving - Slip-form construction of 7.3 m

Coring : Coring was done by the personnel from the District 17 Laboratory of the Texas DOT. Four test sections, each of 61 m length, were selected for detailed survey and coring. Coring of sections 1, 2 and 3 were done on Nov. 27, 1990. Coring of section #4 (STA. 28 to STA. 26) was done on Dec. 11, 1990. The summary of the coring schedule is given in Table A-2. Detailed information on observations made from cores is given in Tables A-3 to A-6.

TABLE A-2. Summary of Coring Schedule

Section Number	Direction	Starting Station Number	Ending Station Number	No. of Cores Taken
1	Southward	529	531	4 (#1-#4)
2	Southward	589	591	6 (#5-1 -#9)
3	Northward	586	584	5 (#101-#105)
4	Northward	28	26	6 (#201-#206)

TABLE A-3. Summary of Observations From Coring - Section 1

	Station/ Location	Lane	Position	Remarks
1	529+	Outside		One longitudinal rebar in core. Core came out intact. No visible weak/failure planes.
2	530+	Outside		Core came out intact. No visible weak/failure plane.
3	529+	Inside		Core came out intact. No visible weak/failure planes. No rebar.
4	530+	Inside	Downstream of minor crack near small spall	Core came out intact. No rebar.

TABLE A-4. Summary of Observations From Coring - Section 2

Core	Station/ Location	Lane	Position	Remarks
5-1	589+58	Inside	Upstream of crack with 13 mm spall, 5 cm from crack. 46 cm from lane marker.	Core & slab failed at mid-depth. A weak plane in core at 2.5 cm depth for a 10 cm length.
5-2	589+59	Inside	Downstream of crack with 13 mm spall. 20 cm from crack but not on spall. 46 cm from lane marker.	Failed plane in core & slab 15 cm below the surface. No other plane of weakness.
6	590+05	Inside	Downstream of spalled crack, but outside the spall 7.5 cm away. 1.8 m from lane marker.	Sample split at 2.5 cm. depth along an existing failed plane in slab. Plane of weakness continued beyond spall.
7	590+13	Inside	At corner where 2 cracks meet. 46 cm from edge of lane outside 13 mm deep spall.	Excessive air voids in core. No weak or failed plane apparent.
8	589+58	Outside	1.5 m from edge. Downstream of non-spalled crack.	Significant air voids in core. No apparent weak planes or failed planes. Longitudinal r/f in core.
9	590+05	Outside	0.3 m from lane marker on 13 mm spall downstream of crack.	Failed plane at 9 cm depth. No other weak planes evident.

TABLE A-5. Summary of Observations From Coring - Section 3

Core	Station/ Location	Lane	Position	Remarks
101	585-584	Outside	1.2 m from lane marker. Upstream of 13 mm spalled crack.	Core came out intact. No visible defects.
102	585-584	Outside	1.2 m from lane marker. Downstream of 13 mm spalled crack, on spall.	Core came out intact. No visible defects.
103	584	Outside	0.6 m from lane marker and downstream of crack, on 2.5 cm spall.	Core came out intact. No visible defects.
104	584	Inside	Middle of lane, Upstream of 2.5 cm spalled crack.	Core failed 10 cm from surface. Weak plane at 2.5 cm from surface.
105	584	Inside	Middle of lane. downstream of 2.5 cm spalled crack. On the spall.	Core failed 10 cm from surface. Weak plane at 2.5 cm depth below the spall.

TABLE A-6. Summary of Observations From Coring - Section 4

Core	Station/ Location	Lane	Position	Remarks
201	27 to 26	Outside	Upstream of crack and 13 mm deep spall between two cracks in the middle of lane.	Core intact. Weak plane clearly visible beyond the spall at 2.5 cm depth.
202	28 to 27	Inside	On 2.5 cm spall upstream of crack.	Core intact. Weak plane below spall at 3.8 cm depth. Weak plane is only in half of the core.
203	28 to 27	Inside	Downstream of crack opposite core #202.	Core intact. 7.6 mm long aggregate-mortar separation 7.6 mm below surface.
204	27 to 26	Inside	Upstream of crack and 2.5 cm deep spall.	Core intact. No weak planes.
205	27 to 26	Inside	D/S of same crack for core #204.	No spall. Weak plane at 2.5 cm Core broke into two at weak plane while coring.
206	27 to 26	Inside	Core taken so that it is on both sides of the crack at small crack.	Transverse crack visible along the depth of core, but core intact. Weak plane at 13 mm

Beltway 8 Frontage Road in Harris County

Construction year: 1987.

Location: On the northbound feeder road of Beltway 8 in Houston between the Bissonet and Bellaire streets.

Pavement :
- Surface - 17.6 mm CRCP with 2 layers of 16 mm steel.
- Base - 15 cm Cement stabilized base
- Subbase - Lime stabilized subgrade
- Subgrade - Clay

Mix Design:
- Cement Content - 8.5 sacks/m^3
- Coarse Aggregate Factor - 0.76
- Water content - 25.2 l/sack
- Air factor - 3 %
- Slump - 3.8 to 5 cm.

Other Information :
- Cement - TXI, Katy and Hunter plants.
- Water - City of Houston
- Admixtures - AEA-Daravair M (20 ml/45 kg suggested, 15 ml used)
- Retardant - Daratard 17
- Fly ash. - None.

Aggregates : Refer to Table A-7 below.

TABLE A-7. Aggregates for Beltway 8 West Loop Frontage Road

Aggregate	Source	Aggregate Type	Specific Gravity	SSD Unit Wt. (Kg/m^3)	% Solids
Coarse Aggregate	TXI, Altair	River Gravel	2.62	1615	62.3
Fine Aggregate	TXI Altair	River Sand	2.63	1660	63.03

Construction: Paving - Southbound, 7.6 m. pass, 4.3 m pass.
Northbound, 12 m wide single pass.

Texas DOT sources familiar with the construction of the highway indicated that the section between Beechnut and Westheimer streets was constructed in two stages. Available evidence suggest that one section was from Beechnut to Westpark, and the other, northwards of Westpark.

Coring : Coring was done on May 13, 1991, by the personnel from TxDOT District 12 laboratory. Of the three lanes, only two inside lanes were cored. A summary of all observations made from cores is given in Table A-8.

A major portion of this pavement was filmed using the ARAN unit of the Texas DOT with the purpose of selecting an appropriate test section for coring purposes.

Observations : The following observations were made from this test section.

1. Spalling was first observed in 1989, two years after construction.
2. There is very little spalling southbound. Most of the spalling is northbound between Bellaire and Bissonet.
3. Spalling is not limited to the inside lanes only. It is distributed among all three lanes of the pavement.
4. Rebar was out of place at most coring locations. The bottom layer was close to the bottom of the slab, with no significant cover.
5. Most cores had a plane of weakness(delaminations) close to the surface.
6. Most cores failed at the plane of re-bar. It was not clearly evident if there was an already established plane of weakness at that level.

7. Generally, delaminations occur between aggregate and mortar.

TABLE A-8. Summary of Observations From Coring

Core	Lane	Position	Remarks
1	Middle	Middle of lane and downstream of crack.	No delaminations visible. All 33 cm of core came out in-tact.
2	Middle	Same crack as for core #1. 46 cm from inside lane and upstream of crack.	Delamination clearly visible at a depth of 1.3 to 2.5 cm from the surface.
3	Middle	Core taken at the middle of a crack 1.2 m from inside lane.	Delamination visible, but it ends within the core itself. Core was broken at re-bar.
4	Middle	Core taken downstream of crack but beyond large spall. Core was 1.2 m away from middle lane.	Core broke at re-bar level. Minor delamination visible within the top 13 -25 mm.
5	Middle	Core taken at same crack as core #4 and upstream. Core was 1.2 m away from middle lane.	Core broke at the plane of re-bar. No delaminations evident.
6	Inside	Middle of unspalled crack, 1.2 m away from the middle lane.	Core broke into pieces. Delaminations are present.
7	Inside	Downstream of crack with 13 mm spall. 20 cm from crack. Not on spall. 46 cm from lane marker.	Core sample broke into 3 pieces. Delamination present at the top of the slab. Another failure plane at level of re-bar.

Interstate 45 in Leon County

Construction year: 1972.

Location: A 32 km stretch on Interstate 45 extending from SH-7 at Centerville to the Freestone county line.

Pavement :	Surface	-	20 cm CRCP, #5 rebars at 19 cm spacing.
	Subbase	-	10-12 cm asphalt/lime treated subgrade.
	Subgrade	-	According to TxDOT sources, it is sand.
Mix design:	Cement content	-	251.5 Kg/m^3
	Water content	-	23.5 l/sack
	Coarse Aggregate Factor	-	0.80
	Air factor	-	4 percent
	Slump	-	4-5 cm

Aggregates: Refer to Table A-9 below.

The records indicate that 3 combinations of the coarse aggregate types were used in the concrete.

1. 65% East Texas Stone Crushed Limestone and 35% Holsey Bros. Gravel.
2. 65% Gifford Hill Gravel and 35% East Texas Stone Crushed Limestone.
3. 100% Crushed Sandstone East Texas Stone Co.

Other Information:	Cement	-	Atlas Cement Co., Waco.
	Water	-	Local Lake.
	Admixtures	-	AEA Scotch (1035 ml. for 6.1 m^3 of concrete).

Construction: Both highway lanes in one direction were paved in one operation.

Observations: Spalling is almost non-existent in this test section of 129 lane km. The primary mode of failure is punchouts. A quick count of the number of punchout failures indicated the following data.

Number of punchout failures northbound = 5

Number of punchout failures southbound = 16

TABLE A-9. Details on Aggregates for IH-45 in Buffalo, Texas

Category	Source	Aggregate Type	Spec. Gravity	SSD Unit Wt.(Kg/m^3)	% Solids
Coarse Aggregate 1	Blue Mtn. Pit, East Texas Stone Co.	Crushed Calcareous Sandstone	2.64	303	55.7
Coarse Aggregate 2	Holsey Bros., Austonio.	Siliceous Gravel	2.61	1162	63.7
Coarse Aggregate 3	Gifford Hill, Wardlaw Pit.	Crushed Limestone/ Siliceous Gravel	2.65	1562	58.9
Fine Aggregate	Holsey Bros., Austonio.	Siliceous-Limestone Sand	2.66	1517	57.0

IH-10 in Gonzales County

Survey Date: November 7, 1990

Construction year: 1970-71

Location: Approximately 48 km of CRC pavement on Interstate 10 in Gonzales county extending from F.M. 609 near Flatonia up to the Caldwell county line.

Pavement : The typical pavement configuration is indicated below.

Section East of SH-304

Surface - 20 cm thick CRC, with one reinforcement mat.

Subbase - 10 cm black base and lime stabilized subgrade.

Subgrade - Clay.

Section West of SH-304

Surface - 20 cm thick CRC, with one reinforcement mat.

Subbase - 20-25 cm cement-soil mixture.

Subgrade - Sand.

Mix design: Not available.

Aggregates: No information is available, but our observations indicate that it is a crushed stone.

Construction: The two segments of the highway on either side of SH-304 were constructed as separate projects. In both segments all 7.3 m of pavement was laid using the slipform method. Shoulder is asphalt concrete.

Observations: There is no spalling in this test section of 193 lane km. The primary mode of failure is punchouts. A quick count of the number of punchout failures indicated in Table A-10.

TABLE A-10. Data on Punchouts

Direction of Travel	Number of Punchouts	
	West of SH-304	East of SH-304
East-bound	50	139
West-bound	No Data	145
Length of Road	13 km	32 km

IH-10 near Downtown Houston

Construction year: 1971

Location: Between mile posts 771 and 773 on Interstate 10. It is an 8-lane highway, east of IH-45.

Remarks: Construction details of the pavement are not available for this test section. Information for the section west of IH-45 on IH-10 is available, and it is 10 cm CRCP, with aggregates from Parker Brothers, Eagle Lake.

Observations:	This 3.2 km test section is heavily spalled in the two inside lanes. The two outside lanes are not spalled at all. Observation of spalls indicate that the aggregate is a river gravel.

IH-610 West Loop

Survey date:	February 07, 1991 (using ARAN)		
Construction year:	1968		
Location:	Between the Glenmore and Jason Streets. It is an 8-lane highway, south of US-59 intersection in the west IH-610 loop.		
Pavement:	The pavement surface is 10 cm thick CRC, with one reinforcement steel mat with #5 bars at 19 cm as longitudinal steel, and #4 bars at 75 cm as transverse steel.		
Mix design:	Cement content	-	277.1 Kg/m^3
	Water content	-	21 l/sack
	Coarse Aggregate Factor	-	0.79
	Air factor	-	3 percent
	Slump	-	1.2 to 5 cm
Aggregates:	See Table A-11 below		
Other Information:	Cement - Type I Cement from Trinity, Houston.		
	Admixture - Solar 25, 118 ml (AEA)		
Construction:	No information is available.		
Observations:	The pavement is extensively cracked, and spalled as well. The spalls are not limited to the inside lanes only.		

TABLE A-11. Aggregates for IH-610 West Loop in Houston

Category	Source	Aggregate Type	Spec. Gravity	SSD Unit Wt. (km/m^3)	% Solids
Coarse Aggregate	Horton & Horton, Eagle Lake, Texas.	Gravel	2.57	1616	62.9
Fine Aggregate	Horton & Horton, Eagle Lake, Texas.	Sand	2.60	1616	62.7

US-59 in Wharton County

The test section was in service for around 20 years. It is located between Wharton and El Campo in Texas DOT District 13. No detailed investigations were done in this section. However, the remaining non-overlaid sections indicated the following:

1. River gravel was used as the coarse aggregate in concrete.
2. There was extensive spalling in both directions of the highway.
3. Most of the spalling was in the inside lane.
5. Texas DOT sources in Yoakum district office have noticed that spalling occurred 5 to 7 years after placement of concrete. They also said that there is very little spalling in the longitudinal joints or cracks.

Petrographic Analysis of Concrete Cores

TABLE A-12. Results From Petrographic Analysis of Cores From BW-8 in Houston

Core No.	Observations
3	Core thickness was 33 cm. 3-year old concrete. Two-layer reinforcement. Siliceous gravel coarse aggregate. Sub angular aggregate shape. Core taken through a transverse crack with crack extending to a 25 cm depth. Occasional poor bond of aggregate to mortar. Uniform color and smooth texture of matrix. Delaminations at 2.5, 4, and 8 cm (at rebar) depths, and most delaminations occur around a brown porous chert. Delaminations are separated and filled with road film that obscures some of the secondary deposit features. Areas immediately surrounding the cracks exhibit limited hydration.
7	Core thickness was 33 cm. 3-year old concrete. Two-layer reinforcement. Siliceous gravel coarse aggregate. Subangular aggregate shape. Core was taken in an area between transverse cracks. Poor bond of aggregate to mortar around chert. Some chert particles fractured. Color of matrix changes throughout core. Smooth texture of matrix. Delaminations at 2.5, 4, 8 cm (at rebar) depths and most delaminations occur around a brown porous chert. Delaminations at aggregate-paste contact where bleed channels are also seen. Areas immediately surrounding the cracks exhibit limited hydration. Secondary deposits are present throughout the depth of core.

TABLE A-13. Results From Petrographic Analysis of Cores From SH-6 in Bryan/College Station

Core No.	Observations
4	Core thickness was 20 cm. 20-year old concrete. One-layer reinforcement. Siliceous and calcareous river gravel coarse aggregate. Subangular aggregate shape. Core was taken through a transverse crack, with vertical crack extending through full depth of core and bond breaker. Surface of core is spalled across 3/4 of the surface, with no other delaminations. Crack width is smaller at the depth of rebar. Adequate bond of aggregate to mortar. Fewer bleed channels present. Areas immediately surrounding the cracks exhibit limited hydration. Better degree of hydration seems to have slowed the onset and intensity of attacks by secondary deposits such as calcium hydroxide and ettringite.
5	Core thickness was 20 cm. 20-year old concrete. One-layer reinforcement. Siliceous and calcareous river gravel coarse aggregate. Subrounded aggregate shape. Core not taken through a transverse crack. Top 2.5 cm of core is completely separated from the rest of the core, and no other delaminations were observed. Adequate to poor bond of aggregate to mortar, with the bond at the top of the core being particularly weak. Fewer bleed channels present. Paste fairly well hydrated. Areas immediately surrounding the cracks exhibit limited hydration. Better degree of hydration seems to have slowed the onset and intensity of attacks by secondary deposits such as calcium hydroxide and ettringite.

Observations From Concrete Cores

Test Section in SH-225 in La Porte, Texas

TABLE A-14. Summary of Observations From the Coring Operation at the SH-225 Test Section in La Porte, Texas

Core #	Test Section Description	Lane	Delami-nated ?	Remarks
1	Procrete curing	Inside	No	
2	Procrete curing	Outside	Yes	Delaminations at 6.3 cm depth, and at top rebar depths on both sides of random crack.
3	Standard cure, Skewed rebar	Inside	Yes	Delamination at 4 cm depth on one side of crack (only 5 cm long).
4	Standard cure, Skewed rebar	Outside	Yes	Delaminations at 6.3 and 11.4 cm depths (on opposite sides of the transverse crack).
5	Cotton mat cure	Outside	Yes	
6	Cotton mat cure	Outside	No	Core taken at crack branching.
7	Standard cure	Inside	Yes	Delaminations at 2.5 cm depth and at top rebar.
8	Polyethylene cure	Outside	No	
9	Standard cure, 0.9 m. saw cuts	Inside	No	Core taken at intersection of saw cut and longitudinal crack.
10	Standard cure, 0.9 m saw cuts	Outside	No	
11	Standard cure, 1.5 m saw cuts	Outside	No	
12	Standard cure, 1.5 m saw cuts	Inside	No	
13	Standard cure, 1.5 m saw cuts	Outside	No	

Test Section in US-290 in Cypress, Texas

TABLE A-15. Summary of Observations From the Coring Operation at the US-290 Test Section in Cypress, Texas

Core ID/ Sub Section	Coarse Aggregate	Curing Method	Position of Core	Observations
1 I-A	100% Limestone	Polyethylene Film	Centerline Sawcut	No indication of delaminations.
2 I-A	100% Siliceous gravel	2 coats of regular TxDOT compound	Centerline Sawcut	No indication of delaminations.
3 I-A	100% Limestone	Polyethylene Film	Transverse Crack	Core heavily damaged.
4 I-A	67% Limestone 33% Siliceous gravel	1 coat of regular TxDOT compound (Type II)	Transverse Crack	No indication of delaminations.
5 I-A	33% Limestone 67% Siliceous gravel	1 coat of regular TxDOT compound (Type II)	Transverse Crack	Very fine 2.5 cm long delamination at 4 cm depth.
6 I-A	100% Siliceous gravel	Type II	Transverse Crack	Very fine 2.5 cm long delamination at 4 cm depth.
7 I-A	33% Limestone 67% Siliceous gravel	Poly-Film	Transverse Crack	No indication of delaminations.
8 I-A	33% Limestone 67% Siliceous gravel	2 coats of regular TxDOT compound	Transverse Crack	No indication of delaminations.

TABLE A-15. Continued

Core ID/ Sub Section	Coarse Aggregate	Curing Method	Position of Core	Observations
9 I-B	100% Siliceous gravel	Linseed Oil	Transverse Crack	Delamination at 4 cm depth underneath an aggregate particle. Signs of a developing spall.
10 I-B	100% Siliceous gravel	Water-Based Compound	Transverse Crack	Very fine de-bonding cracks at 1.2 cm and 5 cm depths. Crack length is 1.2 cm.
11 I-B	100% Siliceous gravel	Water-Based Compound	Transverse Sawcut	1.2 cm long de-bonding crack underneath aggregate particle.
12 I-B	100% Siliceous gravel	Water-Based Compound	Transverse Sawcut	One de-bonding crack above aggregate very close to the surface.
14 III-B-1		Type I	Transverse Crack/ Double Crack Inducer	Delamination underneath aggregate at 2.5 cm depth. Also indicates a developing spall.
15 III-B-I		Type I	Transverse Sawcut	2.5 cm long de-bonding cracks on top of aggregate particle at 2.5 cm depth.
16 III-B-I		Type I	Transverse Crack/ Single Crack Inducer	Three de-bonding cracks both above and below aggregate particles at 2.5, 4 and 5 cm depths.

TABLE A-15. Continued

Core ID/ Sub Section	Coarse Aggregate	Curing Method	Position of Core	Observations
18 III-B-3		Type II compound withheld 1 hour before placement	Transverse Crack/ Double Crack Inducer	Two areas of de-bonding cracks underneath aggregate particles at 2.5 to 5 cm depth
19 III-B-3		Type II compound withheld 1 hour before placement	Transverse Sawcut	Several de-bonding cracks both above and below aggregate particles at 2.5 cm depth.
20 III-B-3		Type II compound withheld 1 hour before placement	Transverse Crack/ Single Crack Inducer	Delamination at 2.5 to 5 cm depth.

APPENDIX B

PRELIMINARY ANALYSIS OF SPALLING DATA

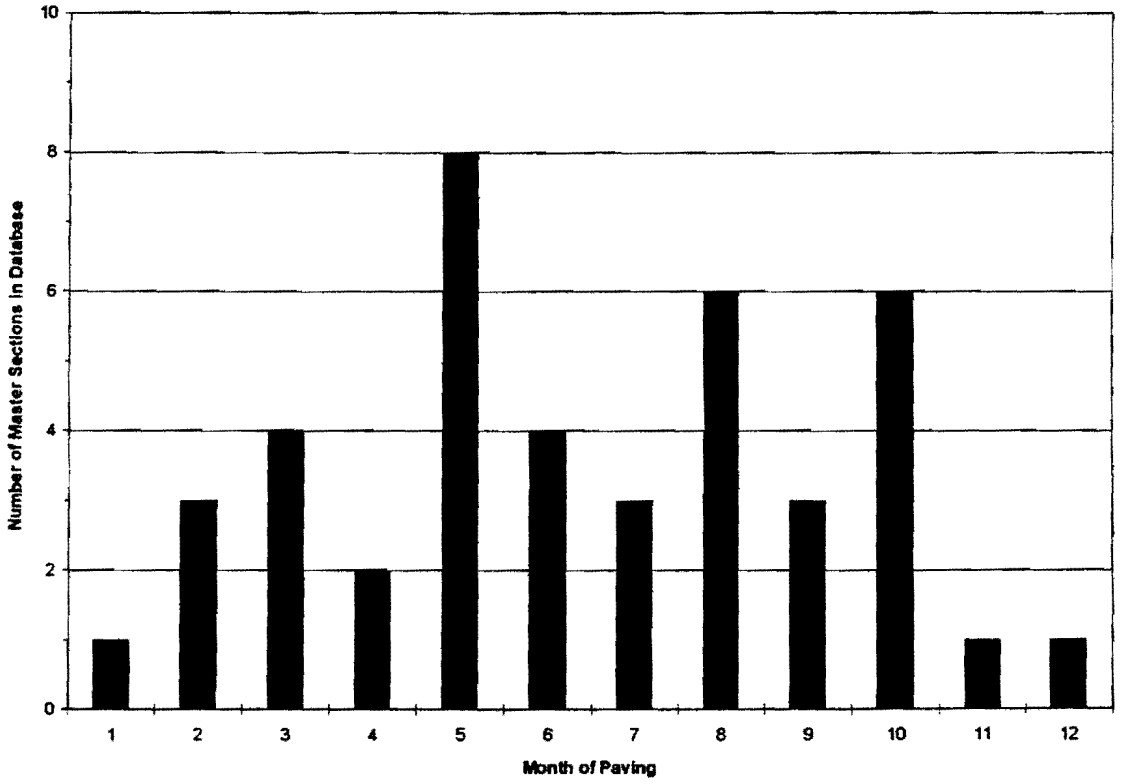

FIG. B-1. Number of Master Sections Available in TRPD, by Paving Month

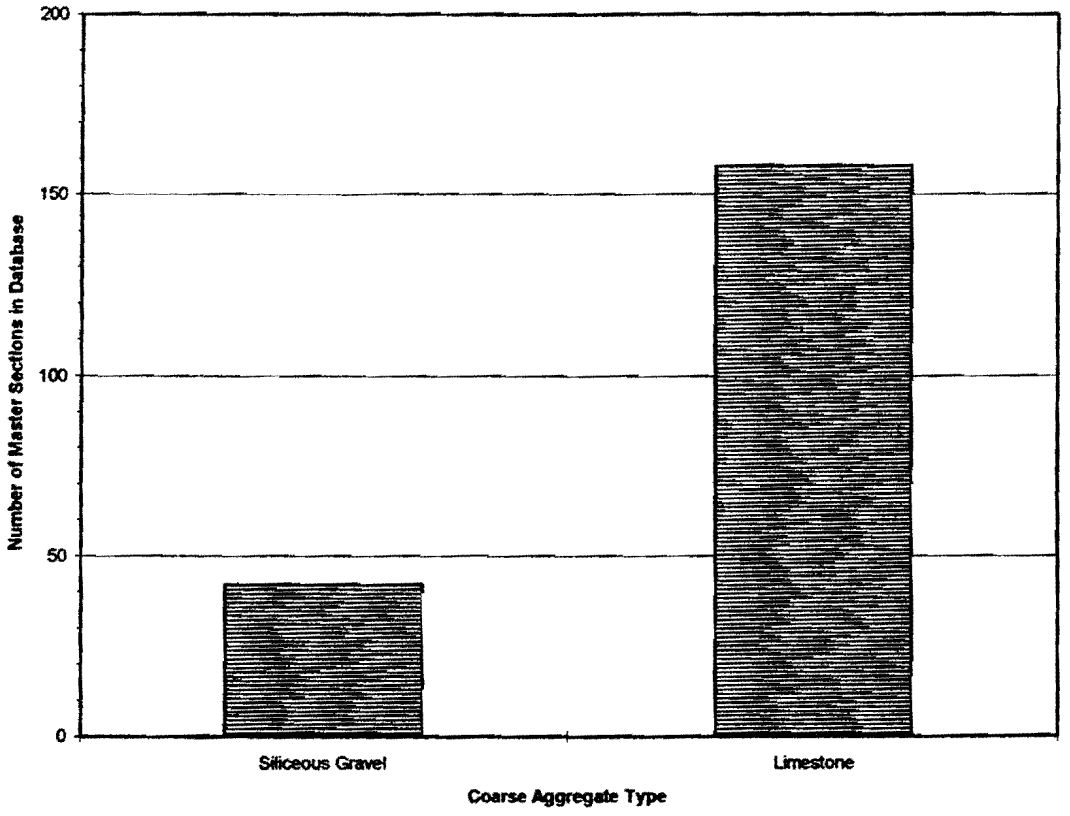

FIG. B-2. Number of Master Sections Available in TRPD, by Coarse Aggregate Type

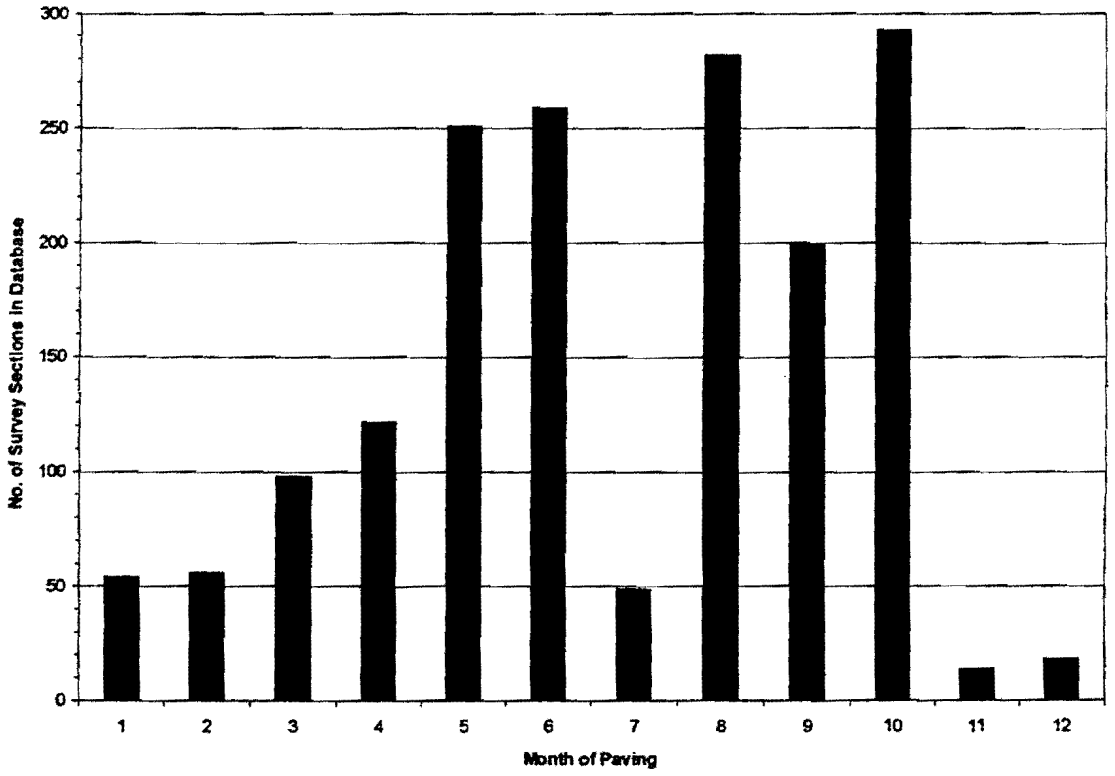

FIG. B-3. Number of Survey Sections in the Database by Paving Month

APPENDIX C

LABORATORY TEST DATA

TABLE C-1. Results From Phase I of Split Tensile Tests for Different Gradations

Coarse AggregateType	Gradation	Replicate Number	3-Day		7-Day	
			Max. Load (lbf)	Fracture Toughness (K_{IC})*	Max. Load (lbf)	Fracture Toughness (K_{IC})*
Siliceous Gravel	38 mm-Opt	1	17500	461.89	19300	509.40
	38 mm-Opt	2	16980	448.16	18330	483.80
	38 mm-Gap	1	16400	432.86	23630	623.68
	38 mm-Gap	2	19650	541.18	22520	594.38
	19 mm-Opt	1	18890	498.58	24560	648.23
	19 mm-Opt	2	17710	467.43	21390	564.56
	19 mm-Gap	1	16000	422.30	24170	637.93
	19 mm-Gap	2	19500	514.68	22970	606.26
Limestone	38 mm-Opt	1	20450	539.75	22510	594.12
	38 mm-Opt	2	24020	633.98	24440	645.06
	38 mm-Gap	1	18820	496.73	24820	655.09
	38 mm-Gap	2	23240	613.39	24530	647.44
	19 mm-Opt	1	20860	550.57	24740	652.98
	19 mm-Opt	2	23810	628.43	21780	574.85
	19 mm-Gap	1	19100	504.12	21500	567.46
	19 mm-Gap	2	18560	489.87	23490	619.99

***Units = psi - $\sqrt{in}$ (1 psi - $\sqrt{in}$ = 1.099 Mpa - $\sqrt{m}$; 1 in = 2.54 cm ; 1 lb_f = 4.448 N)**

TABLE C-2. Laboratory Data for Concrete Moist-Cured at 21.1°C With Siliceous River Gravel Coarse Aggregate

Age of Concrete (Hours)	Replicate Number	Specimen Length (ℓ) in cm	Maximum Load (P) in lbf	Nominal Stress (σ_0) in Mpa	Fracture Toughness (K_{IC})*
12	1	14.6	1444.1	183.6	120.63
12	2	14.6	1823.6	231.8	152.34
12	3	14.6	2246.3	285.6	187.65
24	1	14.6	6609.8	840.4	552.16
24	2	14.6	8040.1	1022.2	671.64
24	3	14.6	6473.3	823	540.76
72	1	14.6	14193.8	1804.6	1185.7
72	2	14.6	16692.8	2122.3	1394.5

***Units = psi - $\sqrt{\text{in}}$ (1 lb_f = 4.448 N; 1 psi = 6.89 Mpa ; 1 psi - $\sqrt{\text{in}}$ = 1.099 Mpa - $\sqrt{\text{m}}$; 1 in = 2.54 cm)**

TABLE C-3. Laboratory Data for Concrete Moist-Cured at 21.1°C With Crushed Limestone Coarse Aggregate

Age of Concrete (Hours)	Replicate Number	Specimen Length (ℓ) in cm	Maximum Load (P) in lbf	Nominal Stress (σ_0) in Mpa	Fracture Toughness (K_{IC})*
12	1	14.5	1302.8	166.5	109.13
12	2	14.5	1233.0	157.6	103.28
12	3	14.5	1467.64	187.6	122.94
26	1	14.6	6648.01	845.2	555.35
26	2	14.6	7045.82	895.8	588.58
26	3	5.625	5768.0	749.6	487.16
72	1	14.6	12455.1	1583.5	1040.46
72	2	14.6	13528.7	1719.7	1130.14

***Units = psi - $\sqrt{\text{in}}$ (1 lb_f = 4.448 N; 1 psi = 6.89 Mpa ; 1 psi - $\sqrt{\text{in}}$ = 1.099 Mpa - $\sqrt{\text{m}}$; 1 in = 2.54 cm)**

TABLE C-4. Laboratory Data for Concrete Moist-Cured at 40.5°C With Siliceous River Gravel Coarse Aggregate

Age of Concrete (Hours)	Replicate Number	Specimen Length (ℓ) in cm	Maximum Load (P) in lbf	Nominal Stress (σ_0) in Mpa	Fracture Toughness (K_{IC})*
13	1	14.6	8894.7	1130.9	743.03
13	2	14.6	7489.5	952.2	625.65
13	3	14.6	7985.6	1015.3	667.09
24	1	14.6	14087.5	1791	1176.82
24	2	14.6	14044.5	1785.6	1173.23
24	3	14.6	13135.7	1670.1	1097.31
72	1	14.6	19037.3	2420.4	1590.31
72	2	14.6	17397.5	2211.9	1453.32

***Units = psi - $\sqrt{\text{in}}$ (1 lb_f = 4.448 N; 1 psi = 6.89 Mpa ; 1 psi - $\sqrt{\text{in}}$ = 1.099 Mpa - $\sqrt{\text{m}}$; 1 in = 2.54 cm)**

TABLE C-5. Laboratory Data for Concrete Moist-Cured at 21.1°C With Lime-Treated Siliceous River Gravel Coarse Aggregate

Age of Concrete (Hours)	Replicate Number	Specimen Length (ℓ) in cm	Maximum Load (P) in lbf	Nominal Stress (σ_0) in Mpa	Fracture Toughness (K_{IC})*
12	1	14.7	2934.5	371.1	244.47
12	2	14.7	2565.8	324.5	213.75
12	3	14.3	2049.5	266.4	173.10
24	1	14.5	8757.5	1119.5	733.57
24	2	14.5	7881.0	1007.5	660.15
24	3	14.5	8401.4	1074	703.74
72	1	14.5	17322.8	2214.5	1451.03
72	2	14.6	16268.7	2068.4	1359.03

***Units = psi - $\sqrt{\text{in}}$ (1 lb_f = 4.448 N; 1 psi = 6.89 Mpa ; 1 psi - $\sqrt{\text{in}}$ = 1.099 Mpa - $\sqrt{\text{m}}$; 1 in = 2.54 cm)**